AFIT/GSO/ENY/97J-1

# ANALYSIS OF TETHERS IN SAMPLING NEAR EARTH OBJECTS

THESIS

John W. Wong, Captain, USAF

AFIT/GSO/ENY/97J-1



Approved for public release; distribution unlimited

The views expressed in this thesis are those of the author and do not reflect the official policy or position of the Department of Defense or the U. S. Government.

AFIT/MS/ENY/97J-1

# ANALYSIS OF TETHERS IN SAMPLING NEAR EARTH OBJECTS

John W. Wong, B.S.
Captain, USAF

Approved:

Christopher D. Hall — 2 Jun 97

Dr Christopher D. Hall, Chairman
Assistant Professor of Aerospace and Systems Engineering — date

William E. Wiesel Jr — 2 June 97

Dr William E. Wiesel, Jr.
Professor of Astronautical Engineering — date

James T. Moore — 2 Jun 97

Dr James T. Moore, Lt Col, USAF
Associate Professor of Operations Research — date

AFIT/GSO/ENY/97J-1

# ANALYSIS OF TETHERS IN SAMPLING NEAR EARTH OBJECTS

THESIS

Presented to the Faculty of the Graduate School of Engineering

of the Air Force Institute of Technology

Air University

In Partial Fulfillment of the

Requirements for the Degree of

Master of Science

John W. Wong, B.S.

Captain, USAF

JUNE, 1997

# Acknowledgements

My eternal gratitude goes to my thesis advisor and committee, Dr Christopher Hall, Dr William Wiesel, and Lt Col (Dr) James Moore, for enduring this endless period with me and finally seeing me through to completion.

I also wish to identify certain people who, whether they knew it or not, made a big difference: Gary Brandstrom, for his camaraderie and help in my previous, ill-fated TEX effort; Frank Desamours, for being Frank (pun intended!); and finally, a good friend and former GSO, Dan Hrovat, for his support and encouragement as I walked through dark times. I have left out many people who helped or encouraged me in one form or another, but they are not forgotten. Thank you all!

This one is for you, Janelle, for being born two weeks into my life at AFIT.

John W. Wong

# Preface

This thesis investigates the feasibility of sampling near earth asteroids from an orbiting spacecraft using a tethered lander/sampling device. A proposed SAIC point design for a tethered asteroid sampling mission is reviewed, and parameters of suitable asteroidal targets are developed based on the design. Numerical models of tether motion are built by modifying tether dynamics found in literature reviews. Results indicate that the tethered sampling approach is feasible for at least the first two of the three mission phases, (deployment, attachment, sample retrieval) with the final phase being inconclusive and requiring further investigation.

# Table of Contents

# List of Figures

# List of Tables

Table Page

# Abstract

This study investigated the feasibility of a SAIC proposal to sample Near Earth Objects (NEOs) from an orbiting spacecraft using a tethered landing device. The parameters for suitable targets were derived from an analysis of a proposed point design as applied to current knowledge of NEOs. Tether strength and lifetime for the point design were also assessed. First order modeling of tether dynamics showed that deployment and attachment to a NEO are feasible. The dynamics of retrieving a sample via a crawler unit which crawls up the tether requires further exploration.

# ANALYSIS OF TETHERS IN SAMPLING NEAR EARTH OBJECTS

## I. Introduction

This thesis investigates the feasibility of using a tethered sample collection device on an electrically propelled "prospector" spacecraft to acquire and return fairly large samples of asteroidal or cometary material to the vicinity of earth. The examples and assumed point design characteristics are based on a SAIC study conducted for the NASA Lewis Research Center in 1995 (31).

### 1.1 Background.

There is very little compositional and structural data on Near Earth Objects (NEOs). Most existing data has been inferred through the study of photometric or radiometric observations, or extrapolated from the occasional meteorite (13). The uncertainty of our data affects the formulation of strategies to deflect threatening objects (8), and also influences mission planning for a mining or science rendezvous. A series of sample return missions to NEOs would provide key structural information on NEOs and revolutionize basic scientific research into the geology and history of our solar system (10).

The interest in cometary and asteroid exploration is not new. In 1984, the Space Science Committee of the European Science Foundation and the Space Science Board of the US National Academy of Sciences formed a working group to determine a program of joint space exploration missions. The group made several recommendations, one of which was that electric propulsion be developed and applied to asteroid and comet rendezvous and sampling missions. Meanwhile, the European Space Agency created a list of four basic missions in their 1984 report "European Space Science - Horizon 2000"

that included a cornerstone mission to a primordial body [asteroids or comets] with the intent of returning a sample (12).

Several fly-by missions to NEOs have already been attempted (35). For example, the European spacecraft ISEE 3 was renamed ICE (International Cometary Explorer) for its 1985 fly-by of comet P/Giacobini-Zinner. Halley's comet was greeted in 1986 by Giotto and several other international spacecraft, and more recently, the Galileo spacecraft imaged the asteroids Gaspra and Toutatis while on course to Jupiter. A recent casualty, the Ballistic Missile Defense Organization (BMDO) spacecraft Clementine, was supposed to rendezvous with the asteroid Geographos, but it failed during its moon mapping phase in 1995 (7).

### 1.1.1 Why the SAIC study was commissioned.

All of these missions were designed around chemical propulsion for maneuvering, course correction, and momentum dumping. Chemical propellants have several limitations with regards to deep space missions, including corrosion, stability, freezing, explosive hazards, and mass of the propellant feed hardware (36:240-246). The low specific impulse ($I_{sp}$) afforded by common bipropellant fuels, such as nitrogen tetroxide and hydrazine ($I_{sp}$ = 283 seconds), requires a relatively large mass fraction of propellant ($m_p$) for a given $\Delta V$ as compared to high $I_{sp}$ systems (i.e. Hall effect thrusters or ion thrusters), which can have specific impulses in the thousands of seconds.

It is readily apparent that the use of electric propulsion can be used to reduce net spacecraft mass or improve $\Delta V$ capability, or a combination of both. The vast majority of spacecraft sizing studies involving electric propulsion have been confined to Earth-orbit raising (orbital transfer vehicles), or to stationkeeping and attitude control. The NASA Lewis Research Center, Advanced Concepts Group is extensively involved in the analysis, development, and testing of electric propulsion devices, and contemplated the use of solar electric propulsion (SEP) in an asteroid sampling mission to increase the size of the returned sample. Thus, they commissioned a SAIC study in 1995 (31) for preliminary mission sizing and estimated sample return sizes in a SEP asteroid sampling

mission. The SAIC report applies the current state-of-the-art in electric propulsion to an interplanetary mission and goes so far as to provide a target, launch date, high-level point designs of systems, and a rough cost estimate.

### 1.1.2 Current NEO sampling approaches.

The typical sampling procedures and methodologies proposed for NEO missions have been based on proven technologies. The European Space Agency (ESA) project Champollion, formerly known as Rosetta, will rendezvous, land, and collect soil samples with a scoop arm and core samples with a low power drill (12). This technology was demonstrated during the Viking missions, and Martin Marietta developed extensive feasibility and engineering studies in the late 1970's with the lander/rover concept(21). The pro to this approach is that relatively pristine subsurface samples can be obtained from desired locations. The con is that the mission suffers from a high mass penalty, complexity, and the risks from landing.

The NEARS project at Johns Hopkins is designed to come close to an asteroid surface and fire a pyrotechnic sampling device into the asteroid, then the sampling device is reeled back to the spacecraft by an attached line. The sampling device has a "six-shooter" design, so that after each firing a new "cartridge" rotates into position for subsequent sample collection. The advantages of this approach are in avoiding the risks of landing, and reduction of mass in the sample collection system and spacecraft structure. The disadvantages are the small sample sizes (<100 grams), and limited number of samples that can be collected. There may also be some hazard associated with hovering over a surface without human control in realtime.

In either case, the returned sample size is on the order of a few kilograms. Both concepts discard the spacecraft upon return to earth, and deliver the samples by deorbiting an aerobraked capsule. These and other NEO missions are described in greater detail in Appendix A.

### 1.1.3 SAIC proposed sampling approach.

The SAIC study (31) proposed a different mission and sampling strategy to work around the major constraints in the feasibility study. These constraints (goals) were to have low mission cost, maximize the sample return mass, and use solar electric propulsion. Consequently, the SAIC "Asteroid Prospector Mission" plan calls for sizing a spacecraft to use a Delta II 7925 booster to achieve a heliocentric orbit, and then xenon ion thrusters for primary propulsion into a transfer orbit to the target.

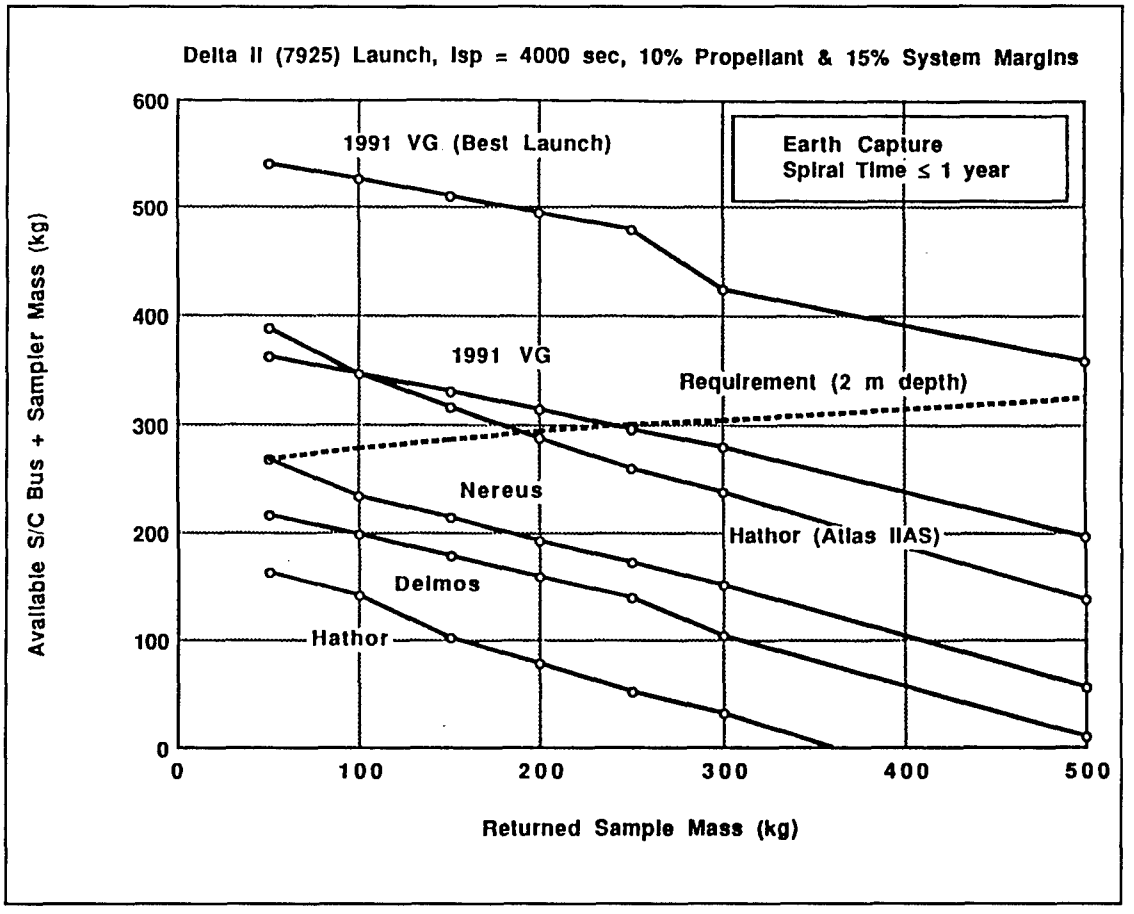


**Figure 1.1 SAIC Target Performance Map for the Asteroid Prospector Mission (31:4.14)**

The general results of the sample return assessment are shown in Figure 1.1. The study assumed a spacecraft of approximately 1000 kg total mass (different point designs were optimized for each mission), and xenon ion propulsion with specific impulses ($I_{sp}$)

between 3000-4500 seconds. The total required power was varied between 5 and 10 kilowatts (kWe) for propulsion and spacecraft functions. The Delta II could not meet the Hathor mission requirements, so the constraints were relaxed to allow launch on an Atlas IIAS.

The circular points represent the data points generated in the study. Note that several hundred kilograms of NEO material can be returned from selected asteroids to an earth orbit. (The "earth capture spiral time" reflects the need to bring the returning spacecraft and sample from a high altitude to Low Earth Orbit, where it can be retrieved.) The expected return was highly sensitive to the target choice and launch geometries of earth and the target, and ranged from about 50 kg in the Nereus mission to just over 500 kg in an "ideal" mission to asteroid 1991VG.

Since the design parameters require a lightweight spacecraft and sampling device, SAIC assessed three types of sampling devices, the penetrating projectile, the lander (with two options: robotic arm/scoop, or robotic excavation device), and a tethered sample collection device. Their analysis recommended that a simple screw conveyor device on a landing platform would be most appropriate to this mission due to mass constraints and risk management.

The SAIC recommendation is to lower the sample collector to the surface of the asteroid on a tether. The collection device bores in to a specified depth, and when its downward motion is restricted, transports material up into a Sample Canister Assembly (SCA), which then climbs the tether (using a Tether Climbing Motor) to the spacecraft in orbit. A notional depiction of the landing platform and SCA is illustrated in Chapter 2.

The return concept also differs from current missions. The proposed operation returns both the spacecraft and the sample to LEO for recovery by either docking with a space station or a rendezvous with a shuttle orbiter. This may allow the spacecraft to be refurbished on orbit and deployed on another mission if deemed cost effective.

### 1.1.4 Tethers--an elegant solution?

The discussion of tethers as a retrieval method in the literature is somewhat limited. The concept of tethering small rocket-propelled penetrators so they could be reeled back to a hovering spacecraft was originally suggested by Dr Paul Penzo of the Jet Propulsion Laboratory in NASA's *Tethers in Space Handbook* (24). This is also the approach taken by NEARS (34).

An extended-visit lander/core sampling device attached by tether to an orbiting object has not been identified prior to this study, but has several remarkable advantages if it is feasible. Tethers would allow a relatively fragile spacecraft to stand off from an asteroid and thereby reduce the risks associated with rendezvous and landing. Moreover, the solar arrays and other extendable equipment on the spacecraft would not have to be ejected or stowed, thus reducing spacecraft complexity and weight, and the use of a conducting tether would allow the spacecraft to use its solar arrays to power the sampling device. This alone is a significant difference--Champollion has a power budget of 100W for its core sampling drill, versus the potential for several kilowatts available in a tethered sampling system using a conducting tether.

There are other advantages to a tethered sampling system. A tethered sampling system offers the possibility of sampling from several locations with lowered risk and lowered fuel consumption. After samples have been retrieved, possibly by a "crawler" unit on the tether similar to the Tether Climbing Motor postulated above, the sampling device and tether can be discarded, thus reducing the mass of the return vehicle while increasing the returned sample size. It may even be desirable to use the tether to transfer momentum from the asteroid into the spacecraft on its return to earth, as a kind of slingshot.

## 1.2 Research Objectives

The objectives of this study are to investigate the feasibility of using space tethers for stand-off sampling of Near Earth Objects, determine the key parameters of such a

mission, develop a trade space for the parameters, and hypothesize a mission profile for tether-employed sampling of NEOs.

## 1.3 Scope of Research

This research presents the trade space for mission parameters of an asteroid sampling mission akin to the SAIC proposal. Constraints and bounds are developed for the various phases of operations (tether deployment, attachment to and sampling of the asteroid, and sample retrieval to the orbiting spacecraft) once the spacecraft has been placed into orbit around the asteroid. Other portions of the mission, such as the trajectory analysis to and from the target body, are beyond the scope of this work. This study is only meant to provide a first order analysis of employing tethers to retrieve asteroid samples, so some issues may be identified and deferred for future work.

The dynamics of tether motion for the deployment of a tether and its attachment to the surface of an asteroid is based on the text *Dynamics of Space Tether Systems*, by Vladimir Beletsky and Evgenii Levin (6). The dynamics of crawler motion are treated in a paper by Ronald Glickman and Samuel Rybak (14), of Ball Aerospace, and form the basis of modeling for crawler motion when the tether is attached to both an asteroid and orbiting spacecraft.

# II. Literature Review

The history of proposed tethered space objects is concisely summarized in the preface to *Dynamics of Space Tether Systems*, by Beletsky and Levin(6) and the NASA *Tethers in Space Handbook* (22). In short, the idea of connecting two (or more) objects in space has actually been around for over a century, having first been proposed by Tsiolkovsky in 1895 and subsequently reinvented many times since. The following sections will not discuss the historical aspects, but rather the many ideas which have been proposed which would use tethers, and a brief background on asteroid fundamentals.

## 2.1 Tether concepts.

References (6) and (22) have extensive surveys of proposed tether applications. These varied concepts are combined and summarized in Table 2.1, and can be combined to form an almost limitless number of applications. For further reading, reference (22) lists 43 detailed applications of these basic concepts.

**Table 2.1 Summary of proposed space tether concepts**

| Application | Concept |
|---|---|
| Artificial gravity | Orbital station and tethered counterweight spin about mass center. |
| Gravity gradient stabilization | Tether system rotates synchronously with orbital revolution |
| Microgravity: improve living conditions | Centrifugal forces from rotating tether system can eliminate free floating objects |
| Microgravity: fluid transfer | Centrifugal forces (microgravity) force liquids to drain from one tank to another; would allow propellants to be stored at a safe distance |
| Interferometry | Tether is a long baseline for multiple sensors |
| Passive reflector array | Many reflectors joined by a tether in geosynchronous orbit |
| Solar power station | Vertical tether with multiple power collectors; low end beams power to Earth |
| Rotating solar sails | Multiple tethers used to control thin-film solar sails |
| Stabilization | Multiple tethers connecting a spacecraft and counterweight |

**Table 2.1 (continued)**

| Application | Concept |
|---|---|
| Electrodynamic tethers: propulsion | Current applied to an electrodynamic tether interacts with the Earth's geomagnetic field and accelerates the spacecraft/tether system. Proper phasing can alter all orbital elements without using propellants |
| Electrodynamic tethers: power generation | The electrodynamic tether cuts Earth's magnetic field lines and generates current at the expense of orbital velocity |
| Electrodynamic tethers: power conversion | Convert chemical energy (thrusters modify orbital speed) to electricity (using electrodynamic tether) at high efficiency, perhaps as high as 90% |
| Electrodynamic tethers: power management | Use tether to provide peak power generation or to augment power while spacecraft is in eclipse. Altitude is recoverable on sunlit side of Earth. |
| Electrodynamic tethers: power accumulation | Use propulsion concept to gain orbital energy over a long period of time, then expend a large amount of power in a short time with power generation |
| Electrodynamic tethers: generate and receive radio | Conducting tethers could act as very long antennas |
| Upper atmosphere: science | An orbiting shuttle tows an aerodynamic probe through the upper atmosphere; a measuring system of the environment or high-speed wind tunnel |
| Upper atmosphere: photoreconnoisance | An orbiting shuttle tows an aerodynamic probe through the upper atmosphere; higher resolution photos, or stereo photography using shuttle and probe |
| Upper atmosphere: remote aerobraking | Spacecraft tows a balloon through the upper atmosphere until drag forces cause reentry. No propellant need be expended. |
| Gravity and magnetic field measurements | Long tethers allow high resolution measurements of the gravity field and magnetic field |
| Momentum transfer: fuel savings | Orbit boost using two spacecraft connected by tether. Example: Boost shuttle while deboosting external tank, then deboost shuttle while boosting payload. |
| Momentum transfer: docking | Shuttle docks with space station tether at shuttle apogee. Tether is retrieved to bring station and shuttle together, raising shuttle orbit and lowering station orbit. At end of mission, shuttle is lowered, thus restoring original orbits. |
| Momentum transfer: space escalator | Payload connects to a tether in orbit, docking at low end, climbs the tether, then gets a boost at high end. A series of tethers provides the escalator system. The tethers use electrodynamic propulsion to regain altitude |
| Momentum transfer: Lunar space elevator | Anchor a space station past the lunar collinear libration point L2 via tether to the surface. |
| Momentum transfer: substitute for gravity assist | Spacecraft can use asteroids or small bodies to change trajectory similar to gravity assist by using a tether equipped with a penetrator during a flyby. |
| Stationkeeping: Constellations | Constellations of satellites tethered together would not drift and collide. This could be used for space settlements or manufacturing platforms |
| Stationkeeping: Geosynchronous satellites | By using a tether and counterweight, one could station a geosynchronous satellite at half of geosynchronous altitude |
| Asteroid sample collection | Spacecraft shoots tethered rocket propelled sampling tube into body; reels back small sample in capsule. |

## 2.2 Tether experiments.

Tethers have already flown in space. The earliest use of a tether to connect two orbiting objects (excluding astronauts on space walks) is from 1966, during the Gemini 11 and 12 flights, when the vehicle was connected by a 30 meter tether to an Agena upper stage to analyze the steady state and librational dynamics of a tether pair (16). Some

recent applications of tethers have been the joint Italian-U.S. Tethered Subsatellite System (TSS-1) experiment flown on the Space Shuttle in February 1996, the Small Expendable Deployment System (SEDS), and the National Reconnaissance Office's TiPS program.

### 2.2.1 TSS-1.

The TSS-1 experiment was designed to verify the dynamics of tethered subsatellites and obtain data on the use of electrodynamic tethers in power generation. The system consisted of a deployer with an extendible 12 meter boom, the 500 kg subsatellite with instrumentation, and a 20 km, five-layer conducting tether that is 0.113 inches (2.8 mm) in diameter (22).

In the nominal mission, the TSS is deployed upwards, away from the earth over a period of 6.7 hours, remains on station for measurements for 10 hours, then is retrieved in 10.2 hours, with a stop at 2.4 km distance for measurements and to get the "man in the loop" for the final retrieval. In the actual mission, the tether failed at 13 km during an otherwise normal deployment. NASA later determined that the tether generated far more current than expected (nominally 5 kV at 20 km length was anticipated) and that arcing through faulty insulation had severed the tether.

### 2.2.2 SEDS.

According to Reference 22, the Small Expendable Deployer System is a lightweight spinning-reel system designed to deploy a payload attached to a 20 km long tether whose primary objectives are "...to study the dynamics of tether deployment and to validate the SEDS design concept." The system consists of a 16 kg deployer (of which 6 kg is a tether made of Spectra, an Aramid fiber similar to Kevlar) and a 23 kg end mass. The tether is given a slight pre-twist during winding to compensate for the twist as the tether deploys (due to tension in the angled fibers, not an intrinsic torsional stiffness of the tether). Once the payload is ejected, two redundant optical turn-count beams sense the tether deployment length and rate (28).

The SEDS end mass is deployed towards the earth on the tether. When it has reached a vertical position (in about 1 ½ hours), the tether is cut, allowing the end mass to reenter. For further reading on SEDS, an excellent resource is listed in Reference 28.

Beletsky(6) cites the deorbiting of Space Station waste as one future application of this concept, which with a 100 km tether could deorbit up to 2,000 kg of material. This amounts to an application of momentum scavenging, since lowering this mass would raise the Space Station incrementally as well.

### 2.2.3 TiPS.

The Tether Physics and Survivability (TiPS) experiment is a National Reconnaissance Office (NRO) project designed to address two basic conditions for operational tethers—survivability and controllability. According to the director of NRO's small satellite office, Colonel Pedro Rustan(2:24), "...The purpose of this kind of tether is to put something out there and leave it for years. It's a very thin type, and we want to know if it's going to last for weeks, months or years."

The spacecraft consisted of two small endmasses connected by a very thin 2.15 nautical mile tether. The $4 million program was launched piggyback to a classified payload and deployed on June 20, 1996 into a circular orbit at an altitude of 552 nautical miles and inclination of 63.4 degrees. Deployment to the full 2.15 nautical mile length occurred in 42 minutes.

The TiPS tether was constructed of a resilient yarn core surrounded by a Spectra braid, ultimately resulting in a 4.0 kilometer, 2.2 mm diameter non-conducting tether (28). The total tether mass was 5.5 kilograms, and the estimated mean time between failure (MTBF) for this design was estimated at 890 days.

## 2.3 Application to sample collection.

Several missions to Near Earth Objects have been planned and are under construction (Appendix A), but each uses a significantly different sampling methodology. In NASA's *Tethers in Space Handbook, Second Edition*, Dr. Paul Penzo proposes using

small tethered penetrators to collect samples from several places on a body, or even from several bodies. A rotating turret containing several rocket-propelled penetrators shoots a sampling capsule into the surface from a distance of 50-100 meters, and a small explosive charge in the penetrator then seals the capsule and ejects it from the surface for retrieval. This approach was adopted by the NEARS team (32), and is described in both the introduction and in Appendix A.

Dr. Penzo discusses the sequence of events in either a lander or a penetrator sample return scheme as follows:

**Table 2.2 Sample methodology comparison**

| | Conventional approach (lander) | Hovering spacecraft (penetrator capsules) |
|---|---|---|
| 1 | Close range verification (site survey) | spacecraft rendezvous |
| 2 | automated soft landing | tethered penetrator shot into target from 50-100 m |
| 3 | lander attachment to the body | on impact, sample material enters holes in penetrator and fills a sample cup |
| 4 | drill unit cores a sample | explosive seals sample cup, ejects cup for retrieval |
| 5 | lander separation from the body | cup velocity creates tension in tether as it rotates it |
| 6 | automated rendezvous with orbiter | spacecraft thrusters control cup retrieval dynamics |
| 7 | sample transfer to orbiter | other tethered penetrators sample the body/bodies |
| 8 | launch stage ejection | earth return |
| 9 | earth return | |

The relative merits of a single deep core sample and multiple surface samples are dependent upon the goals of the mission. If most asteroids are products of collisions over the eons, several surface samples from the fractured side of an asteroid could provide much of the same information as a core sample. However, a deep core sample provides a more pristine, less "weathered" specimen, as well as more information as to the physical structure of the parent asteroid. Since the morphology of a NEO is an important consideration in developing a defense against asteroids, both the SAIC study and this thesis are oriented towards large core samples.

## 2.4 Basic Principles.

The following sections condense some excellent explanations in the literature. For a more detailed explanation or derivation, see references 4, 22, and 11. For

convenience, the following sections parallel the literature, which does not follow a standardized convention for orienting either the inertial or body-fixed reference frames.

### 2.4.1 The origin of gravity gradient forces in tethers.

Figure 2.1 illustrates a tethered system in circular orbit about M in the plane of the paper. M rotates about the y-axis, which points up from the plane of the page to form a right-handed orthogonal triad. "Centrifugal" accelerations do not really exist, but we will use the term to denote the negative of the acceleration needed to keep an object in curvilinear motion. This is to identify a difference between the actual acceleration needed to remain in a particular orbit, versus the existing gravitational acceleration for the tethered end bodies. The magnitude of the "centrifugal" accelerations and forces can be derived by differentiation of the position vector of an object, and they are caused by the use of a rotating reference frame.

Normally, the "centrifugal" acceleration of an orbiting spacecraft is equal and opposite to the gravitational attraction. However, for a tethered pair of objects this is only true near (not at) the center of mass of the system, but not at either end. This condition arises because the mass center of the two tethered objects is constrained to travel at constant angular velocity $\Omega$, as are the two endmasses, $m_1$ and $m_2$, by virtue of the physical connection of the tether. The situation is depicted in Figure 2.1.

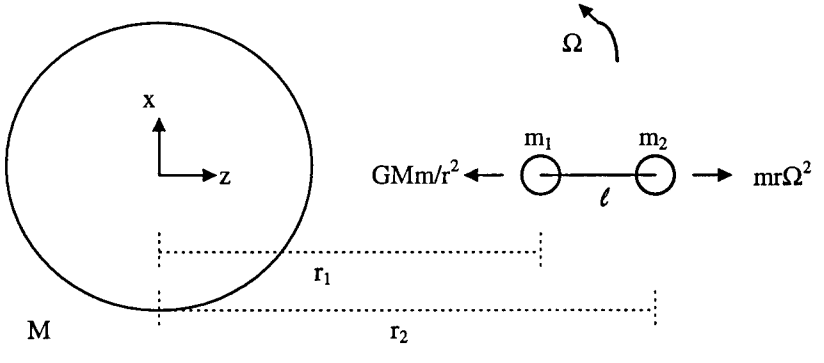


**Figure 2.1 Gravity gradient forces**

The equations for the gravitational and required radial ("centrifugal") forces are shown in Equations 2.1 and 2.2, where G is the universal gravitational constant, $r_0$ is a generic distance between the centers of mass of two bodies, M and m represent the masses of the primary and orbiting bodies, respectively, and $\Omega$ is the orbital angular velocity of the orbiting mass:

$$F_{gravity} = -\frac{GMm}{r_0^2} \tag{2.1}$$

$$F_{centrifugal} = mr_0\Omega^2 \tag{2.2}$$

Gravity gradient forces arise from two connected objects in orbit because the lower body experiences a greater gravitational force than the upper body, and the upper body experiences a greater "centrifugal" force, thus causing a tension force (not shown) in the tether. Somewhere along the tether, the gravitational and centrifugal forces will balance, which is called the "zero-g" point. If we define $R_0$ = distance from center of large body to zero-g point, and m = total mass of the tethered system:

$$F_z = -\frac{GMm}{R_0^2} + mR_0\Omega^2 = 0 \tag{2.3}$$

which rearranges to:

$$R_0 = \left(\frac{GM}{\Omega^2}\right)^{\frac{1}{3}} \tag{2.4}$$

Gravity is nonlinear with distance, so the mass center of the tether system will not coincide with the zero-g point. How do these forces change with radial distance from the zero-g point? Consider a point on the tether along the z-axis (radial direction) at a distance $z$ from the zero-g point. By summing the partials of the gravitational and centrifugal forces with respect to the R, the distance from our chosen point to the center

of mass (CM) of the primary body M, and neglecting the tether mass, we can make the approximation:

$$F_z \cong z\left(\frac{\partial F_{gravity}}{\partial R} + \frac{\partial F_{centrifugal}}{\partial R}\right) \tag{2.5}$$

Using the gravity terms and centrifugal terms from Equation 2.1, this becomes:

$$\begin{aligned} F_z &\cong z\left(2\frac{GMm}{R^3} + m\Omega^2\right) \\ &\cong z\left(2m\Omega^2 + m\Omega^2\right) \end{aligned} \tag{2.6}$$

Note that in the radial direction, this shows that the net force experienced on a mass not located at the zero-g point is actually two parts gravity gradient, one part centrifugal. Refer back to our rotating coordinate system in Figure 2.1: note that for $z>0$ (masses above the zero-g point), the gravity gradient force is directed upwards, and conversely, for $z<0$ (closer to earth than the zero-g point) the gravity gradient force is directed downwards. Arnold (4) provides detailed derivations of the gravity gradient forces along all three axes, which are summarized in the equations below.

$$\begin{aligned} F_x &= 0 \\ F_y &= -m\Omega^2 y \\ F_z &= 3m\Omega^2 z \end{aligned} \tag{2.7}$$

### 2.4.2 Libration.

Gravity gradient stabilized systems are subject to perturbatory forces which cause oscillation about the point of stability, or *libration*. The major factors include the oblateness of the earth, solar pressure, atmospheric drag, and in the case of an electrodynamic tether, the electromotive force from a conductor cutting through the

earth's magnetic lines of force. The following section summarizes the derivation of the equations of motion (4). Suppose a tethered system deviates from the vertical by some small amount, as shown below, with an in-plane (x-z) angle of θ and an out of plane (y-z) angle ϕ:

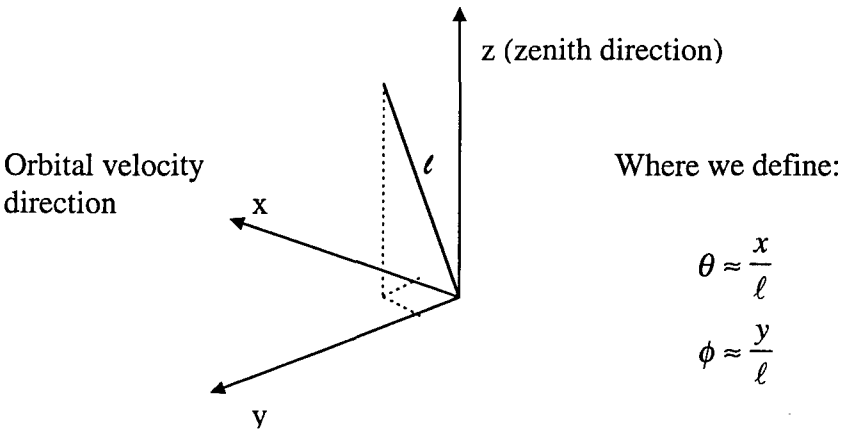


**Figure 2.2 Reference frame for libration analysis**

From Equation 2.5, we can see that the $F_z$ and $F_y$ gravity gradient forces will cause a torque on the system. The torques are found by multiplying the appropriate forces along the moment arms and summing:

$$\begin{aligned} \tau_\theta &= -F_z x \\ &= -3m\Omega^2\ell^2\theta \end{aligned} \tag{2.8}$$

$$\begin{aligned} \tau_\phi &= -F_z y - \ell F_y \\ &= -3m\Omega^2\ell^2\phi - \Omega^2\ell y \\ &= -4m\Omega^2\ell^2\phi \end{aligned} \tag{2.9}$$

According to Arnold (4), the equations of motion in a rotating spherical coordinate system are:

$$\vec{F} = m\hat{r}\left[\ddot{r} - r\dot{\phi}^2 - r\cos^2\phi\left(\dot{\theta}+\Omega\right)^2 + r\Omega^2 - 3r\Omega^2\cos^2\theta\cos^2\phi\right]$$
$$+ m\hat{\theta}\left[\ddot{\theta}\, r\cos\phi + 2\left(\dot{\theta}+\Omega\right)\left(\dot{r}\cos\phi - r\dot{\phi}\sin\phi\right) + 3r\Omega^2\cos\theta\cos\phi\sin\theta\right] \qquad (2.10)$$
$$+ m\hat{\phi}\left[r\ddot{\phi} + 2\dot{r}\dot{\phi} + r\cos\phi\sin\phi\,\left(\dot{\phi}+\Omega\right)^2 + 3r\Omega^2\cos^2\theta\cos\phi\sin\phi\right]$$

He then reduces them (for small angles and fixed tether length) to:

$$\ddot{\theta} = -3\Omega^2\theta \qquad (2.11)$$

$$\ddot{\phi} = -4\Omega^2\phi \qquad (2.12)$$

Equations 2.10 and 2.11 show that the frequencies of the in-plane ($\theta$) and out-of-plane ($\phi$) librations are $\sqrt{3}\,\Omega$ and $2\Omega$, respectively. Note also that this is for a dumbbell satellite of two point masses connected by a rigid rod. Chobotov (11) presents a similar derivation of the linearized and uncoupled pitch, roll, and yaw equations of motion, starting from the familiar angular momentum equation and gravity gradient torque vector $T^{(g)}$.

$$\dot{\vec{h}} + \vec{\omega}_s \times \vec{h} = \vec{T}^{(g)} \qquad (2.13)$$

which for a circular orbit, small angular deviations, and application of a 3-1-3 sequential rotation matrix through the Euler angles $\psi$, $\theta$, and $\phi$ to transform from a rotating orbital frame to a body fixed frame, yields

$$\begin{pmatrix} T_1 \\ T_2 \\ T_3 \end{pmatrix} = 3\omega_0^2 \begin{pmatrix} (I_3 - I_2)a_{21}a_{31} \\ (I_1 - I_3)a_{11}a_{31} \\ (I_2 - I_1)a_{11}a_{21} \end{pmatrix} \qquad (2.14)$$

where $[a_{ij}]$ is defined as (11:6):

$$a = \begin{bmatrix} \cos\varphi\cos\psi - \sin\varphi\cos\theta\sin\psi & \cos\varphi\sin\psi + \sin\varphi\cos\theta\cos\psi & \sin\varphi\cos\theta \\ -\sin\varphi\cos\psi - \cos\varphi\cos\theta\sin\psi & -\sin\varphi\cos\psi + \cos\varphi\cos\theta\cos\psi & \cos\varphi\sin\theta \\ \sin\theta\sin\psi & -\sin\theta\cos\psi & \cos\theta \end{bmatrix}$$

Note that for a dumbbell type gravity gradient stabilized satellite, the moments of inertia along the out of plane and velocity vector axes will be identical, and the moment of inertia along the vertical axis will be zero. Thus, in a dumbbell representation of a tethered satellite system, gravity gradient torques do not affect the yaw of the system.

## 2.5 SAIC Point Design Summary.

The SAIC point design for a sampling mission is conceptual, and therefore only the rough sizing of the spacecraft and sampling device is given. The following sections summarize the mission plan and sampling platform parameters.

### 2.5.1 Mission plan.

The SAIC Asteroid Prospector study (29:3.1) showed that the sample return sizes were extremely case dependent upon both the selected target and launch phasing. The SAIC case requiring the lowest transfer energy and the largest sample return is to the asteroid 1991VG. For this reference mission, the best phasing occurs every 25 years, and the next opportunity is in 2016, though the study states several other excellent dates are available, one as soon as 2004.

Launch takes place on a Delta II 7925—to minimize launch costs, the spacecraft was sized to this booster—into a heliocentric transfer orbit to 1991VG around February 8, 2016. Rendezvous occurs on July 8, 2016, after 150 days of flight, and at that time the spacecraft begins a 90 day survey and sampling period around the asteroid. The return flight begins on October 2, 2002, and arrives in the vicinity of earth Aug 2, 2017 (launch + 540 days). The SAIC proposal adds one additional year from the date of earth capture to spiral down to LEO; however there is no actual timeline or sequence of operations

established here. The point design for the sampler assumes a sample core retrieval time of 21 days, which occurs during the 90 day visit period at the asteroid.

### 2.5.2 Sampling platform description.

The SAIC concept for the tethered retrieval system design reviewed several possibilities for sample collection, such as the penetrator concept outlined by Dr Penzo and described in section 2.3, and a lander concept, involving either a robotic scoop arm or some other type of excavation device. The SAIC study team concluded, after an extensive mass trade analysis, that the best approach to collection of large samples is with a lander and screw conveyor collector. Henceforth, the combined lander and sample collection hardware will be referred to as the "lander" or "sampling device".

The lander consists of a trussed, shock-absorbing structure whose legs are driven into the asteroid by the impact of landing, as in Figure 2.3. Rocket propelled anchors (not illustrated) are also shot into the surface for additional support. Once the attachment of the lander to the asteroid is complete, a screw device bores into the asteroid to a specified depth. The screw then ceases boring, but continues to turn and transports sample material into a Sample Canister Assembly (SCA). The SCA separates from the lander and uses a small motor to climb the tether back to the spacecraft. The tether is sized as 2 mm aluminum core with a 0.5 mm Kevlar and insulation wrap (8.2 kg for the 500 m design) and is designed to transmit 200-300 W of power.

The sizing of this design has limited the screw rotation rate to 0.0003 RPMs, which results in a long collection time (21 days) for the proposed 2 meter deep sample. This approach was also taken by the Champollion ("Rosetta") design team, for three reasons: limited power, unknown properties of the sample material, and reduction of the torque placed on the sampling device and its anchors. The mass of the hardware associated with the sample collection is shown in Table 2.3.

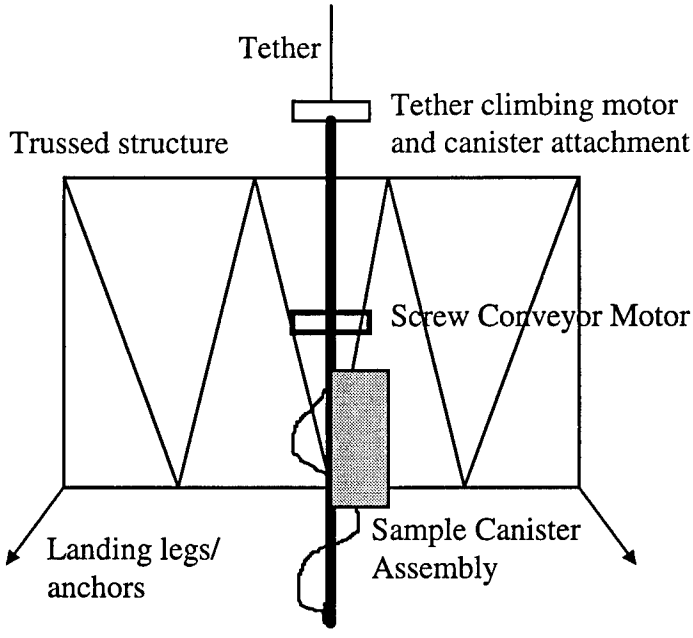


**Figure 2.3 Notional design of tethered sampling system lander**

**Table 2.3 SAIC point design mass summary**

| | |
|---|---|
| **Lander** | |
| Structure and subsystems | 104.9 kg |
| Sample Canister Assembly | 13.2 kg |
| Tether (500 m) | 8.2 kg |
| **Spacecraft** | |
| Docking mechanism | 5.0 kg |
| Communications | 0.8 kg |
| Deployment device | 0.5 kg |
| **Total mass of sampling systems** | **132.6 kg** |

We will also have to estimate the mass of the spacecraft in orbit around the target body. Since the SAIC calculations indicate a total launch mass of 1097 kg for the reference mission in 2016, subtracting the launch vehicle adapter (52 kg), lander system mass (126 kg), and half of the propellant mass (the total propellant mass is 440 kg), this leaves the orbiting spacecraft mass as approximately 700 kg. We will use the following

mass figures in the simulation and analysis of deployment, collection, and retrieval of the asteroid sample: spacecraft, 700 kg; lander/sampler, 120 kg; sample mass, 300 kg.

As a cautionary note, the actual mass and design of an asteroid sampler must be sized to the particular mission profile, which includes choosing an appropriate target and launch phasings, determining the launch mass margins for that set of conditions, and designing the sampling spacecraft within those limits.

# III. Methodology

In this chapter, we establish the relationships between asteroid physical parameters that constrain the SAIC point design, such as size, density, and rotation rate. We then examine the parameters for the tether design and address tether strength and lifetime issues. Finally, we consider the three phases of sample taking, which include deploying the sampler, extended on-orbit sampling, and retrieval of the desired sample.

## 3.1 Space environment.

Current studies (26) estimate the total population of asteroids greater than 1 kilometer in diameter at approximately 1500. Since this figure includes main belt asteroids, such as Ceres and Vesta, the number of large Near Earth Objects (NEOs) is actually much less. Therefore, this thesis targets asteroids between 100 meters and 1 kilometer in diameter to offer a trade study for a larger, and perhaps more accessible, population of NEOs.

Of the almost 6000 asteroids that have been discovered, the 500 or so asteroidal Near Earth Objects are classified in one of three categories, Atens, Apollos and Amors. Table 3.1 lists some commonly accepted definitions (3) and the current populations (20) of NEOs , where "a" represents the semimajor axis of the orbit:

**Table 3.1 Major categories of NEOs**

| Class | Definition | Population |
|---|---|---|
| Aten | a<1.0 AU, aphelion>0.983 AU | 22 |
| Apollo | a<1.0 AU, perihelion<1.017 AU | 183 |
| Amor | a>1.0 AU, perihelion<1.017 AU | 185 |

Asteroids are also classified by composition (derived from studies of meteorites and photometric and spectral analysis). Asteroids tend to fall into three major classifications--chondrites (C), stony (S), or metallic (M)--which respectively represent bodies consisting mainly of carbon/silicate compounds, silicates/metals, and nearly pure

nickel-iron. There are also a few other categories for rare types. The percentages of these objects in the asteroid population (3) are approximately 75% C-type (albedo ~0.03), 17% S-type (albedo 0.10-0.22), and most of the remainder being M-type (albedo 0.10-0.18).

The asteroid selected by SAIC for their point design, 1991VG, is currently believed to have the following physical parameters (22):

**Table 3.2 SAIC Target Body: 1991VG**

| Type | Class | H =Visual Magnitude | Diameter (m) | Rotation Rate | perihelion (AU) | aphelion (AU) |
|---|---|---|---|---|---|---|
| C | Apollo | 28.8 | 10.8 | unknown | 0.976 | 1.077 |

The diameter of 1991VG was not given. However, it was readily interpolated from a visual magnitude conversion table provided in Reference 20.

### 3.2 Physical mission constraints.

Any employment of a tethered landing and sampling vehicle must take into account both the gravity gradient forces and rotational behavior of the target body. The SAIC study proposes the lowering of a tethered sampling platform, which suggests that 1) the asteroid must have a gravity field of sufficient strength, whatever that strength is, to employ a tether and gravity gradient forces, and 2) that the spacecraft-tether-sampler system, when attached to an asteroid, must be oriented with the rotation of the body in such a way to prevent being wound into the asteroid like a yo-yo due to the long visit time--21 days (29).

#### 3.2.1 Gravity constraints.

Reference 22 states that the gravitational acceleration in orbit around a central body of mass M varies as $GM/r^3$ , and thus the gravity gradient acceleration is linearly dependent on the density of the central body, not its size. This can be shown by using Equation 2.1 and the relationship F = ma to form

$$a = \frac{GM}{r^2} \tag{3.1}$$

where G is the universal gravitational constant, M is the mass of the asteroid, and r is the distance from the center of mass of the asteroid. Since the gravity gradient is a radial acceleration dependent only upon distance from the center of mass, it is equivalent to the derivative of Equation 3.1 with respect to r. Hence

$$\frac{da}{dr} = -\frac{2GM}{r^3} \tag{3.2}$$

Equation 3.2 gives a gravity gradient acceleration on the order of 0.3 milligee per kilometer in LEO ($2.68 \times 10^{-6}$ m/s$^2$ per meter, at an altitude of 300 km). Table 3.3 shows a comparison of the gravitational accelerations and gradients for some representative bodies. The computed acceleration gradient, in m/s$^2$ per meter altitude, for a low orbit around small asteroids is shown in Figure 3.1.

**Table 3.3 Gravity and gravity gradient comparisons**

| | Radius (m) | Density (g/cm$^3$) | Mu (m$^3$/s$^2$) | Altitude (m) | Gravity (m/s$^2$) | Gradient (m/s$^2$ per m) |
|---|---|---|---|---|---|---|
| Earth, surface | 6378145 | 5.5 | 3.9887E+14 | 0 | 9.804831 | 3.07E-06 |
| Earth, LEO | 6378145 | 5.5 | 3.9887E+14 | 300000 | 8.9437 | 2.68E-06 |
| Earth, HEO | 6378145 | 5.5 | 3.9887E+14 | 10000000 | 1.486961 | 1.82E-07 |
| Earth, GEO | 6378145 | 5.5 | 3.9887E+14 | 40000000 | 0.185439 | 8E-09 |
| Sun, surface | 6.4E+08 | 1.8113 | 1.3271E+20 | 0 | 324.0063 | 1.01E-06 |
| Sun, 1 AU | 6.4E+08 | 1.8113 | 1.3271E+20 | 1.5E+11 | 0.005887 | 7.84E-14 |
| Asteroid, surface | 50 | 3 | 0.1048128 | 0 | 4.19E-05 | 1.68E-06 |
| Asteroid, in orbit | 50 | 3 | 0.1048128 | 100 | 4.66E-06 | 6.21E-08 |
| Asteroid, surface | 500 | 3 | 104.812799 | 0 | 0.000419 | 1.68E-06 |
| Asteroid, in orbit | 500 | 3 | 104.812799 | 500 | 0.000105 | 2.1E-07 |

We can see that there is a considerable difference in the magnitude of gravitational accelerations involved. Note that the solar gravitational acceleration at 1 AU is an order of magnitude larger than that of the asteroid size range, but the solar gravity gradient is negligible. This indicates that the sun cannot be neglected as a perturbatory source. This data also shows an asteroidal gravity gradient an order of magnitude smaller than that found in LEO; however, we can adjust our operating parameters by either selecting a larger asteroid, a lower orbit, or using both techniques to increase the gravity gradient.

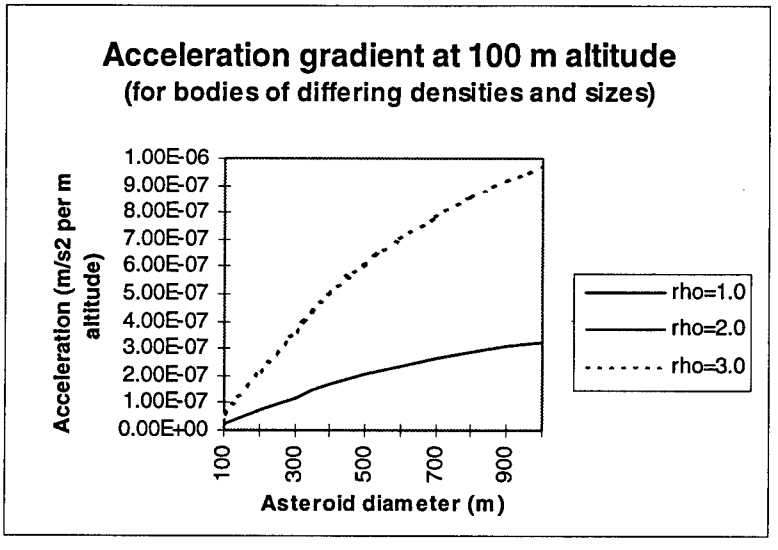


**Figure 3.1 Acceleration gradient for small asteroids**

We will assume that the gradients shown in Figure 3.1 are what we will be working with. Are these gravity gradients sufficient to capture and orient a tethered satellite? According to Chobotov (11), gravity gradient capture occurs when the total kinetic and potential energy of the system the less than some "threshold" capture energy $E_t$, which is where the satellite starts tumbling. This corresponds to a satellite which oscillates between $\pm 90^{\circ}$ on any axis. Chobotov derives a series of equations starting with the spacecraft angular momentum in circular orbit:

$$\dot{\vec{h}} + \vec{\omega}_{sc} \times \vec{h} = \vec{T}^{(g)} \tag{3.3}$$

where

$$\vec{h} = \omega_1 I_1 \hat{e}_1 + \omega_2 I_2 \hat{e}_2 + \omega_3 I_3 \hat{e}_3$$
$$\vec{T}^{(g)} = T_1^{(g)} \hat{e}_1 + T_2^{(g)} \hat{e}_2 + T_3^{(g)} \hat{e}_3$$

and a orbiting (rotating) frame whose components lie along the radial direction, orbital angular momentum vector, and opposite the velocity vector as shown in Figure 3.2:

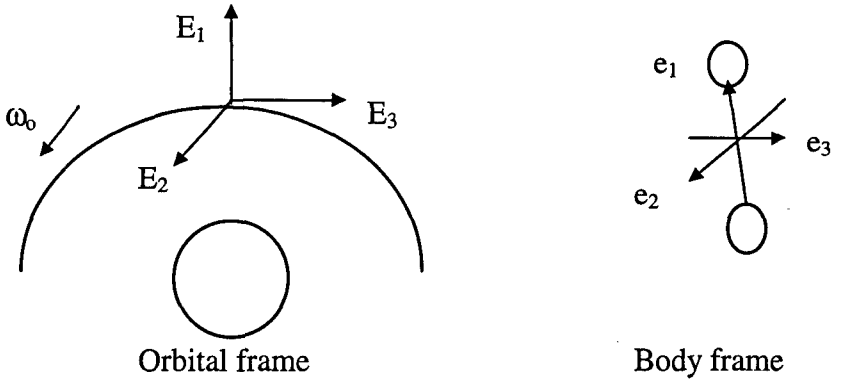


**Figure 3.2 Orbiting and body frames for Chobotov's equations**

The angular deviations $\theta_1$, $\theta_2$, and $\theta_3$ are sequential rotations between the orbital (rotating) and body reference frames about the respectively numbered axes. After using the appropriate rotation matrix, linearizing for small angular deviations, and simplifying, the restoring torques become:

$$\begin{aligned} T_1 &= -\omega_0 (I_2 - I_3)\, \theta_1 \\ T_2 &= -3\omega_0 (I_3 - I_1) \theta_2 \\ T_3 &= -4\omega_0 (I_2 - I_1) \theta_3 \end{aligned} \tag{3.4}$$

where the *negative* of the coefficients for each $\theta$ is called the *gravity gradient constant* $K^{(g)}$ (e.g. $K_1^{(g)} = \omega_0 (I_2 - I_3)$). The threshold capture energy ($E_t$) for any individual axis

is found by adding the potential energy ($E_p$) and kinetic energy ($E_k$) corresponding to the "almost tumbling" condition along that axis:

$$E_t = E_p + E_k$$

$$\int_0^{\frac{\pi}{2}} (gravity\_torque)d\theta = \int_0^{\theta} (gravity\_torque)d\theta + \frac{1}{2} I\dot{\theta}^2 \tag{3.5}$$

$$\int_0^{\frac{\pi}{2}} (\frac{K^{(g)}}{2}\sin 2\theta)d\theta = \int_0^{\theta} (\frac{K^{(g)}}{2}\sin 2\theta)d\theta + \frac{1}{2} I\dot{\theta}^2$$

Chobotov arrives at the critical angular capture rate for that axis

$$\dot{\theta} = \sqrt{\frac{K^{(g)}}{2}}\cos\theta \tag{3.6}$$

Substitution of the respective gravity gradient constants back into this equation gives:

$$\begin{aligned} \dot{\theta}_1 &= \omega_0 \sqrt{\frac{I_2 - I_3}{I_1}}\cos\theta_1 \\ \dot{\theta}_2 &= \sqrt{3}\omega_0 \sqrt{\frac{I_3 - I_1}{I_2}}\cos\theta_2 \\ \dot{\theta}_3 &= 2\omega_0 \sqrt{\frac{I_2 - I_1}{I_3}}\cos\theta_3 \end{aligned} \tag{3.7}$$

Thus, the capture of a satellite into a gravity gradient stabilized configuration is dependent on the orientation of the satellite and its moments of inertia. Under our assumptions of point masses and a massless tether, the moment of inertia in the radial direction ($\theta_1$) is effectively zero. Thus, capture may not occur along the yaw axis.

Referring to Equation 3.7, note that gravity gradient capture appears to be independent of the magnitude of the gravity gradient acceleration. The associated capture

rates for the $\theta_2$ (roll, or out-of-plane axis for tethers) and $\theta_3$ (pitch, or in-plane rotation axis for tethers) are plotted in Figure 3.3 and Figure 3.4.

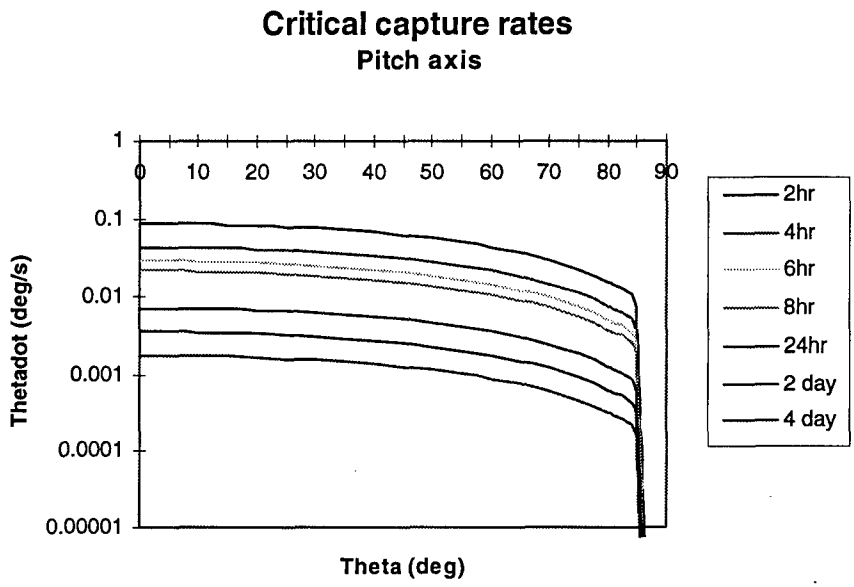


**Figure 3.3 Critical capture rates - pitch axis**

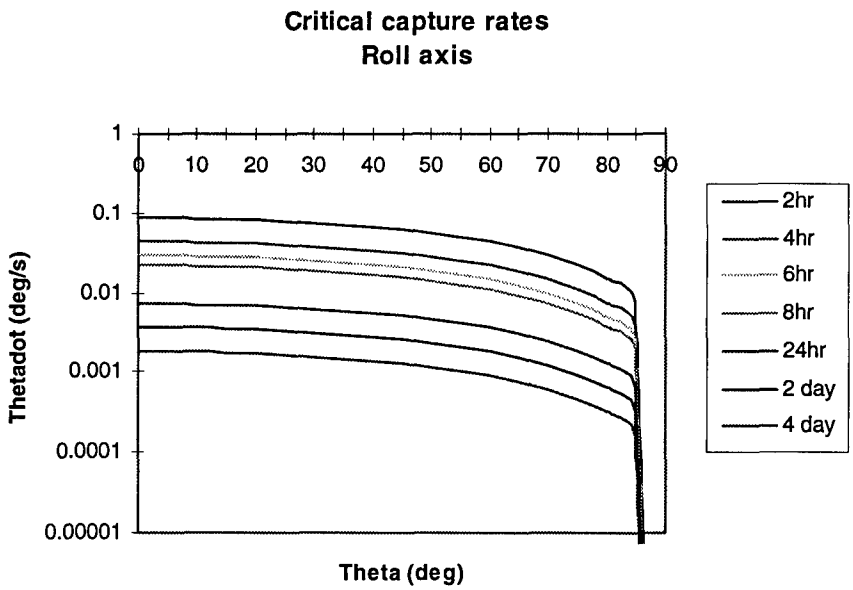


**Figure 3.4 Critical capture rates - roll axis**

The steep drop in the curves of Figure 3.3 and Figure 3.4 is due to the use of a semilogarithic plot of the cosine functions as they approach $\theta=90^0$.

### 3.2.2 Rotation constraints.

According to Dr. Paul Penzo (24), most asteroids have a rotational period between two hours and four days. The following table shows some of the extremes to be encountered in the asteroid population at large (20):

**Table 3.4 Asteroid extremes**

| Name | Size (km) | Shape | Rotation rate | Comment |
|---|---|---|---|---|
| 1995HM | 0.1x 1.0 | Spindle | 97 minutes | Fastest rotation known |
| Ceres | 914 | Spherical | unknown | Largest asteroid |
| Toutatis | two bodies: 4 and 2.5 km | Contact binary objects | two motions of 5.4 , 7.3 days | Unique rotation with no periodicity |

Two more questions, which are particularly important in asteroid defense considerations, are what is the composition of the body, and what is the morphology (physical structure)? Proposed structures vary from solid , dense objects to loose aggregations ("rock piles"), and include concepts of inhomogeneous materials "glued" together by carbon compounds or ice (9). Our interest lies primarily in sampling carbonaceous chondrites—which are thought to contain ice, carbon compounds, silicates, and metals—so for simplification, this study will assume spherical bodies with a homogeneous density between 1.0 and 3.0 $g/cm^3$.

### 3.2.3 Geometry limitations.

A tethered sample system is essentially a cable connecting the surface of a body to the center of mass of the sample system at synchronous orbit. For the initial study, let us only consider the synchronous orbit to be perpendicular to the asteroid axis of rotation, analogous to flying in geosynchronous orbit over the equator. Since this involves a trade of the gravitational sphere of influence (SOI) of the asteroid and the rotation rate, we can

determine an appropriate range of sizes versus rotational speeds that can be sampled. Applying Equation 3.8 for sphere of influence calculations (5) and the conditions that the spacecraft be in a circular synchronous orbit above the surface and within the sphere of influence (i.e. $r_{asteroid} < R < R_{SOI}$ ),

$$\frac{R_{SOI}}{R_{sun}} = \left( \frac{m_{asteroid}}{m_{sun}} \right)^{\frac{2}{5}} \tag{3.8}$$

$$v_{circular} = \sqrt{\frac{\mu}{R}} = R\omega \tag{3.9}$$

we can derive the following for the fastest rotational speed (R=r):

$$\begin{aligned} \omega_{R=r} &= \sqrt{\frac{\mu}{R^3}} \\ &= \sqrt{\frac{G(\frac{4}{3}\pi r^3 \rho)}{r^3}} \\ &= \sqrt{\frac{4}{3} G\pi\rho} \end{aligned} \tag{3.10}$$

and the slowest rotational speed (for this assume $R_{sun}$= 1.0 AU, or 1.496 x $10^{11}$ m):

$$\begin{aligned} \omega_{R=Rsoi} &= \sqrt{\frac{\mu}{R^3}} \\ &= \sqrt{\frac{Gm_{asteroid}}{\left[ R_{sun} \left( \frac{m_{asteroid}}{m_{sun}} \right)^{\frac{2}{5}} \right]^3}} \\ &= k m_{asteroid}^{-0.1} \end{aligned} \tag{3.11}$$

where $k=2.13 \times 10^{-4}\ kg^{0.1}\ sec^{-1}$.

The plot of these bounds for a series of asteroidal masses of $\rho=3.0\ g/cm^3$ is in Figure 3.5 below. The maximum values of $\omega$ are 5.29, 7.48, and $9.16 \times 10^{-4}$ rad/s ($\rho$=1.0, 2.0 and 3.0 $g/cm^3$, respectively) for the asteroids. This equates to minimum rotational periods of 3.3, 2.3, and 1.9 hours for the tethered spacecraft sampling approach to be feasible. The upper limit for rotational period (at the sphere of influence edge) for these asteroids are 121.7, 130.5, and 135.9 hours respectively.

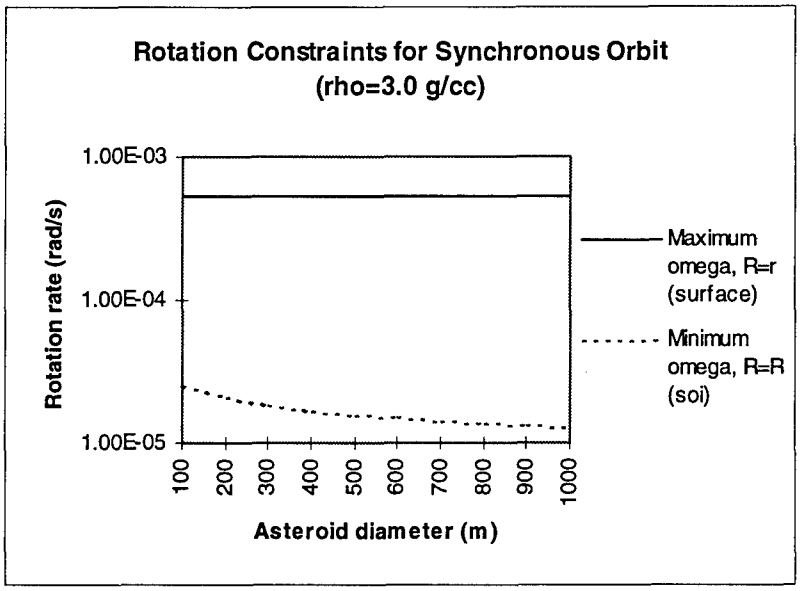


**Figure 3.5 Rotation constraints for synchronous orbit**

### 3.3 Tether considerations.

Now that we have established bounds on the physical parameters of target bodies for a tethered sampling approach, we must consider the material properties of tethers for engineering and mission design. Since tethers of up to 20 km length have already been employed in experiments such as TSS-1 and SEDS in low earth orbit (see Chapter 2), the material break strength of a shorter tether around a small asteroid should not be a problem. Accordingly, we will start by bounding the range of tether lengths useful under the mission assumptions of this study, then continue with strength and lifetime issues.

### 3.3.1 Tether length assessment.

The calculations in the preceding section used the physical limitations of body size, density, and rotation rate to generate the feasible range of synchronous orbits. The lower bound, of course, is the speed at the surface of the body, or where the altitude is close to zero. The upper bound is at the edge of the sphere of influence, which from Equation 3.7 and correcting to give altitude over the surface, is in the following ranges:

**Table 3.5 Sphere of influence altitudes**

| | Altitude to edge of sphere of influence (m) | | |
|---|---|---|---|
| Diameter (m) | ρ=1.0 g/cc | ρ=2.0 g/cc | ρ=3.0 g/cc |
| 100 | 299 | 411 | 492 |
| 500 | 2160 | 2930 | 3490 |
| 1000 | 5037 | 6806 | 8092 |

The minimum length of tether would probably include a few tens of meters, for safety. However, the maximum practical length of tether needed, based on an upper rotation period of four days, asteroid diameter of 1000 meters and density 3.0 g/cm$^3$, works out to be 6313 meters, as shown in Figure 3.6:

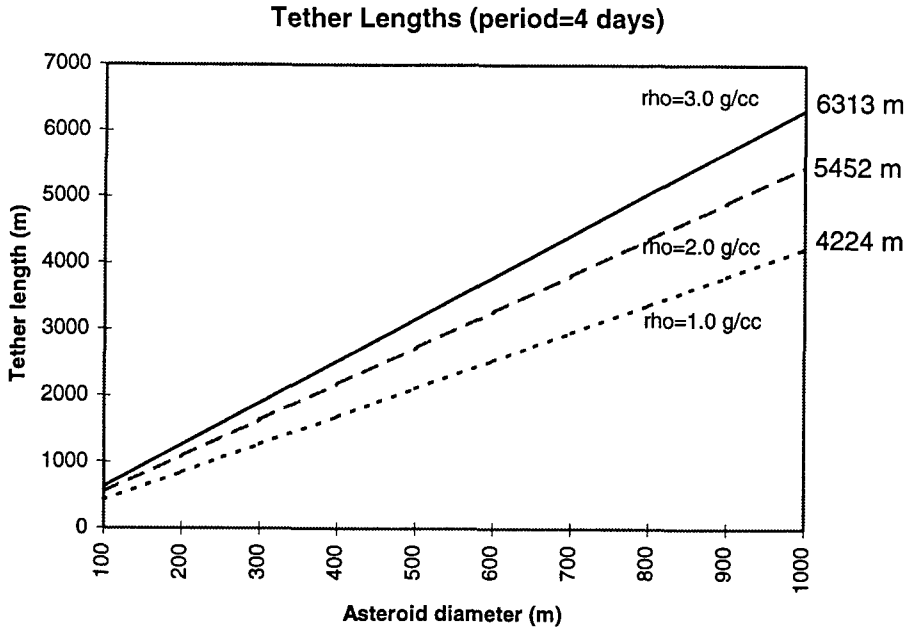


**Figure 3.6 Tether lengths for a four day orbital period**

Linear scaling of the SAIC point design assumptions (8.2 kg/500 m of tether, 5 kg for the reel) gives a modified design estimate of 103.5 kg for the tether and 63 kg for the dispenser. This is an unacceptably high fraction of the total mass of the vehicle and needs to be reduced by an order of magnitude. If we lower the requirement for rotation rate to a period of two days, the tether length drops to 3792 meters (same assumptions as above), giving a tether mass of 62.2 kg and reel mass of 37.9 kg.

If we constrain the tether to a maximum length of 500 m, we must seek targets with a period of 5.4 hours or less. Thus, from these calculations and section 3.3.1 above, the SAIC point design can only operate practicably with the higher density ($\rho$ = 3.0 g/cm$^3$) asteroids whose periods are between 1.9 hours and 5.4 hours. The SAIC design with lower density ($\rho$ = 1.0 g/cm$^3$) asteroids has a more relaxed range of periods, which range from 3.3 hours to 9.3 hours for the tether point design. Combining these two ranges, we might generalize our target criteria to seek asteroids with rotational periods between four and eight hours. The relative altitudes for this range are shown in Figure 3.7 and Figure 3.8.

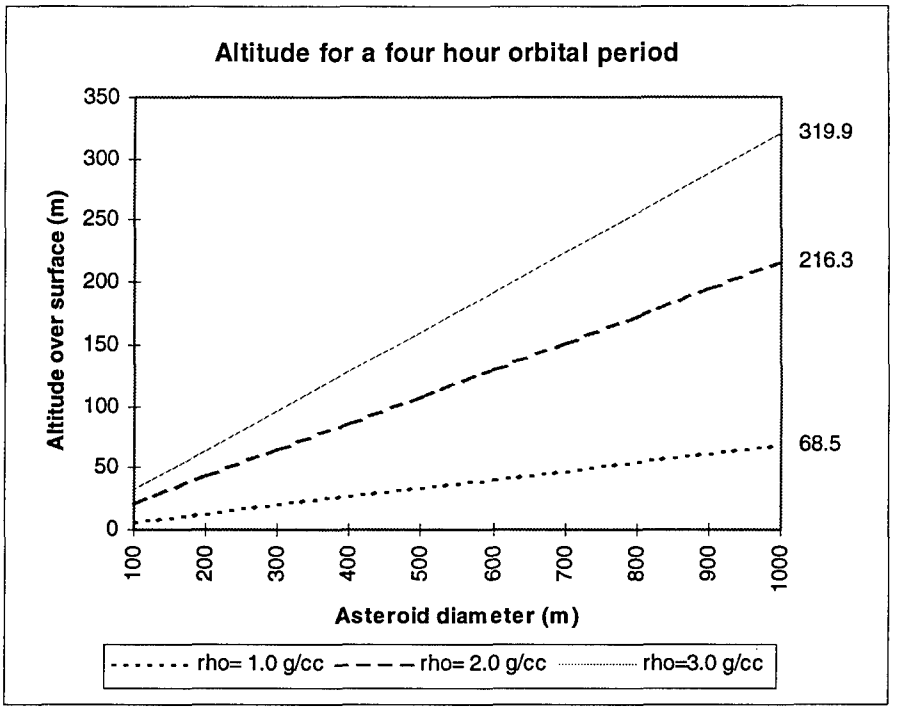


**Figure 3.7 Tether length for synchronous orbit - 4 hour period**

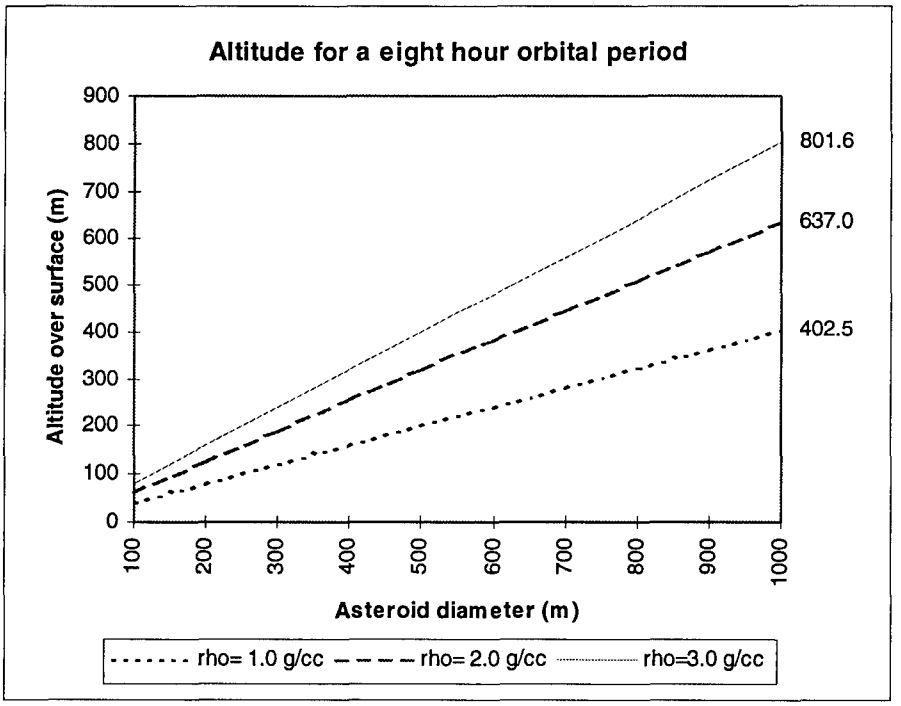


**Figure 3.8 Tether length for synchronous orbit - 8 hour period**

### 3.3.2 Tether material properties.

Tether material strength is a limiting factor in many of the proposed concepts (see Table 2.1) for earth orbiting applications. The tether must be able to support its own weight, as well as the tension from the gravity gradient forces at work. Following Beletsky and Levin (6:35), some commonly accepted measures for tether design are the *break tension* $T_*$ , the *break length* (on the surface of the earth) $l_*$, and the *break length in orbit* $L_*$. These measures assume tethers of uniform cross sectional area $f$ , material specific strength $\sigma_*$, and the following relationship:

$$T_* = \sigma_* f \tag{3.12}$$

Since the break tension is the gravitational force on a tether of break length $l_*$ and linear density $\rho$, (the linear density is the mass per volume, $\rho_m$ , times the cross sectional area $f$):

$$\begin{aligned} l_* &= \frac{T_*}{\rho g} \\ &= \frac{\sigma_*}{\rho_m g} \end{aligned} \tag{3.13}$$

The forces on an orbiting tether are due to the gravity gradient, which we derived in Equation 2.6 as approximately $3m\Omega^2 z$, where $z$ is the vertical displacement from the zero gee point. Rewriting this for the break length in orbit, $L_*$, we get:

$$T_* = 3m\Omega^2\left(\frac{L_*}{2}\right) \tag{3.14}$$

which after substituting $m=\rho L_*$ gives

$$L_* = \frac{1}{\Omega}\sqrt{\frac{2T_*}{3\rho}} = \frac{1}{\Omega}\sqrt{\frac{2\sigma_*}{3\rho_m}} \tag{3.15}$$

Applying this to the SAIC design and materials data, as shown below, we get break tensions of $T_*$= 18.8 kN (Al) and $T_*$=110.0 kN (Kevlar 49) for the SAIC design, and break lengths of thousands of kilometers. The important point is that the Kevlar wrap provides considerable mechanical support for a conducting tether.

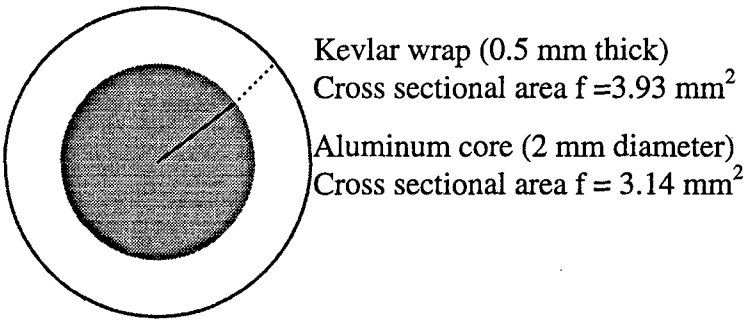


**Figure 3.9 SAIC Notional tether design**

**Table 3.6 Material properties for Aluminum and Kevlar 49 (6:35)**

| Material | $\rho_m$ (g/cm$^3$) | $\sigma_*$ (kN/mm$^2$) | E (kN/mm$^2$) | $l_*$ (on earth) (km) | $l_*$ (LEO) (km) |
|---|---|---|---|---|---|
| Aluminum | 2.7 | 0.6 | 70 | 22 | 335 |
| Kevlar 49 | 1.45 | 2.8 | 130 | 130 | 197 |

### 3.3.3 Tether expected lifetimes.

The expected lifetime of a tether is related to both the diameter and length of the tether and the micrometeoroid flux. The expected flux of meteors ($\Phi$) of mass m (grams) per m$^2$ per second in the range of $10^{-7} < m < 10^2$ grams is (6:38):

$$\log\Phi = -14 - 1.2\log m \tag{3.16}$$

If we assume that the average asteroid has a density of 3.0 g/cm$^3$, then a dangerous particle for a tether of diameter 3 mm would be about one third the tether diameter (1 mm) and have a mass of 1.26 x $10^{-2}$ grams. This gives $\Phi$=1.90 x $10^{-12}$ particles per m$^2$ per second, or on a tether 500 m in length, as in the SAIC point design, a potentially dangerous impact every 2.50 x $10^4$ years. If the average particle is of density 1.0 g/cm$^3$ instead of 3.0 g/cm$^3$, then the expected lifetime of this tether design drops to 6.68 x $10^3$ years.

### 3.4 Equations of motion.

There is a substantial body of literature on equations of motion for tethered spacecraft. Unfortunately, there is no standard choice of reference frames, and assumptions among the different formulations vary widely. Moreover, all formulations appear to be based on an earth centered inertial (ECI) reference frame, which assumes that the gravitational acceleration and coriolis forces due to the sun are dominated (in magnitude) by the central body (the earth), which is clearly untrue for the size of the asteroids we are dealing with. For interplanetary space and small bodies, such as asteroids, the equations of motion must either be rederived or given a correction factor to account for. This topic is covered in some detail in Appendix B.

The assumption of a massless, perfectly flexible tether is a commonly used to simplify theoretical and engineering analyses of tethered systems (6). This assumption should be valid for the SAIC design as well, since the tether mass (8.2 kg) is much smaller than either of the end bodies (126 kg and 700 kg were our assumptions).

Beletsky and Levin (6:63) provide a set of rectilinear equations of motion using the orbital parameters of eccentricity e, focal parameter p, and true anomaly v:

$$\begin{pmatrix} \ddot{x} - 2\dot{y}\omega - \dot{\omega}y - \left(1+2\eta^{-1}\right)\omega^2 x \\ \ddot{y} + 2\dot{x}\omega + \dot{\omega}x - \left(1-\eta^{-1}\right)\omega^2 y \\ \ddot{z} + \eta^{-1}\omega^2 z \end{pmatrix} = \frac{1}{m_A}\begin{pmatrix} T_x + F_x \\ T_y + F_y \\ T_z + F_z \end{pmatrix} \qquad (3.17)$$

where

$$\eta = 1 + e\cos\nu$$

$$\omega = \dot{\nu} = \eta^2\sqrt{\frac{\mu}{p^3}}$$

and the forces $F_x$, $F_y$, and $F_z$, are the components of external forces other than gravity. In spherical coordinates this becomes (6:65)

$$\begin{aligned}
&\ddot{\theta} + \dot{\omega} + (\dot{\theta}+\omega)\left(\frac{2\dot{r}}{r} - 2\dot{\phi}\tan\phi\right) + \frac{3\omega^2}{\eta}\sin\theta\cos\phi = -\frac{F_\theta}{m_A r\cos\phi} \\
&\ddot{\phi} + \frac{2\dot{r}}{r}\dot{\phi} + \left[(\dot{\theta}+\omega)^2 + \frac{3\omega^2}{\eta}\cos^2\theta\right]\sin\phi\cos\phi = -\frac{F_\phi}{m_A r} \\
&\ddot{r} - r\left[\dot{\phi}^2 + (\dot{\theta}+\omega)^2\cos^2\phi + \frac{\omega^2}{\eta}(3\cos^2\phi\cos^2\theta - 1)\right] + \frac{T}{m_A} = -\frac{F_r}{m_A}
\end{aligned} \tag{3.18}$$

where

$$\begin{pmatrix} F_r \\ F_\theta \\ F_\phi \end{pmatrix} = \begin{pmatrix} \cos\theta\cos\phi & \sin\theta\cos\phi & \sin\phi \\ -\sin\theta & \cos\theta & 0 \\ -\cos\theta\sin\phi & -\sin\theta\sin\phi & \cos\phi \end{pmatrix}\begin{pmatrix} F_x \\ F_y \\ F_z \end{pmatrix}$$

These equations describe the relative motion of end body A with respect to the orbiting reference frame attached to body B. In our case, body A will represent the deployed sampling device, and body B will be the spacecraft in orbit. More detailed explanations for the equations of motion in each operating phase of the sampling mission are provided in Appendix B.

### 3.5 Proposed mission plan.

Once the spacecraft/sampler has been placed into orbit around the target body, some period of surveying will be necessary. The shape and size of the orbit is immaterial, until the mission planners have chosen candidate sampling sites on the body. The major

goal at this point is to choose a suitable sampling location in the plane of rotation of the body since the spacecraft will be on station for several weeks.

The spacecraft will then move into a synchronous orbit above the sampling site. This part of the operation will consist of three distinct phases of operations: deployment of the tethered sampling system; attachment to and sampling of the asteroid; and finally, retrieval of a sample from the surface of the body. The SAIC study suggests that the sample retrieval be performed with a canister and climbing motor, which would leave the landed sampling device attached to the asteroid.

There are two possibilities for increasing the amount of sample mass returned to earth. The sampling device could then be discarded, and the tether cut away, to reduce the mass of the returning spacecraft, which is a basic assumption in the SAIC study. Alternately, the tether and sampling device could be used to provide a momentum assist to the returning spacecraft. The dynamics of these alternatives and their effects on the return trajectory are beyond the scope of this study, though they could be examined in future work.

### 3.5.1 Survey orbit.

The purpose of a survey orbit is to observe the target for candidate sampling locations based on physical properties of the object, such as size, rotation rate, rotation mode, and geographical features. For example purposes, an orbit with an eccentricity of 0.5 was chosen so that the periasteroidal altitude would be equal to one target diameter. This orbit provides some flexibility for close and distant observation and gives a reasonable "safe" distance from the asteroid. Under these conditions, a limb-to-limb view of the target subtends angles of 38.94 degrees and 12.76 degrees at periastris and apoastris, respectively. This suggests that a circular orbit at an altitude of at least four times the body diameter is "close enough". (This is approximately the view of a volleyball held at arms length.)

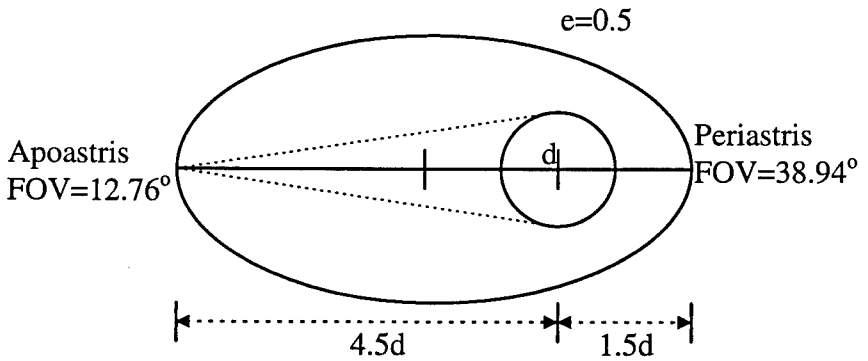


**Figure 3.10 Example survey orbit (e=0.5)**

### 3.5.2 Tether deployment.

Since the tethered sampling device must be deployed towards the asteroid, it will be necessary to slow the sampler orbital velocity to allow it to drop into a lower orbit. Thus, the sampling device should be deployed opposite the direction of the spacecraft velocity vector with some initial velocity v. As the sampler mass separates from the spacecraft, the tether may be either ejected from the spacecraft (tensionless deployment), or unreeled by a small tension force as the sampler mass changes orbit. We will consider both cases in Chapter 4.

As the sampler drops to a lower orbit and the tether deploys, the tethered system assumes a vertical orientation due to the gravity gradient forces. Since the separation of the two end masses (the spacecraft and sampler bodies) increases the moments of inertia of the overall system, and the minimum moment is around the vertical axis, deployment is an inherently stable procedure. Energy dissipation of librational in-plane and out-of-plane forces occurs from friction between fibers in the tether; however, for control purposes the design should have a damper on board.

Current tethered satellite systems in earth orbit use a boom to assist initial deployment and separation, as well as provide additional energy dissipation for libration control. In this formulation we do not consider a boom, as it is not explicitly stated in the SAIC design, and initial separation can be handled by a simple spring ejection system. We will assume that the librations imposed on the spacecraft in orbit can be damped by

viscous fluid dampers, or the torques are sufficiently small for the reaction control system to handle.

### 3.5.3 Attachment and sampling.

The tether will be deployed to leave the sampler end mass close to, but above the surface of the target body. The landing is accomplished by unreeling small lengths of tether to get the sampler within a few meters of its landing position. The SAIC design assumes that the sampler impacts with some force to drive the legs/anchors into the surface, so the last few meters of altitude may be disposed of by either a freefall landing or by decelerating with small rockets or gas jets.

The center of mass of the spacecraft-sampler system is not changed until the attachment of the sampler to the surface of the asteroid. At this point, the spacecraft and tether may be treated as a spherical pendulum attached to the surface of the asteroid. Until the instant of attachment, the center of mass of the spacecraft and lander remained in synchronous orbit; upon attachment, the center of mass of the system is within the body of the asteroid and spacecraft mass is in orbit at supersynchronous altitude.

Since the orbiting spacecraft still has the angular velocity $\omega$ required for synchronous orbit, but is at higher altitude, the tether will be under tension to keep the spacecraft from departing to a higher orbit. The tension also provides a vector component to return the spacecraft towards a vertical (radial) orientation, so this is just a special case of gravity gradient stabilization where one end of the tether is constrained from moving.

### 3.5.4 Tethered retrieval

Retrieval of a tethered object is an inherently unstable process which requires active control throughout the retrieval phase. The magnitude of oscillations in a tethered system grows because the angular momentum of the system remains constant while the moments of inertia of the system decrease (i.e. while the tether is shortened). Thus, libration control and damping should be implemented by both a mission strategy and a

closed loop control law. The subject of control laws is beyond the scope of this effort, and is not discussed further.

Two general approaches to retrieval involve exponential retrieval or uniform retrieval. The premise behind exponential deployment is to find a solution which conveniently describes the system in terms of angular displacement, and thereby provide simple analysis of rotational motions. The uniform deployment strategy is a more "cargo" oriented approach, where a subsatellite is deployed either at a constant rate of change in altitude, or at a constant velocity. It is not possible to fulfill both conditions for uniform deployment while in orbit; for example, if the height changes linearly, the new orbital velocity from Equation 3.9 ( i.e. $v^2 = \mu/R$) changes proportionately as the square root of the deployment distance. There is a third option for the retrieval of an end body, which is to leave the tether in place and allow the subsatellite to climb to the main body. This final approach is the concept of operations in the SAIC study.

### 3.5.4.1 Exponential deployment and retrieval

Using Beletsky and Levin's notation, where $\varphi$ = the out of plane angle, $\upsilon$ = the in plane angle desired for a stationary mode of motion, and $\ell_0$ = initial tether length, the tether length for exponential retrieval (or deployment) varies as (6:400) :

$$deployed\_length = \ell_0 e^{\left(-\frac{3}{4}\omega t \sin 2\upsilon\right)} \tag{3.19}$$

An inherent disadvantage of this approach is obvious—because this is an exponential deployment/retrieval, the rate of change in velocity of the subsatellite will be very small at first, and large toward the end. Another problem is that there must be some initial separation distance $\ell_0 > 0$ for deployment, which places a condition on the initial deployment velocity. Also, by inspection, we see that the most rapid change occurs when $\upsilon = \pi/4$ or $5\pi/4$. For the conditions $\ell_0$ = 1 m (for deployment) or 500 m (for retrieval), $\upsilon = \pi/4$, and a two hour orbit, we find that either deployment or retrieval starts

at 0.0007 m/s and ends 1.32 orbits later with a terminal velocity of 0.327 m/s (total time: 9,495 seconds). The closing speed on a longer tether scales linearly with the tether length; for instance, a 5 km tether has a terminal velocity of 3.27 m/s (total time: 13,013 seconds) under similar conditions.

### 3.5.4.2 Uniform deployment and retrieval.

In the case of uniform deployment and retrieval, the tether length (assumed to be a straight line connecting the two bodies) is simply r = vt, where t is the time (in seconds) from the beginning of deployment. From the radial equation of motion of Equation 3.18 (the third equation), a uniform deployment indicates constant velocity so we can set $\ddot{r}$ =0. If we set the external forces to zero, then to guarantee that the tether tension is always greater than or equal to zero, it follows from necessity that

$$3\cos^2\phi\cos^2\theta - 1 \geq 0 \tag{3.20}$$

which requires the inclination to the vertical be less than 55°. Beletsky and Levin rewrote Equation 3.18 in such a way as to show that Equation 3-20 is actually a binding constraint for maintaining tension (6:398). They also linearized Equation 3.18 for a circular orbit without perturbative forces and with respect to the dimensionless time $\tau = \omega t$ to get

$$\begin{aligned} \ddot{\theta} + \frac{2}{\tau}(\dot{\theta} + 1) + 3\theta &= 0 \\ \ddot{\phi} + \frac{2}{\tau}\dot{\phi} + 4\phi &= 0 \end{aligned} \tag{3.21}$$

which has a general solution of

$$\theta = \frac{1}{\tau}\left[-\frac{2}{3} + c_1 \sin(\sqrt{3}\tau) + c_2 \cos(\sqrt{3}\tau)\right]$$
$$\phi = \frac{1}{\tau}\left[c_3 \sin(2\tau) + c_4 \cos(2\tau)\right] \tag{3.22}$$

where the constants $c_1$through $c_4$ are arbitrary and influence horizontal oscillations during tether deployment. Levin constructs a series expansion based on $1/\tau$ for the trajectory of the deployed satellite (6:404):

$$x = -\dot{s}\left(-\tau + \frac{2}{9\tau} + \frac{10}{81\tau^3} + \ldots\right)$$
$$y = -\dot{s}\left(\frac{2}{3} + \frac{4}{27\tau^2} - \frac{52}{1215\tau^4} + \ldots\right) \tag{3.23}$$
$$z = 0$$

where $\dot{s}$ represents the tether change in length with respect to $\tau$, x is directed outwards along the radial vector opposite the gravitational attraction, y is opposite the spacecraft velocity vector, and z is out of plane. For $\tau >> 1$, this reduces to a surprisingly simple relationship for the horizontal displacement of the deployed subsatellite during a uniform descent:

$$y = -\frac{2}{3}\dot{x} \tag{3.24}$$

where y indicates the horizontal displacement in relation to the radial velocity x (dot), and is due to the Coriolis forces acting during deployment in a rotating frame of reference. If we were to deploy a 500 m tether at 1 m/s from a spacecraft in a two hour orbit, this results in a horizontal displacement of 0.67 m. However, application of Equation 3.23 to this set of parameters indicates this deployment would take almost 160 hours to complete.

### 3.5.4.3 Retrieval along a previously deployed tether.

The SAIC design assumes a Sample Canister Assembly climbing the tether to the orbiting spacecraft, a strategy which may eliminate the growth of libration amplitudes during retrieval. This aspect will be examined in Chapter 4, following an analysis by Glickman and Rybak (14) along the same lines. In essence, for long tethers, the mass of the tether can provide a stabilizing influence on a subsatellite which climbs a previously deployed tether. This methodology will be applied to the sample retrieval method proposed by SAIC on a much shorter tether.

## 3.6 Methodology summary.

In this chapter, we developed the physical parameters of target asteroids, performed a sizing and lifetime analysis for the tether point design, and reviewed the dynamical aspects of each of the three operational phases of the mission (deployment, attachment to the asteroid, and retrieval options).

Target asteroids are assumed to be in the 100 m to 1000 m diameter size range, with densities of 1.0 to 3.0 g/cm$^3$. The maximum and minimum rotation periods for target asteroids, based on the need for a spacecraft to remain in synchronous orbit and the tether point design length of 500 m, varies between 1.9 and 9.3 hours. Furthermore, we note that the asteroid population tends to have rotation rates between two hours and four days, and that a tether of 6313 m length could handle all cases within these bounds. However, this requires a mass trade with the spacecraft that is outside the scope of this effort.

The tether point design is quite adequate for its design function. The tether can withstand loads of over 100 kN, though it is unlikely to experience more than 10 N of tension. Based on the micrometeroid flux in LEO, the SAIC tether has an expected lifetime on the order of 25,000 years. Therefore, it is probably sized for carrying electrical loads from the spacecraft to the lander, though this is also out of scope of this effort.

The various phases of operations were examined in broad detail. Deployment of a tether is an inherently stable process because of the increasing moments of inertia of the system during deployment; conversely, retrieval is an inherently unstable process. Two cases of deployment were shown: exponential and uniform deployment. The exponential deployment case has an ease of formulation based on spherical coordinates, but in practice leads to very slow initial deployment rates and very fast ending deployment rates. The uniform deployment method appears to be a desirable operational procedure, but is restricted to tether swing angles of $55^0$ or less to maintain tether tension. Retrieval in both cases is the opposite of deployment and may be modeled with the same equations.

A third method, the one proposed by SAIC, is to retrieve a sample by sending it in a crawler unit along the tether, as opposed to deploying and reeling in a tether. As this is a feasibility study, and since exponential deployment has already been achieved in LEO, only the crawler concept of sample retrieval will be examined in any further detail in Chapter 4.

# IV. Analysis and Results

This chapter focuses on the dynamics of the tethered sampling mission in each of the three sampling mission phases: deployment of the lander from a synchronously orbiting spacecraft; prolonged attachment of an orbiting spacecraft to the surface of an asteroid; and retrieval of a sample via a crawler along the deployed tether. The case of deployment is modeled after equations of motion for a massless tether, as detailed in Appendix B.

## 4.1 Disturbing and restoring torques.

The main consideration of this analysis is whether environmental torques allow the tethered sampling approach to be feasible. The selection of appropriate moments of inertia ratios for the spacecraft-lander system is not a consideration in this case of passive gravity gradient stabilization (11:104) because the tether length (and hence moments of inertia of the tethered system) is determined by the size, density, and rotational period of the target asteroid. Therefore, we want to ensure that the restoring torques due to the gravity gradient are larger than the perturbing forces for tethered operations.

### 4.1.1 Disturbance torques.

According to Larson and Wertz (17:353), the four major disturbance torques (the text assumes earth orbiting applications) are caused by gravity gradient, solar radiation, magnetic field, and aerodynamic forces. In the case of our asteroid sampling mission, it is probable that only the gravity gradient and solar radiation forces have any significance. The "worst case" gravitational torque, as given by Larson and Wertz, is

$$T_g = \frac{3\mu}{2R^3}\left|I_z - I_y\right|\sin 2\theta \qquad (4.1)$$

where $T_g$ is the maximum gravity torque, $\mu$ is the gravitational parameter of the central body, R is the orbit radius, and $\theta$ is the maximum angle (in radians) of the Z axis from the local vertical. For solar pressure, the equation is

$$T_{sp} = F(c_{ps} - c_g) \tag{4.2}$$

where

$$F = \frac{F_s}{c} A_s (1+q)\cos i$$

and $F_s$ is the solar constant, c is the speed of light, $A_s$ is the surface area of the spacecraft, $c_{ps}$ is the location of the center of solar pressure, $c_g$ is the location of the center of gravity of the spacecraft, q is the reflectance, and i is the angle of incidence to the sun. Since we do not have a detailed design for the spacecraft in this mission, let us assume that the point design, which is sized for 5 kWe, is using solar cells with an end of life efficiency of 16%. The required area of solar cells at 1 AU is therefore 5 kWe/(0.16 × 1358 W/m$^2$), or $A_s$= 22.1 m$^2$. For the worst case, we will also assume ($c_{ps}$ - $c_g$) is approximately 2 meters, q is 0.6 (as used in a Larson example (17:353)), and cos i = 1.

These figures and Equations 4-1 and 4-2 give the results in Table 4.1. This scenario assumes that a 700 kg spacecraft is in a four-hour orbit around a 1000 meter diameter asteroid at 1 AU, and tethered to the surface. The moment of inertia and the gravity torque in Table 4.1 are that caused by the orbiting spacecraft in relation to the attachment point on the asteroid. The case for the tether length $\ell$ = 500 m assumes further deployment of the attached spacecraft for additional stability.

**Table 4.1 Disturbance torques**

| Tether length (m) | Moment of inertia (kg m$^2$) | Gravity torque (N·m per radian) | Solar pressure torque on S/C (N·m) | Solar pressure torque (N·m) on attachment point |
|---|---|---|---|---|
| 373.7 | 9.84E+07 | 28.12391 | 0.00032 | 0.060024 |
| 500 | 1.75E+08 | 49.99807 | 0.00032 | 0.080031 |

Since the spacecraft will have dimensions on the order of a meter, the gravity torque on the spacecraft alone is likely to be four orders of magnitude lower than the torque shown here for the overall tethered system. Therefore, attitude control should not

be a problem, and the reaction control system on the spacecraft should be sized towards required slew rates for the proper operation of spacecraft subsystems.

### 4.1.2 Heliocentric torques upon the tethered system.

This section addresses the magnitudes of two sources of perturbing torques: those caused by the acceleration of a spacecraft around the sun (Coriolis accelerations), and torques which might arise from the solar gravity gradient. The heliocentric Coriolis acceleration ($2\Omega \times v$) acting upon a spacecraft in circular orbit around an asteroid in a 1.0 AU circular heliocentric orbit is derived in Appendix B.

Because $v=r\omega$, and $\omega$ is proportional to $\sqrt{\mu / r}$ (from Section 3.5.4), the magnitude of the Coriolis acceleration is approximately proportionate to the square root of the tether length. Therefore, restoring torques increase faster with increasing tether length than Coriolis forces, and we should try to avoid missions that require low orbits (i.e. short tethers and high angular velocities) around the denser asteroids. The highest overall torques we will use appear when we choose the case of a four-hour orbit for a larger, denser asteroid to maximize the tether length ($\ell$ = 373.7 m, in Figure 4.1) and orbital speed.

The maximum sun-induced Coriolis acceleration in the worst case (1000 meter asteroid, 4 hour orbit) is $1.52 \times 10^{-7}$ m/s$^2$. Since the definition of torque is F×r, this could create a torque of up to 700 kg $\times$ ($1.52 \times 10^{-7}$ m/s$^2$) $\times$ 374 m , or $3.99 \times 10^{-2}$ N·m on the attachment point to the asteroid. The Coriolis accelerations affect orbital motion, not spacecraft attitude, so no torques are placed on the spacecraft itself.

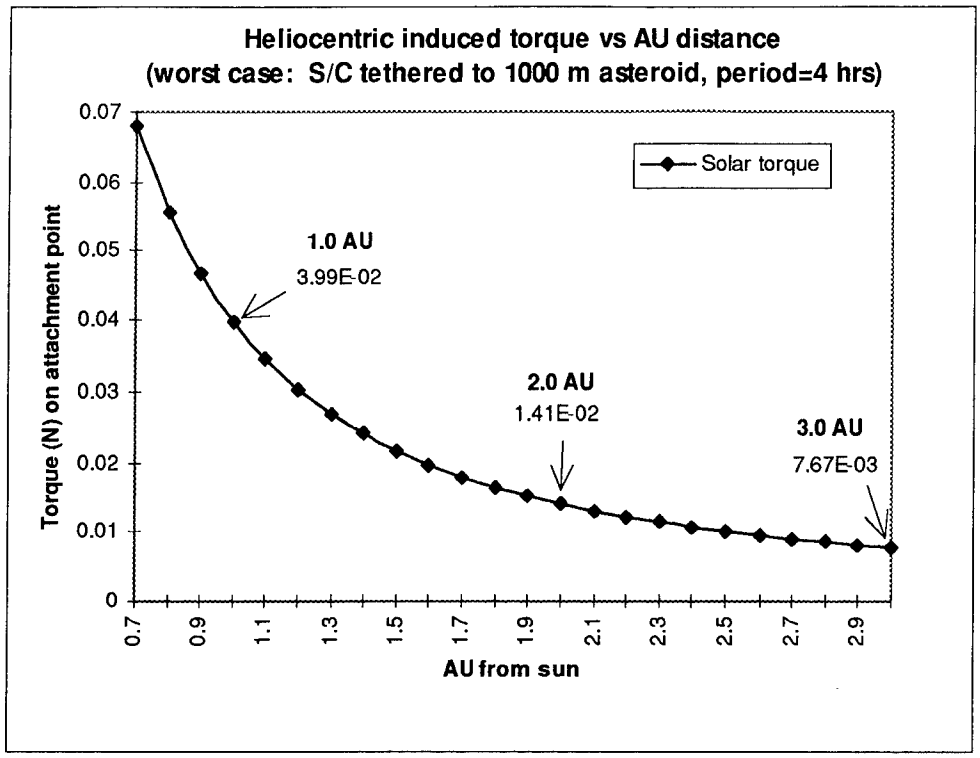


**Figure 4.1 Most stressing case for heliocentric induced torques**

The perturbing torque due to the gravity gradient of the sun at 1.0 AU is entirely negligible over the size of the spacecraft orbit. From Chapter 3, we determined that the gravity gradient is given by

$$\frac{da}{dr} = -\frac{2GM}{r^3} \tag{3.2}$$

where G is the universal gravitational constant, M is the mass of the sun, and r is the distance from the center of the sun. Substituting $\mu_{sun}=1.327 \times 10^{11}$ km$^3$/s$^2$ for GM, and letting r = 1.0 AU = $1.496 \times 10^8$ km (5:429), the gravity gradient acceleration due to the sun is only $-7.93 \times 10^{-14}$ km/s$^2$ per km (or m/s$^2$ per meter). The gravity gradient for the smallest asteroid case (100 m diameter) is still on the order of $10^{-6}$ m/s$^2$ per meter at 500 m altitude. Therefore, solar gravity gradient torques on the tethered system may be ignored entirely.

### 4.1.3 Restoring torques.

Recall from Chapter 2 that the gravity gradient in-plane ($\theta$) and out-of plane ($\phi$) torques on a tethered system, for small angles, are

$$\tau_\theta = -3m\Omega^2\ell^2\theta \tag{2.8}$$

$$\tau_\phi = -4m\Omega^2\ell^2\phi \tag{2.9}$$

where m is the mass of the endbody, $\Omega$ is the orbital rate, and $\ell$ is the length of the tether. The negative sign indicates that the torque acts to restore the tethered system to a vertical position. It is evident that "bigger is better" for the restoring torques, so within mission constraints we should seek to maximize either $\Omega$ or $\ell$, but preferably $\ell$ because it is inversely proportional to $\Omega$ by a power of 3/2 (i.e. orbit radius increases at a faster rate than orbit angular velocity decreases).

The range of restoring torques can be found by examining the cases for largest and smallest torque conditions. The largest forces will be associated with the largest, densest target in our range, and will give the maximum restoring torques; conversely, the smallest forces we can expect to work with will be associated with the smallest, least dense bodies in our target range. We will also keep the tether within a maximum length constraint of 500 meters.

For the first case, a 1000 m diameter asteroid ($\rho$=3.0 g/cm$^3$), 700 kg spacecraft, and a four hour orbital period, gives intermediate results of $\Omega=4.36 \times 10^{-4}$ rad/s and a tether length $\ell$ = 373.7 m. The application of Equations 2-8 and 2-9 above yield in-plane and out-of-plane restoring torques of -56.1 N·m and -74.9 N·m, respectively, per radian from the vertical (-0.98 and -1.31 N·m per degree). This is considerably larger than the torques caused by heliocentric forces in our scenario. If we apply the tether constraint of 500 m to even larger asteroids (diameter > 1000 m), the orbit angular velocity $\Omega$ must be also become greater, and this increases the restoring torques even further.

In the case of the smallest asteroid in our range, a 100 m diameter asteroid ($\rho$=1.0 g/cm$^3$) with a four hour period ($\Omega=4.36 \times 10^{-4}$ rad/s), the tether length is $\ell$ = 8.0

m, and the equations give $-2.55 \times 10^{-2}$ N·m and $-3.41 \times 10^{-2}$ N·m per radian ($-4.45 \times 10^{-4}$ and $-5.95 \times 10^{-4}$ N·m per degree) deviation from the vertical for the in-plane and out-of-plane restoring torques. These are the smallest restoring torques we would encounter over our presumed range of target objects, and it is questionable whether they are of usable magnitude. Fortunately though, the maximum heliocentric Coriolis torque on the attachment point to the asteroid decreases significantly for shortened tethers ($7.05 \times 10^{-6}$ N·m for this case), as does the disturbing torque caused by solar pressure (about $8.0 \times 10^{-6}$ N·m).

Just for comparison, if we were to maximize the restoring torques on the 100 m asteroid above, we would select a target with a four day rotation period. This puts the center of mass of the tethered system at 422.8 m altitude and gives a total tether length of 495 m. The restoring in-plane and out-of-plane torques are then $-1.70 \times 10^{-1}$ N·m and $-2.27 \times 10^{-1}$ N·m per radian ($-2.97 \times 10^{-3}$ and $-3.96 \times 10^{-3}$ N·m per degree) from the vertical, respectively. The maximum disturbing torques due to Coriolis forces and solar pressure in this case are $2.49 \times 10^{-3}$ N·m and $4.96 \times 10^{-2}$ N·m, respectively. One should note that these maximum disturbing forces are dependent on the orientation and velocity of the tethered satellites, and may reinforce or cancel each other.

Although these results show that the asteroid size and density range under consideration have larger restoring torques than disturbing environmental torques, we must also consider the effect of time phasing of these torques. It is possible that resonance in the orbital motion may increase swing angles and rates to levels fatal to accomplishment of the sampling mission.

## 4.2 Tether deployment.

Tether deployment, as stated in Chapter 2, is an inherently stable procedure because the moments of inertia of the tethered system increase during deployment, and then conservation of angular momentum forces libration angles and rates to decrease. Although the equations of motion used here are built for an earth centered inertial (ECI) system, which neglects solar perturbations, the addition of time-dependent solar

perturbational forces back into the equations allows us to numerically evaluate the behavior of tether deployment around small NEOs.

### 4.2.1 Tether slackness.

Tether slackness is an undesirable condition for a deployed tethered system since it removes the tension component necessary for gravity gradient stabilization. This is not saying that free motion is catastrophic during deployment; rather, once a tethered end body has been deployed, we wish to maintain control over the system. One other consideration for maintaining tension in the tether is that free motion of the end bodies will eventually end with a jerk—unless a longitudinal damper is employed—and it is possible that the magnitude of the deceleration is enough to destroy the tether.

From the equations of motion in Appendix B, which are based on the work of Beletsky and Levin (6:362), the tether tension in spherical coordinates is given by

$$T = m_A \omega \ell u \tag{B.35}$$

where $m_A$ is the mass of the deployed body, $\omega$ is the orbital rate, $\ell$ is the length of the tether, and u is

$$\begin{aligned} u &= \dot{\phi}^2 + (\dot{\theta}+1)^2 \cos\ \phi + \frac{1}{\eta}(3\cos^2\phi\cos^2\theta - 1) \\ \eta &= 1 + e\cos\theta \end{aligned} \tag{B.32}$$

Clearly, the tension is positive (the tether is taut) only when u>0. For in-plane ($\theta$), circular orbit motion, $\phi = 0$, so that the tension constraint becomes

$$(\dot{\theta}+1)^2 + (3\cos^2\theta - 1) > 0 \tag{4.3}$$

which has the solution

$$\theta < \cos^{-1}\sqrt{\frac{1}{3}} = 54.7^{o} \tag{4.4}$$

and for out-of-plane ($\phi$), circular orbit motion,

$$\dot{\phi}^2 + (\dot{\theta}+1)^2 \cos\ \phi + (3\cos^2\phi - 1) > 0 \tag{4.5}$$

Equation 4-5 has an obvious solution of $\phi<54.7^{\circ}$ for low angular rates, but also shows a dependence at $\phi=90^{\circ}$ such that the tension is maintained only if

$$(\dot{\theta}+1)^2 < 2 \tag{4.6}$$

thus, $\dot{\theta} < 0.414$ rad/s (23.7 deg/s) is also a limiting condition for the tether maintaining tension when high out-of-plane swing angles are present.

Beletsky and Levin (6:370) provide an analysis of tether jerks and conclude that "...a tether jerk after a phase of free motion could well be fatal...." for a subsatellite in their low earth orbit analysis. After combining and simplifying their equations, the essential equation reduces to

$$v_{*} = T_{*}\sqrt{\frac{\ell}{m_A E}} \tag{4.7}$$

where $v_*$ is the velocity causing tether failure, $T_*$ is the tether break tension in orbit, $\ell$ is the tether length, $m_A$ is the mass of the subsatellite, and E is the modulus of elasticity for the tether. From Chapter 3, we showed that the Kevlar wrap in the SAIC tether point design provided considerable mechanical support (110 kN for Kevlar, vs 18.8 kN for the aluminum core alone). Thus, using the data for Kevlar, $T_*$=110 kN, E=130 kN/mm$^2$, and the limiting case where $\ell$ = 500 m and $m_A$=700 kg, Equation 4-7 gives us the value for the velocity of free motion tether failure as $v_* = 2.58 \times 10^{-1}$ m/s.

Is this a concern? The radii of our asteroids are between 100 and 1000 m, the tethers are between 8 and 500 m in length, and our values of $\omega$ are on the order of $10^{-4}$. The relative velocity a freely orbiting body could develop with respect to the surface, assuming the surface and orbiting body possessed approximately the same initial angular velocity $\omega$, is the difference in orbit radii times $\omega$, or in our case, the tether length times $\omega$. In this case, 500 m/s $\times$ $4.36 \times 10^{-4}$ rad/s = $2.18 \times 10^{-1}$ m/s relative velocity between the surface and orbiting body, which is uncomfortably close to our free motion tether failure velocity of $2.58 \times 10^{-1}$ m/s. Therefore, the asteroid sampling mission should include longitudinal damping in its design for safety.

### 4.2.2 Deployment examples.

The analysis of tether deployment with a time-dependent external force (i.e. the Coriolis forces due to the sun) is shown in the following cases. The equations of motion were numerically integrated for a wide range of parameters, all of which indicated that deployment with a non-inertial asteroid centered reference frame is still a stable process. The deployment can be tailored by implementing a control law based on the tension (which is beyond the scope of this thesis), by manually changing the tension parameters, or by simply allowing the system to evolve naturally until an appropriate deployment profile is found. In the two cases that follow, the lander is given an initial speed via a spring and the tension is allowed to evolve. The two cases are built around the bounding range of asteroid sizes and densities (100 m, $\rho$=1.0 g/cm$^3$, and 1000 m, $\rho$=3.0 g/cm$^3$) and orbit periods of four hours. Heliocentric effects are included in the integration of the equations of motion.

#### 4.2.2.1 Deployment for the smaller, less dense asteroid case.

Asteroids of this size and density ($\rho$ = 1.0 g/cm$^3$) lack sufficient mass to allow orbital periods of less than 3.3 hours (see Chapter 3 for the target parameterization). The following case uses a 100 m asteroid of density $\rho$=1.0 g/cm$^3$, an initial deployment velocity of 0.1 m/s, initial swing angles of $\theta$=$\phi$=10° and swing rates of $\dot{\theta} = \dot{\phi} = 1^{o}$ per second. This case only requires a tether deployment of 8.0 m.

The subplots for Figure 4.2 show the deployment of the end body, where x is in the orbital plane along the velocity vector, y is directed in a nadir direction from the spacecraft in orbit, and $\theta$ and $\phi$ are the in-plane and out-of-plane swing angles measured with respect to the local vertical. From Figure 4.2(a), it appears that total deployment (8.0 m) of the tether could be accomplished in approximately 80 seconds. Subplot (b) shows an interesting oscillation in the rate of change of tether length with a decreasing period. The decreasing nature of the oscillation in $\dot{y}$ suggests that it is somehow coupled to either $\theta$ and $\phi$, or perhaps both. Subplots (c) and (d) show that the tether is behaving as expected, since the swing angles are decreasing as the tether and moments of inertia of the system increase.

Figure 4.3 depicts the evolution of the swing angle rates during the deployment. In the first two subplots, (a) and (b), note that the initial conditions led to a quick change in the swing angle rate, as the end body changed the direction of its motion. However, the swing angle rates were quickly suppressed during the deployment, and reach a near steady state after 60 seconds. The tendency for the tether to assume a vertical position is clearly shown in the phase plane plots (c) and (d), where the swing angles and rates converge on zero

Since this case is representative of the smallest asteroids and gravity gradients under consideration, it appears that tether deployment is not an issue for the size range of our target asteroids.

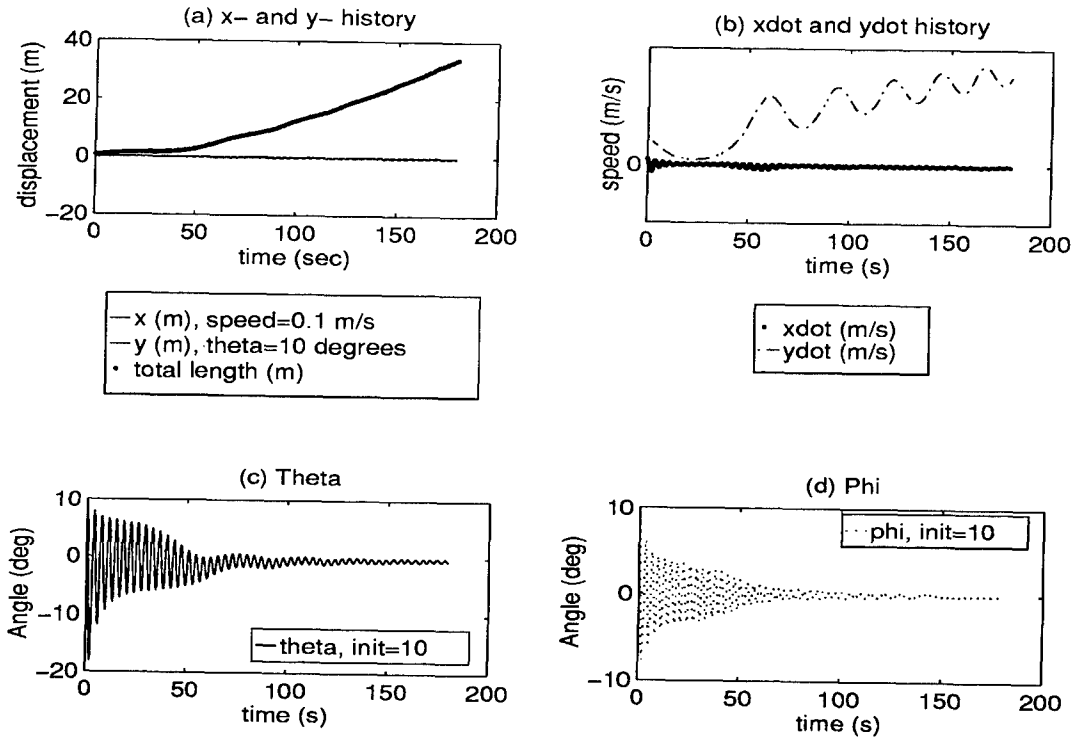


**Figure 4.2 Deployment length and speed: 100 m asteroid, 4 hour orbit**

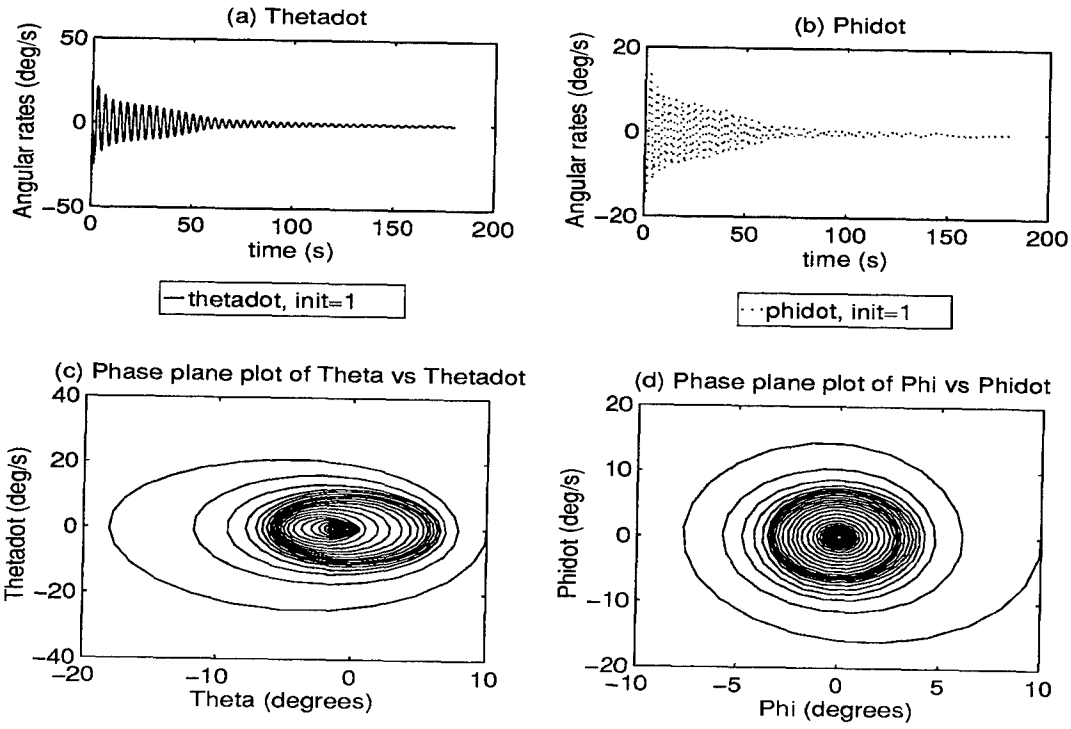


**Figure 4.3 Deployment angles: 100 m asteroid, 4 hour orbit**

#### 4.2.2.2 Deployment for the larger, denser asteroid case.

Referring to Figure 4.4, subplot (a) gives the vertical (y) and in-plane horizontal (x) displacement of the lander as it is deployed. The total deployed tether length is the top curve, and under the conditions of a 1000 m, asteroid of density $\rho = 3.0$ g/cm$^3$, the deployment requirement of 373.7 m is accomplished in approximately 500 seconds. Subplot (b), which shows the x- and y- velocity history of the deployment, also shows the initial deployment velocity of 0.5 m/s. This particular profile was chosen because the vertical descent of the deployed lander is decreasing as it approaches its fully deployed length, and is of a reasonable impact speed. Subplots (c) and (d) show the initial swinging of the tether during deployment, which stabilizes in perhaps 40 seconds, as compared to the 60 seconds needed in the small asteroid case. This is due to the stronger gravity gradient torques in effect.

Figure 4.5 and all the subplots show how deployment becomes more stable over time. However, note in subplots (c) and (d) that the dark areas may correspond to an increase in swing angles and rates, possibly from heliocentric perturbations as the deployment slows down (after 300 seconds). This, however, cannot be read from these figures due to the scaling of the plots.

Notionally, a mission planner would develop a deployment profile to provide the desired tether length in a suitable amount of time, then terminate any further change in length.

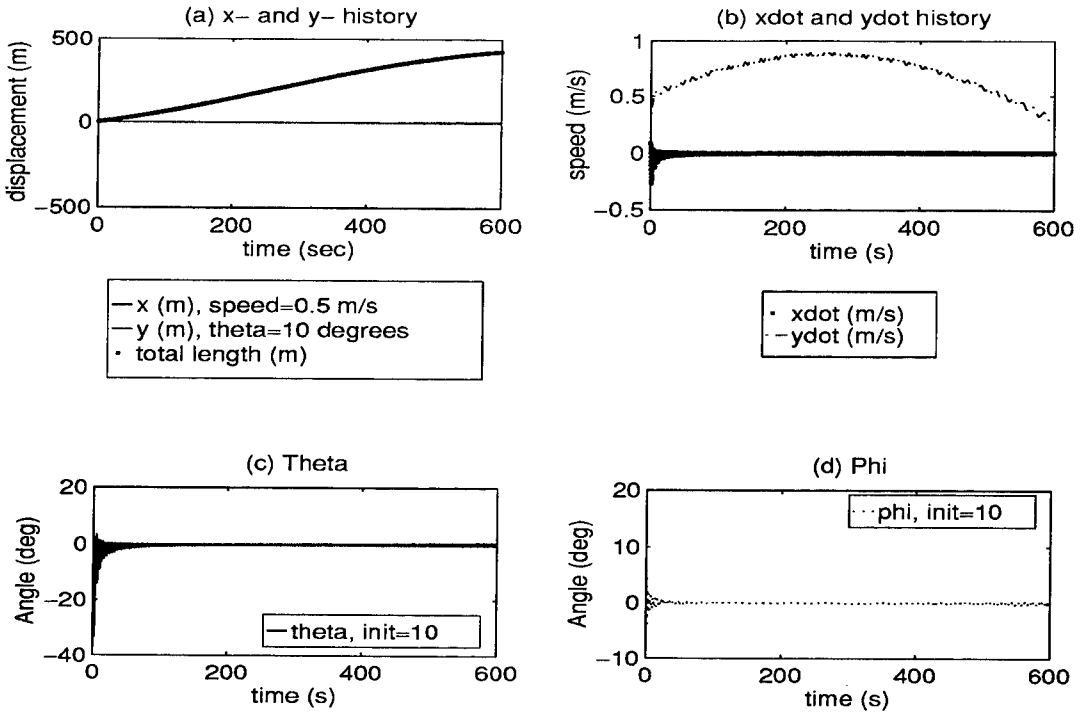


**Figure 4.4 Deployment length and speed: 1000 m asteroid, 4 hour orbit**

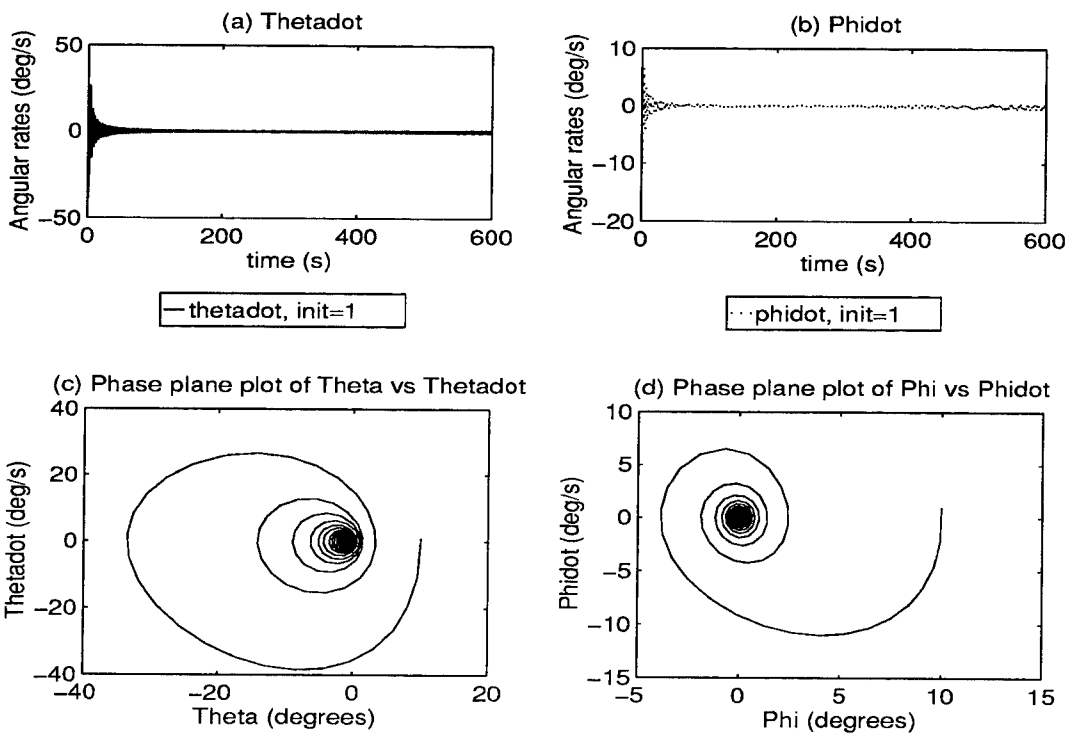


**Figure 4.5 Deployment angles: 1000 m asteroid, 4 hour orbit**

This shows that a four hour orbit (and therefore asteroid rotational period) is a reasonable criteria for successful deployment. What happens for orbit periods less than four hours—when a short tether is employed with a larger asteroid, the orbital speed will be higher, as will the perturbing Coriolis forces.

In the case of a low orbit deployment around a large asteroid, a 700 kg spacecraft could be attached to the surface by a tether as short as19 m. The inertial accelerations due to the sun, which are approximately 0.01 $m/s^2$, lead to maximum disturbing torques of about 160 N·m for a low orbit case, whereas application of Equations 2-8 and 2-9 from Section 4.1 give restoring torques of only 0.58 and 0.77 N·m per radian ($1.01 \times 10^{-2}$ and $1.34 \times 10^{-2}$ N·m per degree) from the vertical. This supports the argument in section 4.1.3 for selecting targets and mission criteria for longer tether lengths to induce the largest practical restoring torques in any given situation. Although deployment is certainly possible with a faster rotating, large asteroid, the visit time for low orbit sampling probably renders this approach infeasible.

Other than choosing a different target, we might try to attach the lander to the asteroid and continue deployment–of the spacecraft–outwards for greater stability. To find a suitable tether length which causes the restoring torques to be x times greater than the perturbing forces for a one degree variation from the vertical, relate the solar torque and Equation 2-8

$$F_{helio}\ell x = 3m\omega^2\ell^2 \tag{4.8}$$

Since we're using a time-dependent heliocentric force, let us forego detailed derivations and simplify this for an estimate of the approximate tether length desired:

$$\ell \approx \frac{F_{helio}x}{3m\omega^2} \tag{4.9}$$

where $\ell$ is the tether length desired, $F_{helio}$ is the maximum heliocentric force anticipated, x is the desired ratio of restoring torques to disturbing torques, m is the mass of the orbiting spacecraft, and $\omega$ is the orbit angular rate. If we assume x=1, then for a two hour orbit and 1000 m asteroid, the spacecraft would have to be deployed to an altitude of at least 437 m. (The nominal tether length for this scenario was 19 m.) Thus, this issue will not be considered further.

## 4.3 Attachment.

In the case of attachment, or anchoring of the lander to the surface of the asteroid, the tether deployment equations of motion may be used once we presume that the lander is now the primary body. The difference is that the "deployed" endmass is now the orbiting spacecraft, and that the in-plane angle $\theta$ is 180° greater than before, to reflect the fact that the tether is pointing outwards from the central body. The tether maximum length constraint is enforced by forcing the radial velocity to zero when the maximum length is reached. This approach also allows us to continue or stop tether deployment at any specified time, though this is considered out of scope for this effort.

The following sections will look at the immediate consequence of attaching to an asteroid (i.e. short term behavior), and follow with a single case of extended operations, since the attachment period could be as long as 21 days (29). Unfortunately, the longest practical time period, due to computer memory and run time, was limited to 15,000 seconds, which covers slightly more than the case of a four-hour orbit. The SAIC mission plan also suggested that the lander impact with some vertical speed to drive anchors into the surface; therefore, it is likely that the attachment phase will start with some initial position away from the vertical, and some initial swing angle and swing rate. We will also allow an additional 0.5 m of tether deployment to occur for braking and to account for uncertainty in actual distance measurements during the mission.

### 4.3.1 Short-term behavior of the attached spacecraft.

This case uses the smallest asteroid in its shortest tether configuration, which is a 100 m asteroid ($\rho$ = 1.0 g/cm$^3$) and four-hour orbit, and the largest asteroid with its

longest tether configuration, which is a 1000m asteroid ($\rho$ = 3.0 g/cm$^3$) and four-hour orbit . The tether was constrained to stop deployment within an arbitrarily short stopping distance (0.5 m) to avoid tether jerking. In these cases, the tension was allowed to evolve naturally, per Equation B-35, until it reached the maximum length constraint.

#### 4.3.1.1 Small asteroid case.

Figures 4.6 and 4.7 show the smallest asteroid case. In Figure 4.6, subplot (a) shows the trajectory of the end body, as seen from the attachment point on the asteroid. The appearance of subplot (a) having two apparent spherical surfaces is due to the assumption that the tether deployment had been snubbed to 0.01 m/s, and that an additional 0.5 m of tether was allowed to deploy.

Subplot (b) describes the tether tension throughout the time period, and subplots (c) and (d) show the swing angle histories. The rather slight tension of about $3.4 \times 10^{-3}$ N does not appear to be consistent with subplot (c), in which the in-plane angle shows a tendency to diverge from the vertical. Although the plots show that most damping occurs within 75 seconds for tension and angle values, longer runs (1500 seconds) show that the divergence of $\theta$ from 180° eventually grows to unreasonable bounds and the results degenerate. Several cases of slightly larger asteroids and longer tethers were run to evaluate this phenomenon, and the degeneracy appears to hold for four hour orbit cases up to asteroids 400 m in diameter ($\rho$=1.0 g/cm$^3$). This behavior also appeared in the higher density ($\rho$=3.0 g/cm$^3$) asteroid cases in this study, so it bears further investigation.

In Figure 4.7, the continuation of the small asteroid case, the swing angles and angular rates are displayed in subplots (a) - (d), and show that the libration in the attached system rapidly dies out. However, the variation in $\theta$ from Figures 4.6(a) is again inconsistent with the plot in Figure 4.7(a), so it may be that there is a problem in the formulation of the equations of motion. The swing angles and rates are used in the Beletsky formulation to determine the tether tension, so it is not surprising that the damping in the swing angle rates closely matches that of the tension history.

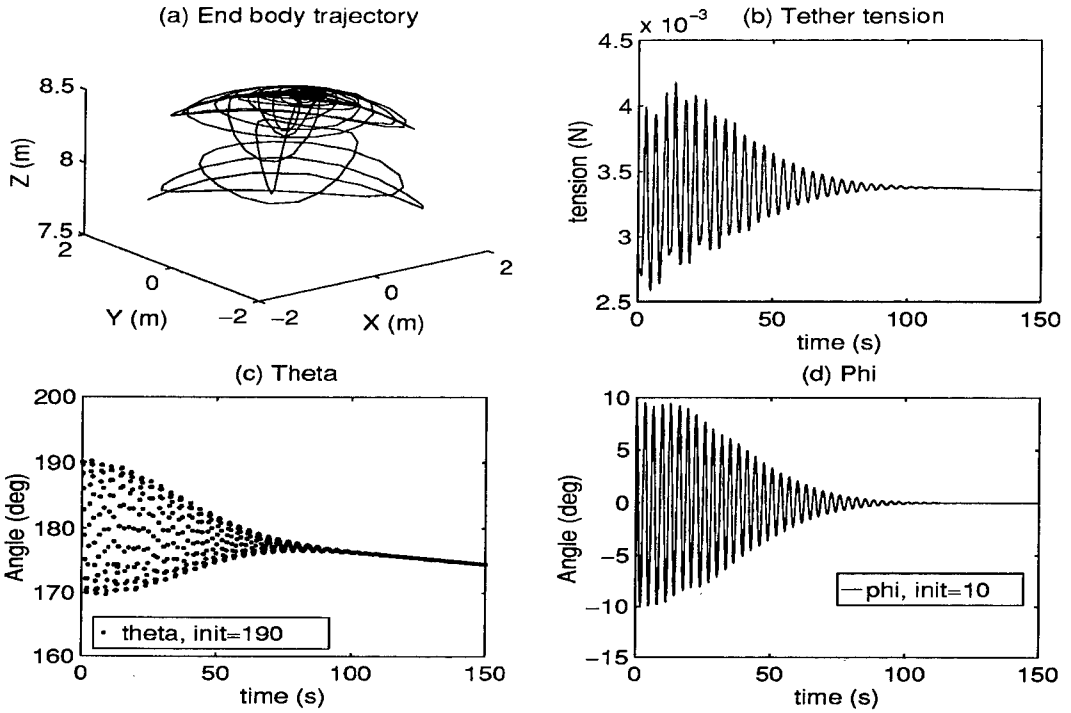


**Figure 4.6 Small asteroid case: theta=190, phi=10, thetadot= phidot = 1**

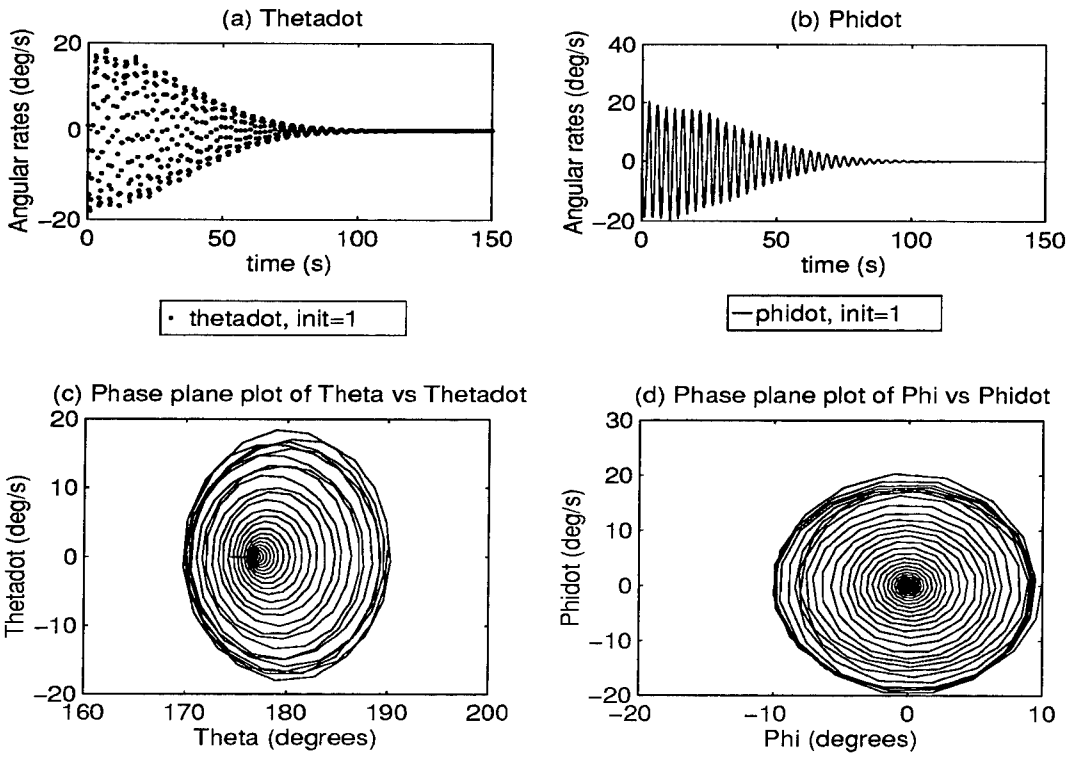


**Figure 4.7 Small asteroid case: angular rates**

#### 4.3.1.2 Large asteroid case.

On the following pages, Figures 4.8 and 4.9 show the behavior of a spacecraft attached by a long tether to a large asteroid. In these cases, the tether length, $\ell = 373.7$ m, is determined by an asteroid 1000 m in diameter ($\rho = 3.0$ g/cm$^3$) and a four-hour orbital period. The tether was allowed an 0.5 m of additional growth, with the assumption that the radial velocity had already been snubbed to near zero (actually, 0.01 m/s). Initial swing angles of $\theta$=190° and $\phi$=10°, and initial swing rates of 1° per second for in-plane and out-of-plane motion were used in this scenario.

In Figure 4.8, most damping of tether tension variations and swing angle oscillations occurred within 500 seconds. The tether tension stabilized at 0.15 N, and again exhibited an inconsistency with the $\theta$, the in-plane angle of the tether. Since the centrifugal force caused by the spacecraft is $mr\omega^2$, which comes to (700 kg × (500+374) × $(4.36 \times 10^{-4})^2$) = 0.12 N, and the gravitational force on the spacecraft, $\mu m/r^2$, comes to 0.095 N, the tether tension due to the local forces should only be about 0.02 N (not including forces due to tether swinging). Therefore, the additional tension forces and the periodic change in tension are caused by perturbative accelerations on the order of $10^{-4}$ m/s$^2$. Heliocentric accelerations ($2\Omega \times v$) are on the order of $10^{-7}$ m/s$^2$, so the likely culprit is asteroid Coriolis forces, which from $2\omega \times v$ would be on the order of $10^{-4}$ or $10^{-5}$ m/s$^2$.

Figure 4.9 shows the behavior of the swing angle rates. In subplots (a) and (b), see that $\theta$ and $\phi$ settle to constant values; however, this is again in conflict with the plot of $\theta$ (Figure 4.8(c)). No explanation has been found for this result, and so we cannot conclude that this motion will be stable in the long run.

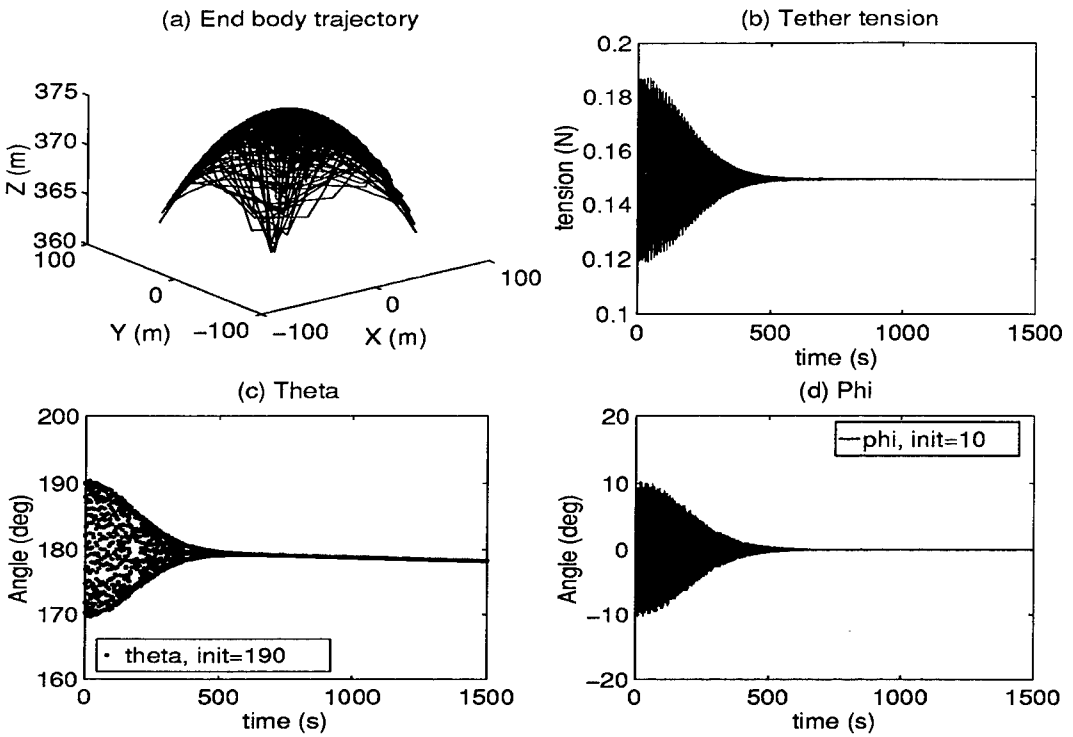


**Figure 4.8 Large asteroid case: theta=190, phi=10, thetadot=phidot=1**

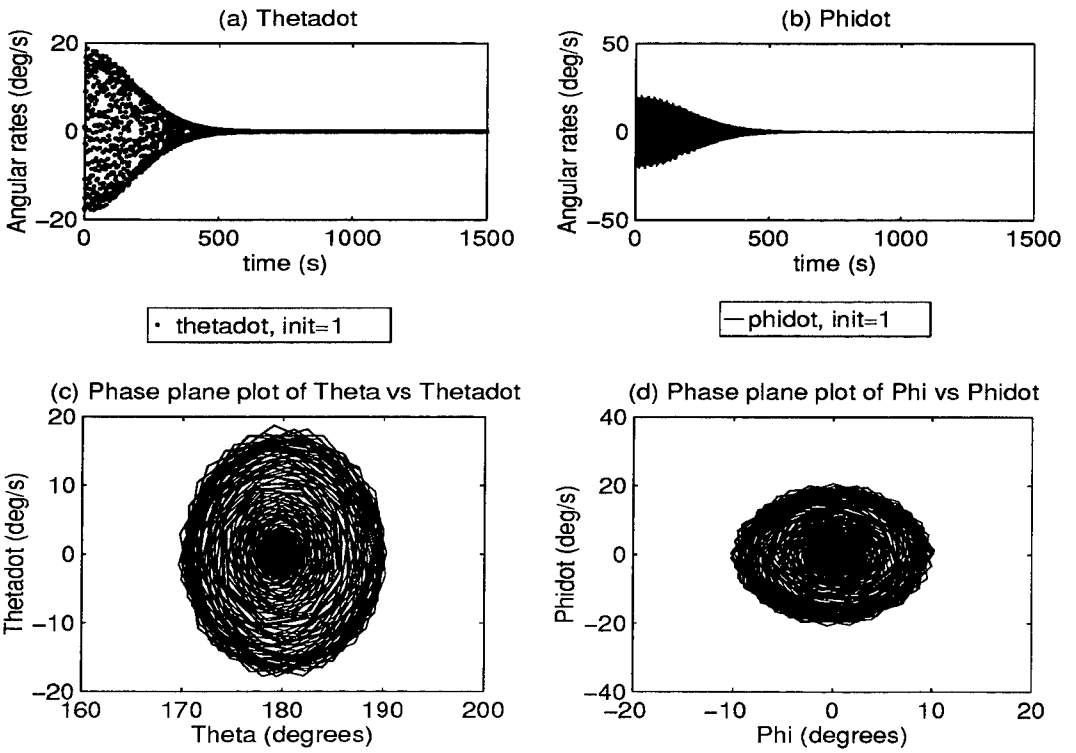


**Figure 4.9 Large asteroid case: angular rates**

### 4.3.2 Long-term behavior of the attached spacecraft.

The following case was run for a four hour orbit case around a large asteroid for a tether near the maximum deployed length. Figure 4.10 and Figure 4.11 are the result of initial angle conditions of $\theta$=190°, $\phi$=10°, and 1° for both in-plane and out-of-plane angular rates

The most striking feature about Figure 4.10 is in subplot (c): it appears that the change in $\theta$, the in-plane swing angle, is directly attributable to the orbit angular rate, since the period of the oscillation in $\theta$ is close to 4 hours (14,400 seconds) if not there exactly. As in the short term case for a large asteroid, the tension converges on a constant value of 0.15 N for the long term. The effects of heliocentric Coriolis accelerations, which should have increased with the increased tether length, do not appear to be influencing the tension. From subplot (a), it appears that the trajectory of the spacecraft remained well behaved throughout an entire orbit.

Figure 4.11, subplots (a) and (b), show a definite tendency for the tether to stabilize and for angular rates to approach zero as the orbit evolves. Subplots (c) and (d) also show the phase trajectories converging on a stable point in the center of the plots. From the results of both Figure 4.10 and Figure 4.11, anchoring the lander and maintaining a tethered spacecraft on orbit is feasible for at least a few hours. It is highly probable, though not certain, that a 21 day tethered mission is feasible too.

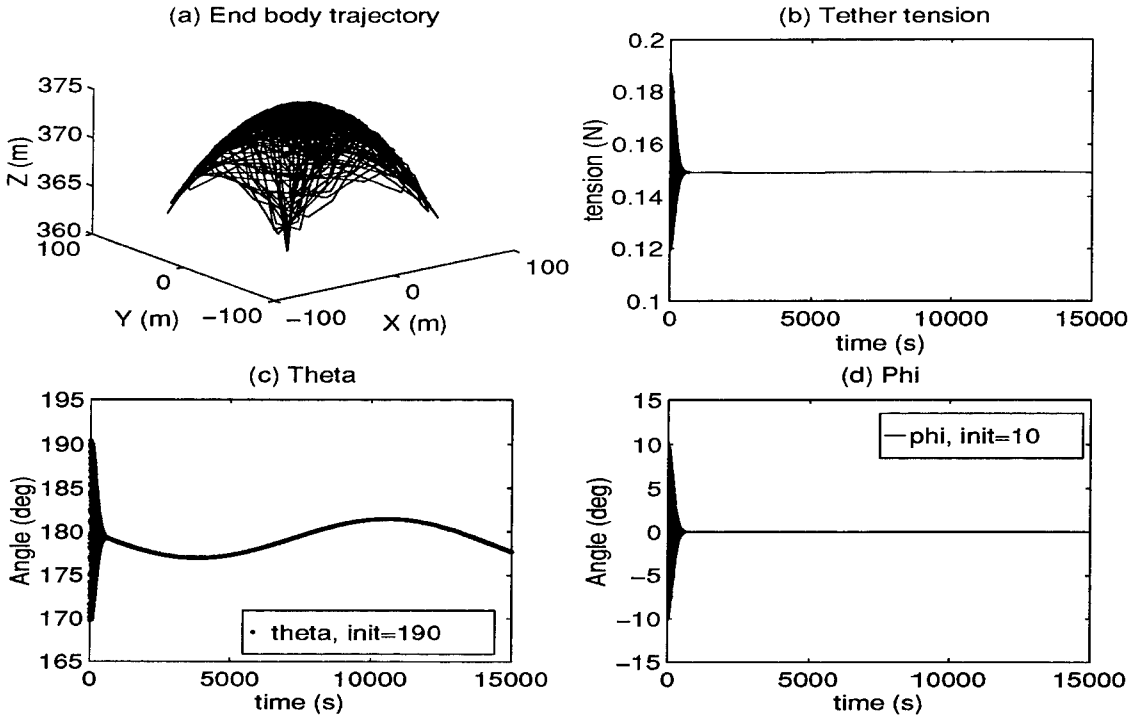


**Figure 4.10 Long term attachment: 4 hr orbit, 15000 second integration**

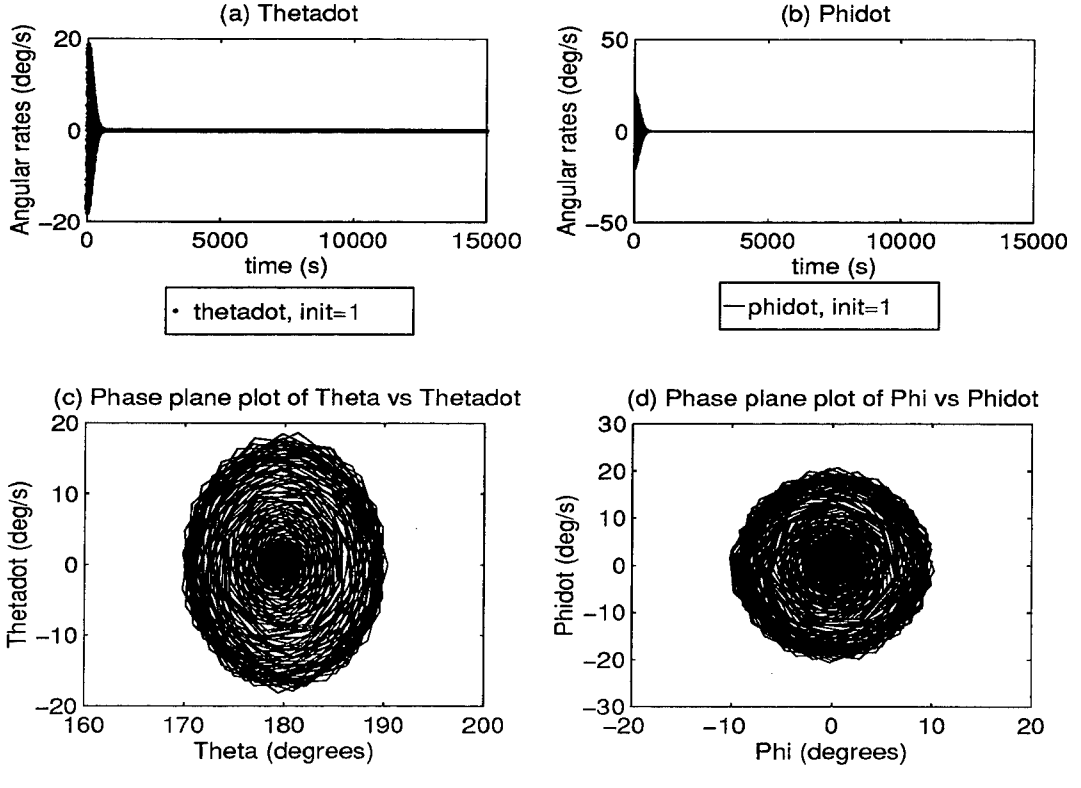


**Figure 4.11 Long term attachment: angular history**

## 4.4 Sample retrieval.

In the paper by Glickman and Rybak (14), a previously deployed tether provided significant stabilization to the retrieval of an end body, which crawled up the tether to the spacecraft. In our case, the lander, having attached to the asteroid surface, is now considered to be the primary body, and the crawler deploys upwards to the orbiting spacecraft. There are two problems with this approach: first, there is a cost in potential energy for raising the crawler out of the asteroid's gravity well, and second, the presence of the crawler is a third body introduced to the tethered system, with unknown consequences on the overall dynamics of the system. Neither of these considerations were addressed by the original authors, and unfortunately, and the scope of this effort is not designed to develop the dynamics of the three-body situation. What makes this even more difficult is that tether tension accelerates the crawler as it climbs. This renders the problem nonconservative unless the asteroid is included in the total energy and angular momentum calculations and minuscule variations in the asteroid angular velocity are tracked.

Figure 4.12 shows the comparison of crawler deployment from the surface of the asteroid when the potential energy concerns are neglected. In subplot (a), the equations of motion for a very short tether with a mass of 5 kg show that crawler deployment is a very slow process. The addition of a 700 kg spacecraft at the far end of the tether, in subplot (b), speeds up crawler deployment by at least two orders of magnitude. Thus, the stabilizing effect of a long tether on crawler retrieval, as described in the literature (14), can be simulated effectively for short tethers by leaving an end mass deployed.

The in-plane and out-of-plane equations of motion provided in the literature are not shown here. Integration of the equations produced highly questionable angular behavior, such as both swing angles smoothly changing direction by $180^0$, with no coupled motion. (This would indicate the tether wraps around the asteroid, but the angular rates did not increase.) This was contrary to the assumptions which used crawler speed to modify the Coriolis torques on the system and maintain a constant Equilibrium Hangoff Angle (EHA), so the equations are not included.

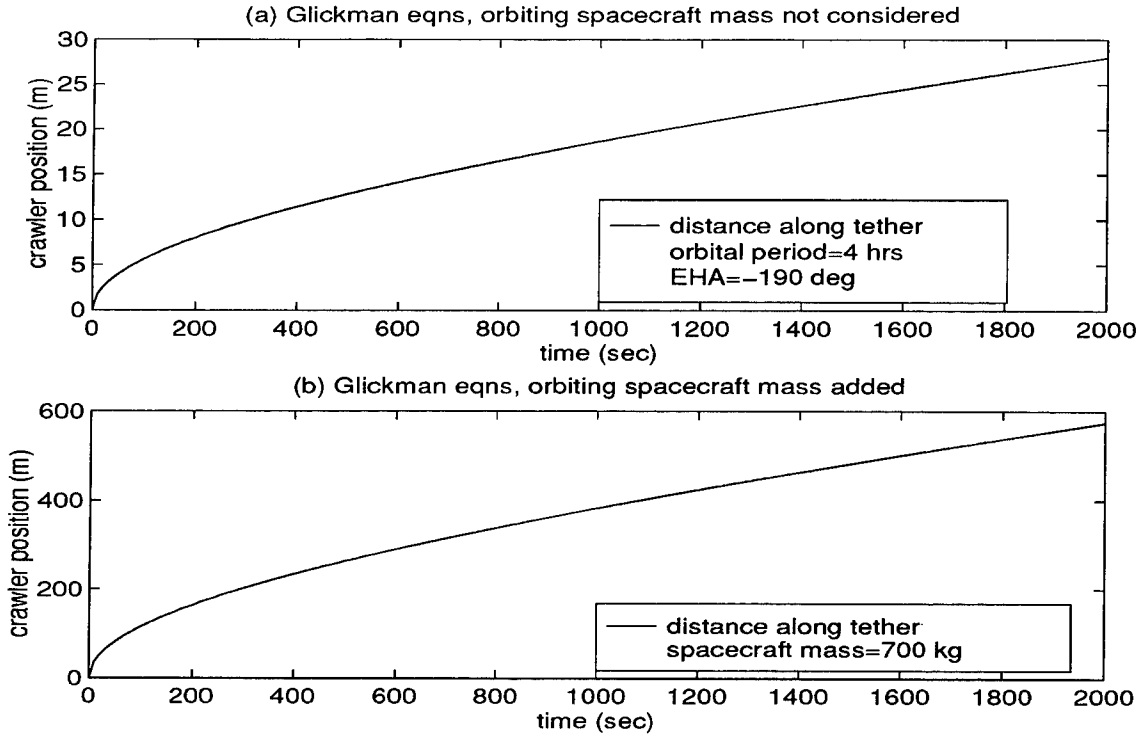


**Figure 4.12 Crawler deployment**

# V. Conclusions

## 5.1 Summary of results.

Based on the point design of the SAIC tethered lander, this thesis assessed the parameters of suitable asteroid targets and tether properties. An analysis of the dynamics of tether deployment, attachment to the asteroid, and retrieval of a sample on the attached tether showed that heliocentric accelerations do affect the motion of the tether, but not substantially. The dynamics of the third phase, sample retrieval, was inconclusive and merits further study.

### 5.1.1 Target selection.

Target asteroid parameters were developed, based on asteroid density, sphere of influence for the asteroid, asteroid rotation rate, and the maximum tether length available (500 m, per the SAIC design). This analysis assumed that the tethered sampling approach requires the spacecraft to be in synchronous orbit with the asteroid prior to deploying the lander.

**Table 5.1 Target selection parameters**

| Asteroid diameter (m) | Minimum rotation period (hrs) | Maximum rotation period (hrs) |
|---|---|---|
| 100 | 3.3 | 9.3 |
| 1000 | 1.9 | 5.4 |

Most asteroids have a rotation period between two hours and four days(24), so this range of asteroid diameters appears appropriate for targeting.

The original target proposed in the SAIC proposal, 1991VG, turns out to have a diameter on the order of 10 meters, and an unknown rotation rate. The sphere of influence for a body this size is approximately 29 meters, and an extremely low

gravitational acceleration ($4 \times 10^{-6}$ m/s$^2$), so this range of bodies was not considered for tether deployment and sampling.

### 5.1.2 Tether properties.

The tether materials and design are sufficient to handle the tension forces expected around the asteroid, which are on the order of a few newtons (the break tension of the design is approximately 110 kN). The tether lifetime for the design is also quite sufficient, since a hazardous impact by a micrometeoroid is estimated only once every 25,000 years for a tether of its size. Presumably, the tether sizing was based on the expected electrical loads and required insulation, though this aspect was not checked.

However, rupture velocity after a period of free flight was a consideration that could not be avoided, regardless of tether strength. Beletsky and Levin (6:370) showed that free flight (i.e. zero tension in the tether) in low earth orbit could easily lead to velocities that, when ending with a jerk, could sever the tether. The distillation of the appropriate equations gives

$$v_* = T_* \sqrt{\frac{\ell}{m_A E}} \tag{4.7}$$

where $v_*$ is the velocity causing tether failure, $T_*$ is the tether break tension in orbit, $\ell$ is the tether length, $m_A$ is the mass of the subsatellite, and E is the modulus of elasticity for the tether. The velocity for free motion tether failure is $v_* = 2.58 \times 10^{-1}$ m/s for the maximum tether length of 500 m, versus the worst case velocity of $2.18 \times 10^{-1}$ m/s. Since the free flight issue is only pertinent when it stops instantaneously, longitudinal damping of tether jerks should be a designed into the mission.

### 5.1.3 Tethered system dynamics.

A substantial body of literature exists for tether dynamics based on an Earth Centered Inertial (ECI) reference frame that neglects heliocentric effects. The dynamical equations for the deployment phase and attachment phase of tethered sampling were

based on tether equations of motion by Beletsky and Levin (6), with a heliocentric "correction" factor added in. Since the correction factor is time-dependent, the body of analysis was performed on the results of the numerically integrated equations of motion. The sample retrieval phase was modeled after the work of Glickman and Rybak (14), who showed that tether mass can provide a very positive stabilizing effect on retrieval.

The equations of motion behave as expected for the first two phases; however, the equations modified for crawler retrieval do not appear to model the motion adequately. One peculiarity was the tendency for the in-plane swing angle $\theta$ to diverge from the vertical without apparent connection to its swing rate or tension in the tether. However, long term modeling showed a periodicity in this behavior matching the orbital rate.

#### 5.1.3.1 Deployment phase of operations.

Tether deployment is a well-understood phase of operations, now that several experiments have flown in space (see Chapter 2 for examples). The deployment equations of motion showed the expected result; namely, that the libration angles in a deployment decrease as the tether deploys. The numerical results show that maximum length of tether can be deployed in 600 seconds or less when either given an initial separation velocity, or if allowed to deploy naturally under forces in the environment. The perturbations due to heliocentric effects, such as the Coriolis acceleration, did not substantially alter the deployment motion or stability of the tethered system.

The tether deployment was also conducted with a constant tension and allowed to proceed past the full deployment to observe the effects of slowing the deployment and eventually reversing direction into a retrieval. The tether showed signs of increasing in-plane and out-of-plane swing angles as it slowed, though the angles did not grow markedly until retrieval, which is normal.

#### 5.1.3.2 Attachment phase of operations.

The attachment phase was modeled on the same set of equations as deployment, except that the tether length was constrained to remain within a maximum length. The short term (<150 seconds) behavior of a spacecraft on a very short tether (8 m) showed a

strong tendency to return to a vertical position. This was somewhat contrary to expectations, since a short tether provides small gravity gradient restoring torques. The mechanism for this behavior remains unclear.

A second case was run for a longer tether (373.7 m) with a larger initial angular displacement. The short term behavior, based on phase plane plots, indicates that the system reduces the swing angles and angular rates toward a constant value as time progresses. Also, the main contribution to tether tension appears to be from asteroidal Coriolis acceleration, not heliocentric accelerations.

The second case, with the longer tether, was then run for as long as practical on a personal computer (15000 seconds of simulation time, which took nearly a day to complete). This time was chosen to be greater than the period of one orbit, so that time dependent perturbations could be detected. The long-term behavior observed, which is shown in Chapter 4, Section 4.3.2, indicates that the attached tether reduced the magnitude of its librations by approximately 90% in the first hour, with little change in the angular rates in the remaining time.

The two cases were also allowed to "deploy" the orbiting spacecraft a small, arbitrary distance immediately after "attachment" to the asteroid. This represented the condition that deployment will generally not stop instantaneously, or that a braking scheme is employed. The case of deploying the orbiting spacecraft to a greater altitude by tens of meters or more for (presumably) more stability was not addressed.

#### 5.1.3.3 Sample retrieval phase of operations.

The case of sample retrieval is inconclusive for now. The equations of motion for retrieving a crawler along a previously deployed tether appear rather elegant in the literature (14:334), but they disregard gravitational attraction from the bodies attached to the tether. This appears to be the downfall in this phase of the modeling and analysis effort, even when heliocentric perturbative accelerations were disregarded.

The equations were modified to assume that crawler retrieval to the spacecraft in orbit was actually a deployment from a massive primary body (i.e. the asteroid). The premise behind the equations is that the crawler speed can be modified to provide a

counteracting torque to Coriolis forces, and this provides a nearly constant retrieval profile, versus the wide variation in speed in an exponential retrieval. However, integration of the angular equations of motion showed the in-plane and the out-of-plane angles blithely moving to $180^{\circ}$ from the initial conditions. This is obviously fatal to mission success since it means the crawler, literally, crashes and burns on the asteroid surface. The problem probably requires a complete reformulation of the situation, and should include gravitational effects from the asteroid, as well as provision for solar perturbations. This is out of scope of this effort, since the sample can be retrieved by other means, such as detaching it from the surface and reeling it in with conventional retrieval procedures.

## 5.2 Conclusions.

### 5.2.1 Feasibility of tethered sampling approach.

The use of tethers to sample asteroids is definitely possible in the deployment and attachment phases of a sampling mission. The possible benefits of keeping the spacecraft in orbit include a lessened risk to the spacecraft than in a landing, better visibility for communications with the earth, and use of the solar panels to provide power down the tether to the sampler. The use of a crawler to return an asteroid sample to orbit has promise, since it eliminates the guesswork of docking a returning vehicle or the hazard of landing the spacecraft.

Clearly, the tension and swing rates derived through simulation are compatible with deployment, since the swing angles and angular rates remain within the initial conditions and decrease over time. The heliocentric correction factor does not appear to affect the overall behavior of the system significantly, and in fact, is actually quite small (about $10^{-7}$ m/s$^2$) for the range of asteroid targets under consideration. These accelerations will remain on this order of magnitude, though slightly smaller, as the distance from the sun increases.

### 5.2.2 Practicality of tethered sampling approach.

The other aspect of an asteroid sampling mission that has not been discussed is the practicality of the tethered sampling technique. Given the low accelerations around the 1000 m asteroids ($4.19 \times 10^{-4}$ m/s$^2$ surface acceleration in our largest case), it may be simpler to land the spacecraft directly; for instance, the impact velocity of a freefall from infinity is the same as the escape velocity, which in the largest case, amounts to 0.647 m/s. The thrust needed to lift a 1000 kg mass off the surface of these asteroids is 0.42 N. Since the xenon ion thrusters in the SAIC point design can provide 250 mN by themselves (29), it is conceivable that augmentation with the existing cold gas reaction control thrusters could eliminate the need for an additional launch mechanism and extra mass.

This leaves two other issues to explore when asking "why" we should use a tether. Perhaps the surface speed of the rotating asteroid is a limiting factor, or that a controlled descent requires more control, mass, and propellant than can be afforded in a direct landing. The surface speed of a 1000 meter diameter asteroid with a two hour rotation period is 0.44 m/s, so the speed does not appear to be a significant problem. The other issue can only be answered when one has an idea of what constitutes acceptable risk to the lander.

### 5.2.3 Suggested enhancements to the tethered sampling approach.

The low gravity torques available in an asteroid sampling scenario might be augmented in several ways. When possible, one should choose a larger or denser target over a smaller or less dense body, though this gives rise to larger Coriolis forces. For bodies 100 meters in diameter or smaller with a low rotation rate, a direct landing of the spacecraft is probably less risky than trying to maintain a tethered orbit, since the low accelerations make the end body susceptible to free motion which could break the tether. A tether might still be used if the restoring force provided by tether tension is augmented by thrust. This case is left for future generations to ponder.

The most risky approach, if the technology and algorithms are sufficiently advanced and reliable, is to use the propulsion system to compensate for solar torquing

around asteroids greater than 100 m in diameter. In this last suggestion, the spacecraft can develop an acceleration of $3.57 \times 10^{-4}$ m/s$^2$ (i.e. 250 mN thrust/700 kg), which is much larger than the solar pressure and Coriolis accelerations (both are about $10^{-7}$ m/s$^2$) for a 1000 m body at 1 AU. Of course, the use of the propulsion system is undesirable from the standpoint that fuel and energy are consumed, though with ion thrusters this does not cause undue concern. The major objection to this approach is because of sample contamination issues, and possibly concerns over the reliability of such an active control scheme.

## 5.3 Issues requiring further study.

This line of investigation could continue on many fronts. The issues requiring further study, in decreasing order of importance, are:

- Reformulation of the crawler retrieval equations of motion
- Long term stability of the attached spacecraft in orbit
- Active control of the attached tether against environmental torques by thrusting
- The effect of deploying multiple tethers from the spacecraft as anchors

As this was an effort to determine the feasibility of the approach, not to determine all of the relationships involved, more detailed modeling and analysis of the vibrational motion of the tether should be performed as well.

# APPENDIX A: NEO missions

There are currently two missions planned to rendezvous with NEOs: the European Space Agency's (ESA) Rosetta mission, and the Johns Hopkins Applied Physics Laboratory (APL) Near Earth Asteroid Rendezvous (NEAR) mission. Another mission which was started but cancelled early in the program was NASA's Comet Rendevous Asteroid Flyby (CRAF), upon which the Rosetta mission is based.

The following sections cover the projects which have particular relevance to this study. The Rosetta mission is of particular significance because it is a sample return mission and deals with many of the concerns involved in such a mission; however, the size and orbital characteristics of the NEAR mission are much closer to the design and analysis conducted by SAIC for NASA Lewis. Clementine is included because it is a noteworthy example of a small interplanetary mission with a limited sensor suite. All three projects are three-axis stabilized and use chemical propulsion.

## A.1 Rosetta

The Rosetta/Comet-Nucleus . Sample-Return (CSNR) mission chosen by the European scientific community is designed to return approximately 10-15 kilograms of cometary material to the earth for study. The major goals, requirements, and constraints of the program are paraphrased from the system definition document as follows (12:111-114):

1. Return three types of samples from a cometary nucleus,: a core sample one to three meters in depth; a volatile sample from the bottom of the core sample; and a surface sample of at least five kilograms. Maintain these samples below 160 K at all times.

2. Plan for a wide range of cometary conditions; accomplish on-comet operations in the shortest possible time.

3. Cope with the actual shape, rotation rate, and gravitational field of the target. This requires an extensive nucleus characterization phase.

4. Sample from a pre-selected site on the target. This requires detailed mapping of the nucleus.

5. Cope with the wide range of physical and compositional characteristics possible. This requires a sampling system able to handle materials from dust to boulders.

6. Plan and implement the mission as a cooperative NASA/ESA venture.

7. Use a spacecraft consisting of three modules: a Mariner Mark-II (MMII) cruise module; a lander module; and an aerobraking [sample return] re-entry capsule.

8. Use a Titan IV-Centaur for launch, and on-board chemical propulsion. [At this point the mission document states the following: "These constraints restrict mission opportunties to near-comet operations at aphelion, which is also the preferred strategy for environental safety considerations."]

9. To comply with safety regulations and planetary protection rules issued by COSPAR [e.g. the two Radioisotopic Thermal Generators on the MMII].

These requirements led to the development of a cruise module based on the NASA Mariner Mark II for the main body, plus a lander and an Earth Return Capsule (ERC) designed by ESA (Figure A.1). The size of the entire spacecraft (2447 kg dry mass), and its requirement to visit a cometary nucleus have placed severe constraints on the sample size, 10-15 kg of material, and the mission design.

The mission consists of eight phases of operations: launch; cruise phase, comet approach; descent and landing; on-comet operations; comet departure; and earth return, and reentry. These phases can be summarized as follows: since the size of the spacecraft prevents a direct heliocentric transfer orbit to the target, the spacecraft is first placed in a low earth orbit by a Titan IV. The Centaur upper stage places Rosetta into a heliocentric earth-to-earth orbit, which takes nearly two years, for a delta V-Earth Gravity Assist (delta VEGA) manuever to increase its energy. Rendezvous occurs near aphelion, between 5 and 6 AU from the sun, and the spacecraft assumes an elliptical orbit around the comet for several weeks to perform mapping of the surface and determination of spin rate, gravity fields, and landing sites.

Once a target landing site is chosen, the spacecraft autonomously closes in (open loop control) to some predetermined distance, on the order of a hundred meters, before switching to cold gas thrusters (closed loop control) for landing. Rosetta is equipped with robotic manipulator arm and a low power drill, and seals several samples of cometary

material into insulated containers. Once sampling is complete, the cruise module and samples separate from the lander for the return trip to earth. The samples are deorbited in a heat shielded aerobraking capsule [a scaled down version of those used in Venus probes], and picked up by helicopter. The RTGs on the cruise module are ejected into a harmless orbit, and the cruise module is allowed to burn up in the atmosphere.

The science package for Rosetta consists of an in-situ imaging system, infrared mapper, neutral mass/ion mass spectrometer, test penetrator, IR-spectral mapper, radar sounder, remote imaging system, radar altimeter, dust counter, and laser range finder. Some additional equipment for sampling purposes includes borehole stratigraphy (i.e. small optical and IR detectors to look at layers in the borehole) and thermal loggers to monitor the temperature profile while sampling. Additionally, the communications package will be used for radio science by 2-way doppler tracking of the comet during the orbit and descent phases.

At the time of this thesis, the target comet for Rosetta is not firmly decided. The first mission proposal was based on a delta VEGA mission to comet Hartley-2 in 2002, with a return in 2010. Further investigation of possible trajectories has shown that a Venus-Earth-Earth Gravity Assist (VEEGA) mission to comet Schwassmann-Wachmann-3 from 2002 to 2011 is of particular interest to ESA for its "enormous launch mass margins" (12:112).

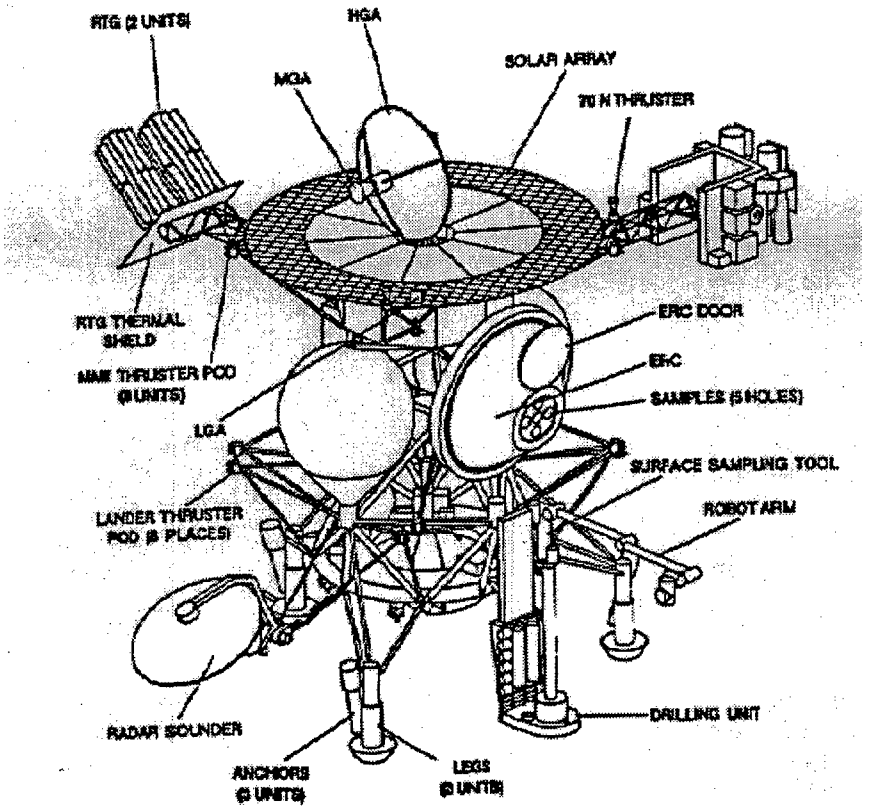


**Figure A.1 Rosetta spacecraft**(rosettafig)

**Table A.1 Rosetta mass budget**(rosettamb)

| Dry masses | | Propellant masses | |
|---|---|---|---|
| Cruise module | 1523 kg | Bi-liquid | 3513 kg |
| Lander | 474 kg | Hydrazine | 68 kg |
| Earth-Return capsule | 297 kg | Cold gas | 39 kg |
| Launcher adapter | 153 kg | | |
| **Totals** | **2447 kg** | | **3611 kg** |

## A.2 Near Earth Asteroid Rendezvous (NEAR)

The Near Earth Asteroid Rendezvous (NEAR) is one of a series of small interplanetary exploration missions in NASA's Discovery program. According to Cheng (10), the primary scientific goals of the mission are to characterize an asteroid's physical (e.g. density, shape, spin state) and geological (e.g. elemental and mineralogical composition, surface morphology) properties, which will require an observation and measurement period of several months.

NEAR is currently under construction at Johns Hopkins APL, and is designed with robustness and simplicity in mind. It is in the shape of an octagonal prism 1.7 meters on a side, and has four fixed gallium arsenide solar panels providing the 70 W of power required by the science payload (25). Like Rosetta, it is also three-axis stabilized and uses chemical propellant for propulsion and attitude control.

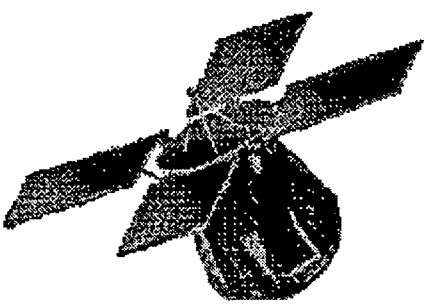

**Figure 2 NEAR spacecraft** (nearfig)

NEAR is scheduled for a February 1996 launch on a Delta II-7925 booster into a heliocentric transfer orbit toward asteroid 2968 Iliya. After NEAR performs the Iliya flyby in August 1996, it will continue on a delta VEGA trajectory past the earth in January 1998, prior to rendezvous with asteroid 433 Eros in January 1999 (10)(25). The total $\Delta V$ for this mission is 5.548 km/s and the C3 is 25.604 $km^2/s^2$.

NEAR will be placed into a 50 km altitude orbit around Eros, which is approximately 36 x 15 x 13 kilometers in dimension, and observe the asteroid for one year. The science package includes a visible imager, X-ray and gamma ray spectrometer, near-IR spectrograph, magnetometer, laser altimeter, and two-way Doppler radar. NEAR is limited to a total wet mass of 805 kg due to the launch capabilities of the Delta II-7925 for this mission.

## A.3 Clementine

Clementine was designed, built, and integrated by the Naval Research Laboratory (NRL) as a joint Ballistic Missile Defense Organization (BMDO) and NASA venture. The primary mission objectives were to test advanced lightweight technologies on a long duration flight, with a secondary mission of science return (i.e. digitally mapping the surface of the moon). The production of the spacecraft was also intended to demonstrate the capability to produce "better, faster, cheaper" spacecraft through streamlined systems engineering and program management (16).

Clementine was constructed of a machined aluminum subfloor with two decks and eight aluminum honeycomb panels containing the electronics. Eight aluminum longerons provided additional stiffness, and two solar panels provided 360 W in earth orbit (Figure A.3). The spacecraft dry mass was approximately 490 lbs (223 kg), and its wet mass was 424 kg (16)(17). This resulted in a launch mass budget as shown in Table A.2 .

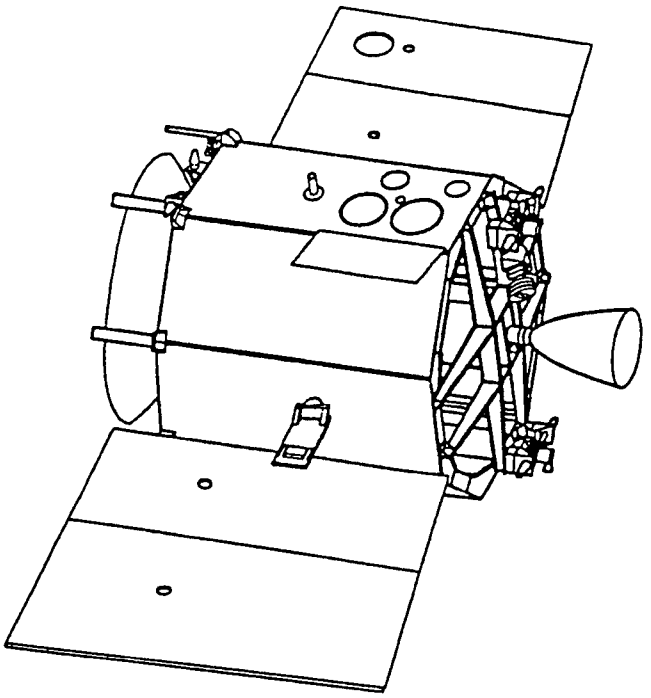

**Figure A.3 Clementine spacecraft.**(clemfig)

**Table A.2 Clementine mass budget.**

| | |
|---|---|
| Spacecraft dry mass | 490 lbs (223 kg) |
| Star 37FM Solid Rocket Motor (SRM) | 2500 lbs (1136 kg) |
| Interstage adapter (for SRM) | 80 lbs (36 kg) |
| Payload adapter | 85 lbs (39 kg) |
| Propellant | (201 kg) |
| **Totals** | **1635 kg** |

The mission was designed to have four phases, launch to LEO (one to seven days), transfer trajectory to lunar orbit insertion (27 days), lunar mapping (two months), and a transfer to asteroid 1620 Geographos (four months). Clementine launched from Vandenberg AFB on a Titan II-G [a former ballistic missile] on 25 January 1994 and entered LEO. The payload was spun up to 60 RPM in preparation for the SRM burn, and after insertion into the transfer orbit, was despun and the solar arrays deployed. The SRM and interstage adapter then separated into a highly elliptical earth orbit to perform a radiation and particle detection experiment, and the spacecraft continued on, entering lunar orbit on 19 February 1994. Clementine's mission effectively ended on 7 May 1995, after completion of the lunar survey, when four of its attitude thrusters fired all of their propellant and spun the craft up to 80 RPM (15).

The science payload consists of two star tracker cameras, a UV/visible camera, near-IR camera, long-wave IR camera, high resolution camera, laser transmitter, charged particle telescope, and dosimeters. The interstage assembly included a radiation experiment and meteoroid counting experiment. The science payload amounted to some 8.0 kg, and required only 67.8 W, according to the summary description provided by Hyman(17).

Clementine proved so successful at such a low cost that a Clementine II mission is under construction by NRL and Johns Hopkins. Again, science return is a secondary mission; the primary purpose is to test BMDO tracking, interception, and intercept vehicle technology on "cold targets" in a treaty-compliant manner. Clementine II will launch three interceptors at three different asteroidal targets. Compositional data will be gathered by a mass spectrometer as Clementine II flies through the debris cloud generated by each impact.

## A.4 Near Earth Asteroid Rendezvous and Sampling (NEARS).

NEARS is a derivative of the NEAR mission described in section A.1.2, and is part of NASA's Discovery program . The NEARS mission will essentially use the NEAR

spacecraft design, but replace the science payload with only that instrumentation needed for landing and sample collection (34). Again, this requires some observation of the asteroid to determine its shape, mass, rotation rate, and assessment of sampling sites, so medium resolution images of the surface will be taken. The mission profile is similar to that of NEAR, except for an additional landing and sampling requirement.

The goal is to return 10-100 grams of material from each of four to six sites on a NEA, using a "six-shooter" pyrotechnic sampling device under development at Johns Hopkins APL. The spacecraft will only make momentary contact with the surface; the sampling tube will penetrate the asteroid, secure a sample, and rebound on a tether to NEARS. Samples will return to earth in an Earth Return Capsule (ERC) by Martin Marietta Astrospace, and will deorbit via aerobraking.

# APPENDIX B: Calculations

## B.1 Basic orbital equations..

The following equations are taken from *Fundamentals of Astrodynamics*, by Bate, Mueller, and White (5).

Periapsis and apoapsis

$$r_{periapsis} = a(1-e)$$
$$r_{apoapsis} = a(1+e) \quad \text{(B.1)}$$

Specific mechanical energy

$$\mathcal{E} = \frac{v^2}{2} - \frac{\mu}{r} \quad \text{(B.2)}$$

Specific mechanical energy

$$\mathcal{E} = -\frac{\mu}{2a} \quad \text{(B.3)}$$

Period

$$\mathcal{T} = \frac{2\pi}{\sqrt{\mu}} a^{\frac{3}{2}} \quad \text{(B.4)}$$

Circular orbit speed

$$v_{circular} = \sqrt{\frac{\mu}{r}} \quad \text{(B.5)}$$

Escape speed

$$v_{escape} = \sqrt{\frac{2\mu}{r}} \quad \text{(B.6)}$$

Gravitational sphere of influence

$$\frac{r_{asteroid}}{R_{sun}} = \left( \frac{m_{asteroid}}{m_{sun}} \right)^{\frac{2}{5}} \quad \text{(B.7)}$$

## B.2 Selection of an appropriate inertial reference frame.

Figure B.1 shows the relative magnitude of inertial accelerations for objects in circular orbit around 1-10 kilometer diameter asteroids (density $\rho = 3.0$ g/cm$^3$ ) when the asteroid body frame is considered inertial. This is based on a similar example (18:104) which showed that lunar motion is poorly represented by an earth centered inertial reference frame. The gravitational acceleration due to the sun at 1.0 AU ($5.91 \times 10^{-6}$ km/s$^2$) is significant, even for our largest asteroid case, so it is apparent that the equations

of motion must be built around a heliocentric inertial reference frame. The earth's gravitation dominates the inertial acceleration in LEO applications, so the assumption of the earth as an inertial reference frame for low earth orbit satellites is still valid.

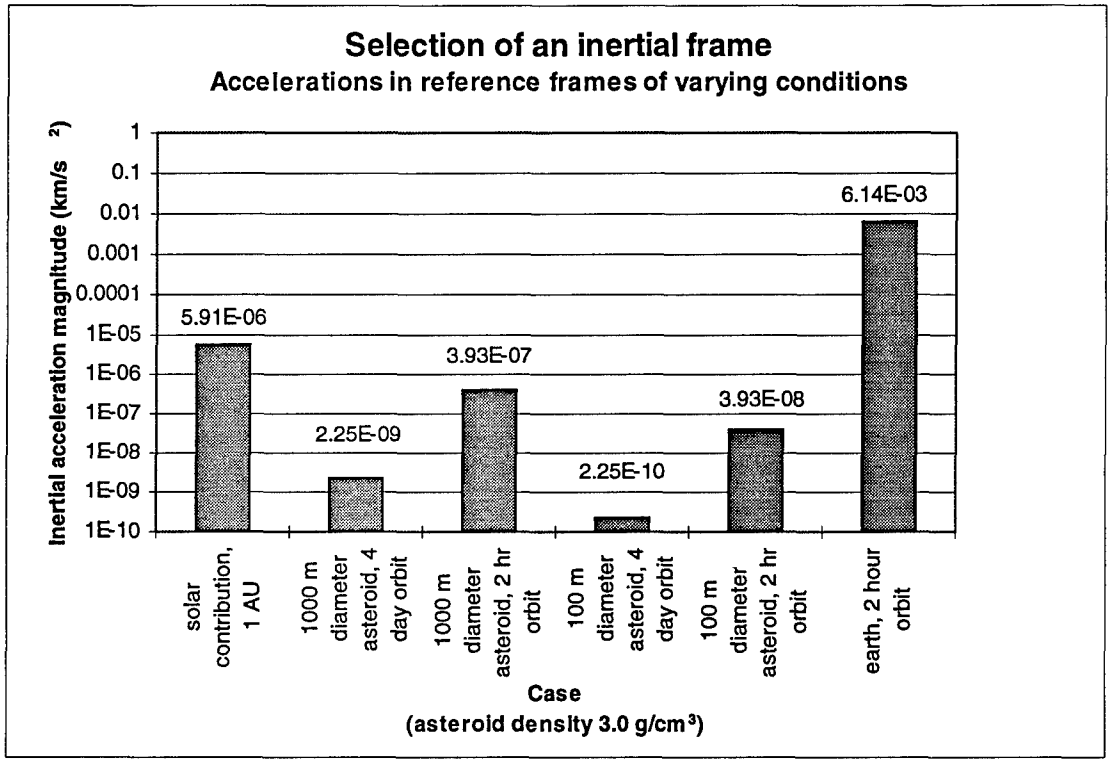


**Figure B.1 Accelerations due to choice of reference frame**

## B.3 Equations of motion in a heliocentric reference frame.

Referring to Figure B.2, we will use a heliocentric inertial reference frame [s], around which the asteroid revolves at angular rate $\Omega$, and a body-fixed reference frame [a], which is fixed at the center of mass of the asteroid with the unit vector $a_3$ aligned with principal axes. The asteroid rotates at angular rate $\omega$ and has a spacecraft of mass m in orbit. In this depiction, the position vector $Ru_R$ defines the position of [a] with respect to [s], and $ru_r$ defines the position of the spacecraft in orbit around the asteroid with respect to the [a] frame.

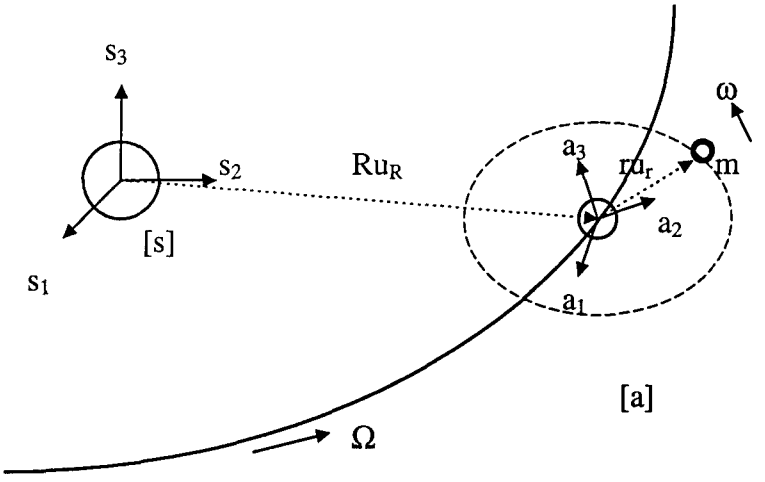


**Figure B.2 Inertial reference frames**

To simplify the problem, assume that [a] is in a circular heliocentric orbit in the equatorial plane of [s], and that the spacecraft is in (approximately) circular equatorial orbit with respect to [a]. We will make the further assumption that R=1.0 AU, so that $\Omega$=1.99 x $10^{-7}$ radians/second, and because of the relative distances involved, that the magnitude of the gravitational acceleration of the sun, $g_{sun}$, is constant on both the asteroid and spacecraft in orbit. Thus, we note the following inertial relationships:

$$\begin{aligned}
\vec{R}^{ms} &= R\hat{u}_R + r\hat{u}_r = \vec{R}^{as} + \vec{r}^{ma} \\
\dot{\vec{R}}^{ms} &= \dot{\vec{R}}^{as} + \dot{\vec{r}}^{ma} + (\Omega+\omega)\times\dot{\vec{r}}^{ma} \\
\ddot{\vec{R}}^{ms} &= \ddot{\vec{R}}^{as} + \ddot{\vec{r}}^{ma} + 2(\Omega+\omega)\times\dot{\vec{r}}^{ma} + \\
&\quad (\dot{\Omega}+\dot{\omega})\times\vec{r}^{ma} + (\Omega+\omega)\times\left((\Omega+\omega)\times\vec{r}^{ma}\right)
\end{aligned} \tag{B.8}$$

By inspection, we can also write down the following equations:

$$R\hat{u}_R = R\cos(\Omega t + \Omega_0)\hat{s}_1 + R\sin(\Omega t + \Omega_0)\hat{s}_2 \tag{B.9}$$

$$r\hat{u}_r = r\cos(\omega t + \omega_0)\hat{a}_1 + r\sin(\omega t + \omega_0)\hat{a}_2 \tag{B.10}$$

The position of the spacecraft in [a] can be related by a Euler rotation to the inertial frame [s]. If we use a 3-1-3 rotation [C] through the angles $\psi$, $\theta$, and $\varphi$ (this is not the same $\theta$ we use to denote the in-plane swinging angle of the tethered spacecraft and lander) to transform from [s] to [a], then

$$[a] = [C][s] \tag{B.11}$$

where

$$\psi = \Omega t + \Omega_0$$
$$\varphi = \omega t + \omega_0$$

and [C] is defined as (11:6):

$$C = \begin{bmatrix} \cos\varphi\cos\psi - \sin\varphi\cos\theta\sin\psi & \cos\varphi\sin\psi + \sin\varphi\cos\theta\cos\psi & \sin\varphi\cos\theta \\ -\sin\varphi\cos\psi - \cos\varphi\cos\theta\sin\psi & -\sin\varphi\cos\psi + \cos\varphi\cos\theta\cos\psi & \cos\varphi\sin\theta \\ \sin\theta\sin\psi & -\sin\theta\cos\psi & \cos\theta \end{bmatrix} \tag{B.12}$$

Additionally, the angular rates can be written as (11:7):

$$\begin{pmatrix} \dot{\psi} \\ \dot{\varphi} \\ \dot{\theta} \end{pmatrix} = \frac{1}{\sin\theta} \begin{pmatrix} \sin\varphi & \cos\varphi & 0 \\ -\sin\varphi\cos\theta & -\cos\varphi\cos\theta & \sin\theta \\ \cos\varphi\sin\theta & -\sin\varphi\sin\theta & 0 \end{pmatrix} \begin{pmatrix} \omega_1 \\ \omega_2 \\ \omega_3 \end{pmatrix} \tag{B.13}$$

Note that there is a singularity at $\theta$=0. Since we specified that the asteroid is rotating about the $a_3$ axis, then $a_3$ is fixed in inertial space at an angle of $\theta$ with respect to $s_3$, and we could simplify Equation B.13 to

$$\dot{\varphi} = \omega_3 \tag{B.14}$$

The acceleration of the spacecraft, m, with respect to inertial space can be found by adding the acceleration terms in Equation B.8. First, the inertial derivative of $Ru_R$ (Equation B.9) is clearly

$$\ddot{\vec{R}}^{as} = -\Omega^2 R\cos(\Omega t + \Omega_0)\hat{s}_1 - \Omega^2 R\sin(\Omega t + \Omega_0)\hat{s}_2 \qquad \text{(B.15)}$$

However, we must acknowledge that the center of mass of the tethered spacecraft-lander system will probably move through some out-of-plane angle $\phi$ during its orbit around the asteroid in reference frame [a], as in Figure B.3 below. Moreover, we do not know if the scalar magnitude of $ru_r$ is constant, so we will have to arrange the equations to take this into consideration.

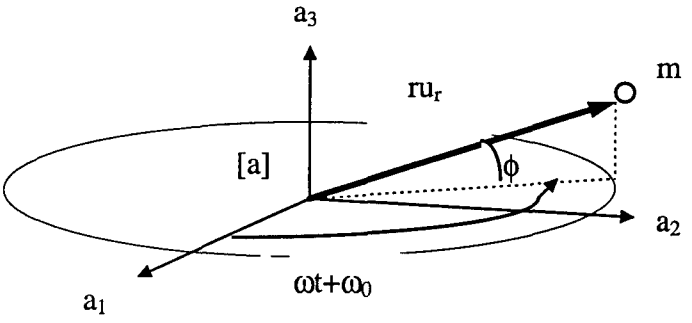


**Figure B.3 Spacecraft center of mass motion**

Thus, we note that

$$\vec{r}^{ma} = r\cos\phi\cos(\omega t + \omega_0)\hat{a}_1 + r\cos\phi\sin(\omega t + \omega_0)\hat{a}_2 + r\sin\phi\,\hat{a}_3 \qquad \text{(B.16)}$$

$$\dot{\bar{r}}^{ma} = \begin{bmatrix} \dot{r}\cos\phi\cos(\omega t+\omega_0)+ \\ r[-\dot{\phi}\sin\phi\cos(\omega t+\omega_0)-\omega\cos\phi\sin(\omega t+\omega_0)] \\ \\ \dot{r}\cos\phi\sin(\omega t+\omega_0)+ \\ r[-\dot{\phi}\sin\phi\sin(\omega t+\omega_0)+\omega\cos\phi\cos(\omega t+\omega_0)] \\ \\ \dot{r}\sin\phi+\dot{\phi}r\cos \end{bmatrix} \begin{bmatrix} \hat{a}_1 \\ \hat{a}_2 \\ \hat{a}_3 \end{bmatrix}^T \tag{B.17}$$

$$\ddot{\bar{r}}^{ma} = \begin{bmatrix} \ddot{r}\cos\phi\cos(\omega t+\omega_0)+ \\ 2\dot{r}[-\dot{\phi}\sin\phi\cos(\omega t+\omega_0)-\omega\cos\phi\sin(\omega t+\omega_0)]+ \\ r\begin{Bmatrix} -\ddot{\phi}\sin\phi\cos(\omega t+\omega_0)+ \\ -\dot{\phi}[\dot{\phi}\cos\phi\cos(\omega t+\omega_0)-\omega\sin\phi\sin(\omega t+\omega_0)]+ \\ [\omega\dot{\phi}\sin\phi\sin(\omega t+\omega_0)-\omega^2\cos\phi\cos(\omega t+\omega_0)] \end{Bmatrix} \\ \\ \ddot{r}\cos\phi\sin(\omega t+\omega_0)+ \\ 2\dot{r}[-\dot{\phi}\sin\phi\sin(\omega t+\omega_0)+\omega\cos\phi\cos(\omega t+\omega_0)]+ \\ r\begin{Bmatrix} -\ddot{\phi}\sin\phi\cos(\omega t+\omega_0)+ \\ -\dot{\phi}[\dot{\phi}\cos\phi\sin(\omega t+\omega_0)+\omega\sin\phi\cos(\omega t+\omega_0)]+ \\ -[\omega\dot{\phi}\sin\phi\cos(\omega t+\omega_0)+\omega^2\cos\phi\sin(\omega t+\omega_0)] \end{Bmatrix} \\ \\ \ddot{r}\sin\phi+\dot{r}\dot{\phi}\cos\phi+\ddot{\phi}r\cos\phi+\dot{\phi}(\dot{r}\cos\phi-\dot{\phi}r\sin\phi) \end{bmatrix} \begin{bmatrix} \hat{a}_1 \\ \hat{a}_2 \\ \hat{a}_3 \end{bmatrix}^T \tag{B.18}$$

Equation B.18 provides the effects of a rotating coordinate frame around [a]. We could now write our the equations of motion in the heliocentric inertial frame by substituting Equation B.15 and Equation B.18 into Equations B.8. However, a great deal of literature exists for tether equations of motion based on an earth centered inertial frame (see next section), so if we could find a correction factor to adapt the equations to a heliocentric frame, we could build on that work. Therefore, we will rewrite Equations B.8 as follows:

$$\ddot{\bar{r}}^{ma} = \ddot{\bar{R}}^{ms} - \ddot{\bar{R}}^{as} - 2(\Omega+\omega)\times\dot{\bar{r}}^{ma} - \left(\dot{\Omega}+\dot{\omega}\right)\times\bar{r}^{ma} - (\Omega+\omega)\times\left((\Omega+\omega)\times\bar{r}^{ma}\right) \tag{B.19}$$

If we had assumed the [a] frame was inertial, and the body m was only accelerated by gravity, then:

$$\ddot{\vec{r}}^{ma} = \vec{g}_{asteroid} - 2\omega \times \dot{\vec{r}}^{ma} - \dot{\omega} \times \vec{r}^{ma} - \omega \times \left(\omega \times \vec{r}^{ma}\right) \tag{B.20}$$

Subtracting the two gives us a heliocentric inertial frame correction factor to the equations of motion in the literature.

$$Inertial\_correction = \ddot{\vec{R}}^{ms} - \ddot{\vec{R}}^{as} - \vec{g}_{asteroid} - 2\Omega \times \dot{\vec{r}}^{ma} - \dot{\Omega} \times \vec{r}^{ma} - \Omega \times \left(\Omega \times \vec{r}^{ma}\right) \tag{B.21}$$

Equation B.21 represents the time-dependent inertial corrections to equations of motion for an asteroid centered reference frame. This term must be added into the asteroid centered equations of motion to compensate for the gravitational acceleration of the sun and resulting Coriolis forces on the spacecraft in heliocentric orbit.

The maximum Coriolis force, $2\Omega\times(\omega r^{ma})$, on the spacecraft occurs when the spacecraft velocity vector $\omega\times r$ is perpendicular to the angular velocity vector of the heliocentric orbit, $\Omega$. Thus, a spacecraft in a two hour orbit (16.1 meters altitude) over a 1000 meter diameter asteroid could experience a Coriolis acceleration of up to $1.72 \times 10^{-7}$ $m/s^2$ due to the sun at 1 AU. Figure B.4 illustrates the maximum Coriolis accelerations that could be experienced around asteroids in equatorial heliocentric orbit.

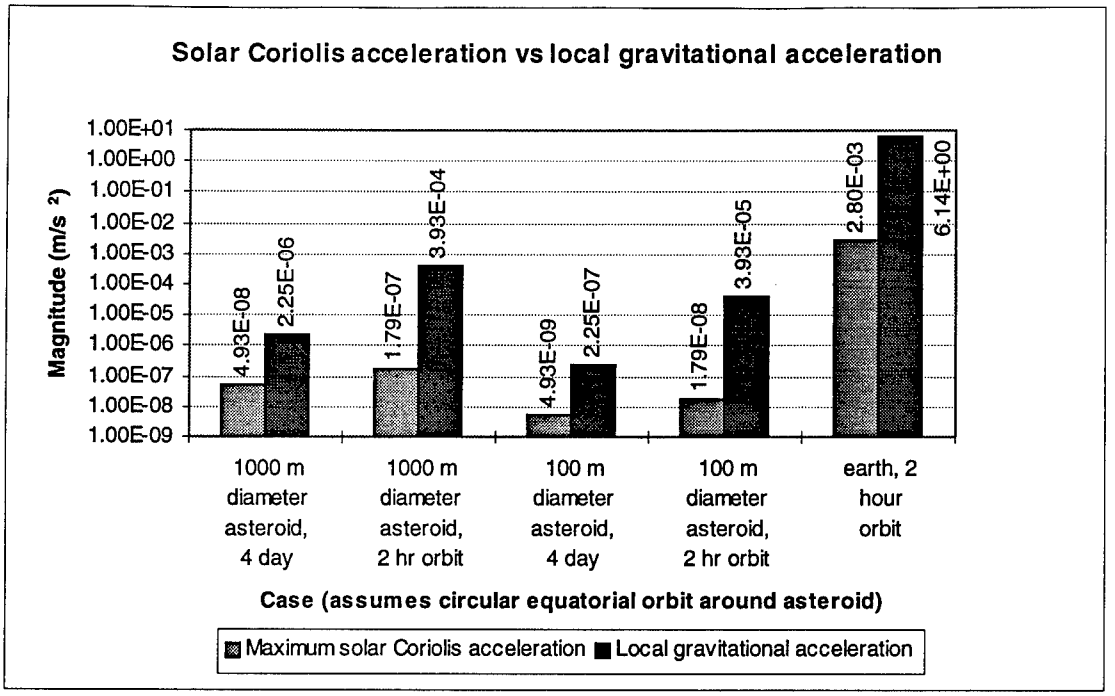


**Figure B.4 Solar Coriolis acceleration on a spacecraft in orbit**

## B.4 Equations of motion for a tethered system.

The various papers and literature on tethered systems share one feature which will make analysis much simpler—they assume that the primary body is much more massive than the deployed body, and thus does not move much from its original circular orbit during deployment. Since these equations are equally valid for deployment toward or away from a central body, we will use this assumption later (when the lander is attached to the asteroid) to presume that the massive primary body at the surface of our spherical asteroid, and the deployed body is the spacecraft in orbit.

This section summarizes the derivation of the equations of motion for a massless, flexible tether, as presented by Beletsky and Levin (6:62). At the end of the derivation, we will add the time-dependent correction to an inertial frame (Equation B.21) as a perturbing "force". The equations are numerically integrated in Chapter 4 to show the angular and positional histories of the tether and deployed end body.

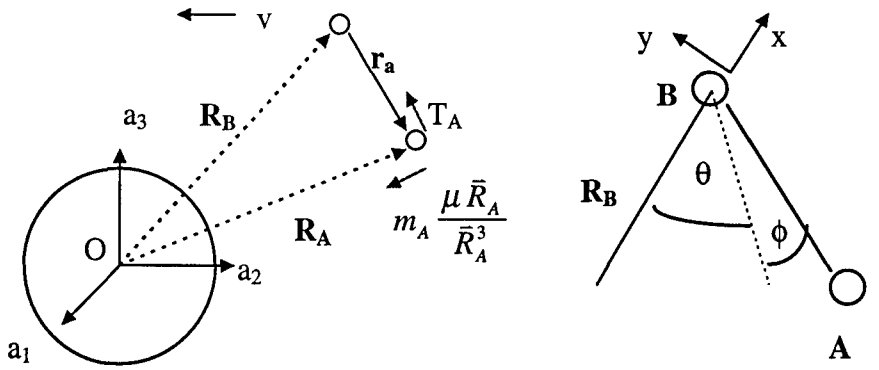


**Figure B.5 Reference frames for tether motion**(fig36)

The assumption of a massless, perfectly flexible tether is a common assumption used to simplify theoretical and engineering analyses of tethered systems (6). We will also assume that there are no forces acting on either end body other than gravity or thrust. Figure B.5 shows an orbital reference frame attached to body B such that $B_x$ points outward along the radius vector, and $B_y$ is in the direction of the velocity vector. The choice of this reference system, as opposed to a center of mass system for the two end bodies, is largely due to the observability of the bodies. Starting with some definitions:

$$\sum \vec{F} = m\ddot{\vec{r}} \tag{B.22}$$

$$\vec{F} = \frac{d}{dt}(m\vec{v}) \tag{B.23}$$

the motion of body A in the inertial frame is affected by the forces of tension (T), gravity, and other perturbing forces ($F_A$, which could include thrusting):

$$m_A \ddot{\vec{r}}_A = T_A - m_A \frac{\mu \bar{R}_A}{\bar{R}_A^3} + \vec{F}_A \tag{B.24}$$

Bringing the terms with the mass of A to the left side, and substituting in body frame derivatives to get the relative motion of A with respect to B:

$$m_A\left[\ddot{\vec{r}}_A+\dot{\vec{\omega}}\times\vec{r}_A+2\vec{\omega}\times\vec{r}_A+\vec{\omega}\times\left(\vec{\omega}\times\vec{r}_A\right)+\ddot{\vec{R}}_B+\frac{\mu\vec{R}_A}{\vec{R}_A^3}\right]=T_A+F_A \tag{B.25}$$

Note that the derivatives of $r_A$ in Equation 3.16 are now with respect to the body frame, whereas the term for $R_B$ is still an inertial derivative. Since the tether system is in orbit, we may assume that

$$\ddot{\vec{R}}_B=-\frac{\mu\vec{R}_B}{\vec{R}_B^3} \tag{B.26}$$

and the linear approximation of the gravity difference is

$$\frac{\vec{R}_A}{R_A^3}-\frac{\vec{R}_B}{R_B^3}\cong\frac{\vec{r}_A}{R_B^3}-3\left(\vec{r}_A\cdot\vec{R}_B\right)\frac{\vec{R}_B}{R_B^5} \tag{B.27}$$

We now replace $r_A$=(x,y,z) with expressions using the in-plane (θ) and out-of-plane (ϕ) angles, and the tether length *r*.

$$\begin{aligned}x&=-r\cos\theta\cos\phi\\y&=-r\sin\theta\cos\phi\\z&=-r\sin\phi\end{aligned} \tag{B.28}$$

Beletsky and Levin convert the equations to orbital parameters of eccentricity e, focal parameter p, and true anomaly ν, to arrive at rectilinear equations of motion (6:63):

$$\begin{pmatrix} \ddot{x} - 2\dot{y}\omega - \dot{\omega}y - (1+2\eta^{-1})\omega^2 x \\ \ddot{y} + 2\dot{x}\omega + \dot{\omega}x - (1-\eta^{-1})\omega^2 y \\ \ddot{z} + \eta^{-1}\omega^2 z \end{pmatrix} = \frac{1}{m_A}\begin{pmatrix} T_x + F_x \\ T_y + F_y \\ T_z + F_z \end{pmatrix} \tag{B.29}$$

where

$$\eta = 1 + e\cos\nu$$

$$\omega = \dot{\nu} = \eta^2\sqrt{\frac{\mu}{p^3}}$$

or in spherical coordinates (6:65)

$$\begin{aligned} &\ddot{\theta} + \dot{\omega} + (\dot{\theta}+\omega)\left(\frac{2\dot{r}}{r} - 2\dot{\phi}\tan\phi\right) + \frac{3\omega^2}{\eta}\sin\theta\cos\phi = -\frac{F_\theta}{m_A r\cos\phi} \\ &\ddot{\phi} + \frac{2\dot{r}}{r}\dot{\phi} + \left[(\dot{\theta}+\omega)^2 + \frac{3\omega^2}{\eta}\cos^2\theta\right]\sin\phi\cos\phi = -\frac{F_\phi}{m_A r} \\ &\ddot{r} - r\left[\dot{\phi}^2 + (\dot{\theta}+\omega)^2\cos^2\phi + \frac{\omega^2}{\eta}(3\cos^2\phi\cos^2\theta - 1)\right] + \frac{T}{m_A} = -\frac{F_r}{m_A} \end{aligned} \tag{B.30}$$

where

$$\begin{pmatrix} F_r \\ F_\theta \\ F_\phi \end{pmatrix} = \begin{pmatrix} \cos\theta\cos\phi & \sin\theta\cos\phi & \sin\phi \\ -\sin\theta & \cos\theta & 0 \\ -\cos\theta\sin\phi & -\sin\theta\sin\phi & \cos\phi \end{pmatrix}\begin{pmatrix} F_x \\ F_y \\ F_z \end{pmatrix}$$

These equations describe the relative motion of end body A with respect to the orbiting reference frame attached to body B. In our case, body A will represent the deployed sampling device, and body B will be the spacecraft in orbit. If we recall that this not truly an inertial frame, then we must add in the inertial correction for the sun by multiplying the spacecraft mass into Equation B.21 to determine the perturbing force F.

### B.4.1 Tensioned deployment.

Equation B.30 may be rewritten as:

$$\ddot{\theta}+\dot{\omega}+(\dot{\theta}+\omega)\left(\frac{2\dot{r}}{r}-2\dot{\phi}\tan\phi\right)+\frac{3\omega^2}{\eta}\sin\theta\cos\phi=-\frac{F_\theta}{m_A r\cos\phi}$$

$$\ddot{\phi}+\frac{2\dot{r}}{r}\dot{\phi}+\left[(\dot{\theta}+\omega)^2+\frac{3\omega^2}{\eta}\cos^2\theta\right]\sin\phi\cos\phi=-\frac{F_\phi}{m_A r} \qquad \text{(B.31)}$$

$$\ddot{r}-r\left[\dot{\phi}^2+(\dot{\theta}+\omega)^2\cos^2\phi+\frac{\omega^2}{\eta}(3\cos^2\phi\cos^2\theta-1)\right]+\frac{T}{m_A}=-\frac{F_r}{m_A}$$

with the quantities

$$u=\dot{\phi}^2+(\dot{\theta}+1)^2\cos\ \phi+\frac{1}{\eta}(3\cos^2\phi\cos^2\theta-1)$$

$$\psi=\frac{\dot{r}}{r}-\frac{e\sin\theta}{\eta} \qquad \text{(B.32)}$$

$$\eta=1+e\cos\theta$$

where e=orbit eccentricity, ν=true anomaly of spacecraft, θ=in-plane angle, ϕ=out-of=plane angle, and r= distance between the spacecraft and subsatellite. To integrate these equations, we must reduce them to a set of first order differential equations. We will assume e=0 and make the following substitutions:

$$\begin{aligned} x_1&=\theta \\ x_2&=\dot{\theta} \\ x_3&=\phi \\ x_4&=\dot{\phi} \\ x_5&=r \\ x_6&=\dot{r} \end{aligned} \qquad \text{(B.33)}$$

to get

$$
\begin{aligned}
\dot{x}_1 &= x_2 \\
\dot{x}_2 &= -2(x_2+1)(\psi - x_4 \tan x_3) - 3\sin x_1 \cos x_1 - \frac{F_\theta}{m_A x_5 \cos x_3} \\
\dot{x}_3 &= x_4 \\
\dot{x}_4 &= -2\psi x_4 - \sin x_3 \cos x_3 \left[(x_2+1)^2 + 3\cos^2 x_1\right] - \frac{F_\phi}{m_A x_5} \\
\dot{x}_5 &= x_6 \\
\dot{x}_6 &= x_5\left[x_4^2 + (x_2+\omega)^2 \cos^2 x_3 + \omega^2(3\cos^2 x_3 \cos^2 x_1 - 1)\right] - \frac{T}{m_A} - \frac{F_r}{m_A} \\
\psi &= \frac{x_6}{x_5}
\end{aligned}
\tag{B.34}
$$

and F is given numerically by application of Equation B.21 and Equation B.30. Beletsky and Levin also note (6:362) that the tension in the tether is given by:

$$T = m_A \omega \ell u \tag{B.35}$$

where $m_A$ is the mass of the deployed body, $\omega$ is the orbital rate, $\ell$ is the length of the tether, and u is the quantity given in Equation B.32. Note that tension is only maintained as long as u>0.

### B.4.2 Attachment to asteroid.

Once deployment and attachment take place, the spacecraft in orbit must remain in place for up to 21 days (29). This requires the use of Equation B.18 with the heliocentric correction (Equation B.21) derived in section B.2. Once again, assuming a massless tether, the center of mass of the spacecraft and lander remained in circular synchronous orbit until the lander attached to the asteroid. At that instant, the spacecraft is still traveling at synchronous orbit rate $\omega$, but at a higher altitude governed by the proportionality of the spacecraft and lander masses. This difference is given by:

$$r' = \frac{m_{lander}}{m_{spacecraft} + m_{lander}} l_{tether} \tag{B.36}$$

A spacecraft in a four hour orbit around a 1000 meter asteroid ($\rho$ = 3.0 g/cm$^3$) is at 320 meters altitude over the surface. Using our point design figures, where $m_{lander}$=120 kg, and $m_{spacecraft}$=700 kg, at the moment of attachment to the asteroid, the center of mass of the spacecraft and lander is still at 320 meters altitude, but the length of the tether (and altitude of the spacecraft) is 373.7 meters. This will be our notional test case.

Now, Equation B.18 was developed from Figure B.3, which shows an out-of-plane angle $\phi$ from the center of the asteroid and reference frame ([a]). The out-of-plane angle, $\phi'$, between the spacecraft position (m) and the equatorial plane of the asteroid, with respect to the attachment point (a′), is easily found by geometry as in Figure B.6.

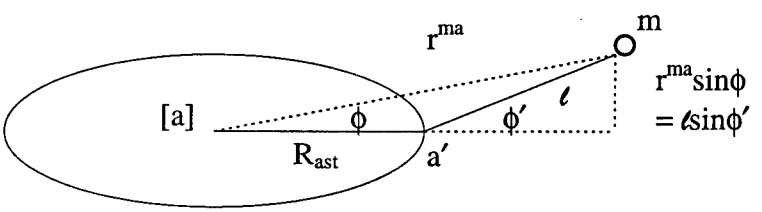


**Figure B.6 Attachment phase of operations**

By inspection, $\phi$ and $\phi'$ are unaffected by the in-plane angle $\theta$ that the spacecraft position makes with the line between the asteroid center and attachment point. Similarly, if we solve for the relationship between the in-plane angles, then $\theta$ (angle with respect to [a]) and $\theta'$ then we have the relationships ([a] on the left, a′ on the right):

$$\begin{aligned} r^{ma} \sin\phi &= \ell \sin\phi' \\ r^{ma} \cos\phi \sin\theta &= \ell \cos\phi' \sin\theta' \end{aligned} \tag{B.37}$$

The motion of the spacecraft should be modeled in the [a] reference frame, as one can easily detect whether the spacecraft eventually impacts the surface of the asteroid, which is when $r^{ma} = R_{asteroid}$. The other constraints are that the tether may not exceed length $\ell$, and for cases where the distance between the spacecraft and attachment point is less than $\ell$, the tension is zero.

However, there is a simpler way to model the spacecraft motion in orbit. Recall from Section B.4 that the primary body is assumed to be so massive that it stays in circular orbit at constant angular rate $\omega$; this allows us to invert the problem and assume that the lander, which is now attached to the asteroid, is the massive body. Thus, by constraining the length of the tether to never exceed $\ell$, and the deployment speed is zero, we can use the equations derived in the previous section.

### B.4.3 Crawler retrieval.

The problem of retrieving a deployed payload has been studied for low earth orbit applications, and normally amounts to reeling in the tethered payload using both a control law and some form of active damping (6)(22). Once the sample is acquired and attached to the tether, we certainly have the option of detaching the sample canister from the attached lander, then reeling it in by proven methods, as in the case of TSS-1. However, in keeping with the spirit of the SAIC proposal, suppose we kept the tether anchored to the lander and the orbiting spacecraft, and allowed the sample canister to "crawl" up the tether? We will adapt a procedure from the literature to see if there an advantage to this approach.

Ronald Glickman and Samuel Rybak (14:317-337) addressed this problem for a spacecraft with a deployed payload in low earth orbit. They assumed a massive primary body in circular orbit at rate $\Omega$, with a payload of mass $m_p$ deployed at a distance +y towards the earth, as shown in Figure B.7 . The orbiting reference frame (tether aligned)

was oriented with -z roughly in the direction of the velocity vector, y along the tether in a nadir direction, and x forming an orthogonal triad. The in-plane angle the tether formed with the nadir was denoted θ, and the out-of-plane angle labeled ϕ.

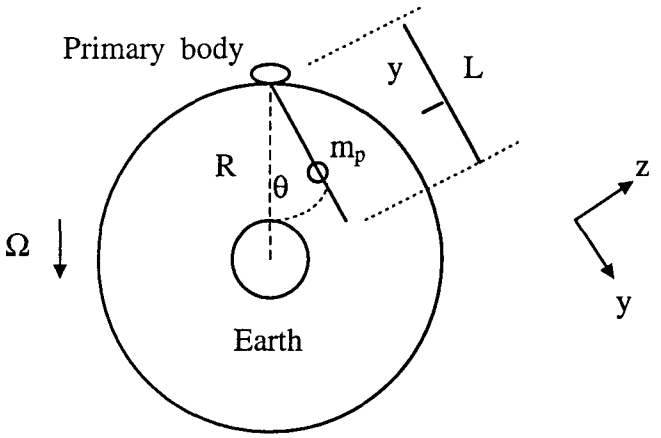


**Figure B.7 Glickman and Rybak reference frame**

After summing the torques on the attachment point to the primary body, and transforming the nadir oriented frame to the tether-aligned frame, they developed a pair of coupled, nonlinear differential equations to describe in-plane (Equation B.38) and out-of-plane (Equation B.39) motion for a crawler system:

$$(3m_p y^2 + \rho AL^3)\Omega^2 \sin\theta\cos\theta\cos\phi + \left(m_p y^2 + \frac{\rho AL^3}{3}\right)\left(\ddot{\theta}\cos\phi - 2(\Omega+\dot{\theta})\dot{\phi}\sin\phi\right) + 2m_p y\dot{y}(\Omega+\dot{\theta})\cos\phi = 0 \quad \text{(B.38)}$$

$$(3m_p y^2 + \rho AL^3)\Omega^2 \cos^2\theta\sin\phi\cos\phi + \left(m_p y^2 + \frac{\rho AL^3}{3}\right)\left(\ddot{\phi} + (\Omega+\dot{\theta})^2\sin\phi\cos\phi\right) + 2m_p y\dot{y}\dot{\phi} = 0 \quad \text{(B.39)}$$

where the $m_p$ is the deployed payload mass and the tether has mass density ρ, area A and a fixed length L, which is assumed to be deployed. Glickman and Rybak examine a situation using a constant in-plane "equilibrium hangoff angle" (EHA), which is an "instantaneous" non-swinging solution for constant θ by tailoring $y\dot{y}$ in the coriolis terms. They first rearrange Equation B.38 for $\phi = 0$ and $\dot{\phi} = 0$ to get

$$\left(m_p y^2 + \frac{\rho A L^3}{3}\right)\ddot{\theta} = -2m_p y\dot{y}(\Omega + \dot{\theta}) - \frac{1}{2}\left(3m_p y^2 + \frac{\rho A L^3}{3}\right)\Omega^2 \sin 2\theta \qquad \text{(B.40)}$$

then, with the assumption that we tailor $\dot{y}$ to give non-swinging values (ie $\dot{\theta} = \ddot{\theta} = 0$),

$$\sin 2\theta_{EHA} = -\frac{2m_p y\dot{y}\Omega}{\frac{\Omega^2}{2}\left(3m_p y^2 + \rho A L^3\right)} \qquad \text{(B.41)}$$

which reduces to

$$\dot{y} = -\frac{\Omega}{4}\left(3y + \frac{\rho A L^3}{m_p y}\right)\sin 2\theta_{EHA} \qquad \text{(B.42)}$$

Now, Glickman and Rybak state (14:323) that the denominator of Equation B.41 has a tether mass gravity gradient term $(\Omega^2/2)\rho A L^3$ which causes a restoring moment regardless of the value of y. They also note that $\dot{y}$ must become quite large as y approaches zero in order to maintain a constant in-plane hangoff angle $\theta_{EHA}$. They term this feature of close-in retrieval as "gravity gradient enhancement".

This enhancement is notable because it provides a workaround to the normal exponential retrieval problem of very low closing speeds, as well as control of the in-

plane swinging of the tether. However, we must also note that the enhancement is most strongly influenced by the length L of the tether, which determines both the mass and inertial properties which stabilize this mode of retrieval. In fact, the example used in the literature assumed a tether of 100 km in length in earth orbit, which provided exceptionally favorable results for retrieval rates and stability. We are examining a short, very low mass tether, which is vastly different from the conditions in Glickman's paper.

To adapt this to our purposes, we will assume that the primary body from Figure B.7 is the lander, attached to the surface of our spherical asteroid of radius R at the equator. This then becomes a problem of *deploying* the sample canister away from the asteroid, which is easily handled by causing the crawler to travel in the new +y direction, which is along the tether pointing towards the orbiting spacecraft. Also, we note that the terms in the denominator of Equation B.41 are really the torques caused by the gravity gradient and moments of inertia of the lander and tether, so by analogy we may add in a term ($3m_{spacecraft}L^2$) to account for the restoring torques due to the spacecraft in orbit. This modifies Equation B.42 and gives

$$\dot{y} = -\frac{\Omega}{4}\left(3y + 3\frac{m_s L^2}{m_p y} + \frac{\rho A L^3}{m_p y}\right)\sin 2\theta_{EHA} \tag{B.43}$$

As for oscillatory buildup in the tether, one may intuitively expect the oscillations to decrease during this "deployment". Glickman and Rybak provided an analysis of oscillations based on the introduction of a coriolis control torque (14:329). Since control laws are beyond the scope of this thesis, the resulting equation is simply restated here:

$$\theta_{MAX}(n) = -\frac{\alpha}{3}\left\{1 - (-1)^n \exp\left[-\frac{\alpha n \pi \Omega}{2\omega}\right]\right\}, n = 1,2,3... \tag{B.44}$$

where

$$\omega = \Omega\sqrt{3 - \frac{\alpha^2}{4}}$$

$$\alpha = -3\theta_{EHA}$$

which are simply constants introduced for clarity. For retrieval, $\alpha<0$, or for deployment, $\alpha>0$, so from Equation B.44 there is an exponential increase in swing angle for retrieval, and an exponential decrease in swing angle for deployment. However, the increase in swing angle during retrieval is quite modest compared to the oscillatory buildup of a normal tether retrieval (14:329), and does not exceed about three degrees in their case of an eight hour retrieval over a 100 km tether.

# APPENDIX C: Matlab Programs

## C.1 Deployment.

The files used in the deployment integration are

| | |
|---|---|
| deploy1.m | Main program and plotting subroutines |
| deploy2.m | The ode45 integration routine |
| Fhistory.m | Plot option for heliocentric forces in orbiting frame |
| helio.m | Heliocentric "perturbing" forces |
| cross.m | Cross product (e.g. cross(*vector1*,*vector2*)) |

Only deploy1.m and deploy2.m are provided here—the others files are in section C.4.

---

```
%        Filename:  deploy1.m
%        Integrating the Levin and Beletsky equations with a
heliocentric correction
%
clear all;

global omegasuninit theta omega omegainit ma mspace muast r T Fhist;
omega=4.36e-4;            %2 hr--8.73e-4, 1 day = 7.27e-5, 4 day =
1.818e-5
omegasuninit=0; omegainit=0; ma=120; mspace=700; Fhist=[0 0 0 0];

% Problem parameters
initlength=.5; rho=1; diam=100;
G=6.67e-11; mass=4/3*pi*((diam/2)^3)*rho*1000;
muast=G*mass; r=(muast^.5/omega)^(2/3);


%give initial deployment speed and direction (specify in deg, m/s)
speed=0.1;
ejectiontheta=10; ejectionphi=10.0; %theta is in-plane angle from
vertical
ejectthetadot= 1.0; ejectphidot=1.0; %phi is out-of-plane angle
theta=ejectiontheta*pi/180; thetadot=ejectthetadot*pi/180;
phi=ejectionphi*pi/180;phidot=ejectphidot*pi/180;


% initial state vector for integration
X0=[theta thetadot phi phidot initlength speed];
t0=0; tf=180;

[t,X]=ode45('deploy2',t0,tf,X0);
```

---

```
%       Length vs. time in subplot 1, xdot and ydot for subplot 3
%       Postprocess X state vector to get total deployment length
for i=1:size(t);
r(i)=X(i,5);
exx(i)=X(i,5)*cos(X(i,3))*sin(X(i,1));
exxdot(i)=X(i,6)*cos(X(i,3))*sin(X(i,1)); ;
why(i)=X(i,5)*sin(X(i,3));
zee(i)=X(i,5)*cos(X(i,3))*cos(X(i,1));
whydot(i)=X(i,6)*cos(X(i,3))*cos(X(i,1)); ;
end
%

figure('Name','Tether displacement');
subplot(321), plot(t,exx,'g',t,why,'-b', t,r,'.r')
xlabel('time (sec)')
ylabel('displacement (m)')
title('(a) x- and y- history')
legend(['x (m), speed=',num2str(speed),' m/s '],['y (m),
theta=',num2str(ejectiontheta),' degrees'], ['total length (m)'])

subplot(322), plot(t,exxdot,'.g', t, whydot,'-.b')
xlabel('time (s)')
ylabel('speed (m/s)')
legend(['xdot (m/s)'],['ydot (m/s)'])
title('(b) xdot and ydot history')


subplot(325), plot(t, X(:,1)*180/pi,'g')
xlabel('time (s)')
ylabel('Angle (deg)')
legend(['theta, init=',num2str(ejectiontheta)])
title('(c) Theta')

subplot(326), plot(t, X(:,3)*180/pi,':r')
xlabel('time (s)')
ylabel('Angle (deg)')
legend(['phi, init=',num2str(ejectionphi)])
title('(d) Phi')


%       all plots won't all fit in one figure window, unfortunately
figure('Name','Angular displacement history');
subplot(321), plot(t, X(:,2)*180/pi,'g')
xlabel('time (s)')
ylabel('Angular rates (deg/s)')
legend(['thetadot, init=',num2str(ejectthetadot)])
title('(a) Thetadot')

subplot(322), plot(t, X(:,4)*180/pi,':r')
xlabel('time (s)')
ylabel('Angular rates (deg/s)')
legend(['phidot, init=',num2str(ejectphidot)])
title('(b) Phidot')

subplot(223), plot(X(:,1)*180/pi, X(:,2)*180/pi)
xlabel('Theta (degrees)')
ylabel('Thetadot (deg/s)')
title('(c) Phase plane plot of Theta vs Thetadot')
```

```
subplot(224), plot(X(:,3)*180/pi, X(:,4)*180/pi)
xlabel('Phi (degrees)')
ylabel('Phidot (deg/s)')
title('(d) Phase plane plot of Phi vs Phidot')

%Fhistory                %option to look at heliocentric factor
```

---

```
%     Integrating the Beletsky and Levin tether differential equations
with heliocentric terms
%     Filename:  deploy2.m
%
function Xdot=deploy2(t,X)
%
%X is [theta, thetadot,phi,phidot, r, rdot]

global  omegasuninit theta omega omegainit ma mspace muast r T Fhist;

F=helio(t,X);            %ugly, but you can't integrate these time
dependent equations otherwise
Fhist=[Fhist;t F'];      %comment out most of the time—it slows you down


Xdot(1)=X(2);
Xdot(2)=-2*(X(2)+1)*(X(6)/X(5) - X(4)*tan(X(3)))-3*sin(X(1))*cos(X(1))-
F(2)/(X(5)*cos(X(3)));
Xdot(3)=X(4);
Xdot(4)=-2*(X(6)/X(5))*X(4)-
sin(X(3))*cos(X(3))*((X(2)+1)^2+3*(cos(X(1)))^2)-F(3)/(X(5));
Xdot(5)=X(6);
Xdot(6)=omega*(X(4)^2+(X(2)+1)^2*(cos(X(3)))^2+3*(cos(X(3)))^2*(cos(X(1)
))^2-1)-T/ma -F(1);
```

## C.2 Attachment.

The equations for deployment are modified slightly to limit the tether to a "maxlength" and provide tension only when the tether is taut. The files used in the deployment integration are

| | |
|---|---|
| attach1.m | Main program and plotting subroutines |
| attach2.m | The ode45 integration routine |
| Fhistory.m | Plot option for heliocentric forces in orbiting frame |
| helio.m | Heliocentric "perturbing" forces |
| cross.m | Cross product (e.g. cross(*vector1*,*vector2*)) |

Only attach1.m and attach2.m are provided here—the others files are in section C.4.

```
%        Filename:  attach1.m
%        Attachment phase of operations EOM with a heliocentric
correction
%
clear all;

global omegasuninit theta omega omegainit mspace muast r T maxlength TT;
omega=4.36e-4;                %2 hr--8.73e-4, 1 day = 7.27e-5, 4 day =
1.818e-5
omegasuninit=0; omegainit=0; mspace=700;

% Give parameters
initlength=31.8; rho=1; diam=400; maxlength=initlength + 0.5;
G=6.67e-11; mass=4/3*pi*((diam/2)^3)*rho*1000; muast=G*mass;
r=(muast^.5/omega)^(2/3);
TT=[0 0];                                    %tension by time

% give initial conditions(specify in deg, m/s)
thetainit=190; thetadotinit=1;
phiinit=10;  phidotinit=1;
speed=.01;      %spherical coord, so speed is really "rdot"
theta=thetainit*pi/180; thetadot=thetadotinit*pi/180;
phi=phiinit*pi/180;phidot=phidotinit*pi/180;

% initial state vector for integration
X0=[theta thetadot phi phidot initlength speed];
t0=0; tf=1500;

[t,X]=ode45('attach2',t0,tf,X0);


%*********************  Postprocessing  ************************

for i=1:size(t);
        exx(i)=X(i,5)*sin(X(i,1))*cos(X(i,3));
        why(i)=X(i,5)*sin(X(i,3));
        zee(i)=-X(i,5)*cos(X(i,1))*cos(X(i,3));
end


%*************************  Plots   ****************************

figure('Name','Attachment phase');
subplot(221), plot3(exx, why, zee)
xlabel('X (m)')
ylabel('Y (m)')
zlabel('Z (m)')
title('(a) End body trajectory')

subplot(222), plot(TT(:,1),TT(:,2))
xlabel('time (s)')
ylabel('tension (N)')
title('(b) Tether tension')

subplot(223), plot(t, X(:,1)*180/pi,'.g')
xlabel('time (s)')
ylabel('Angle (deg)')
legend(['theta, init=',num2str(thetainit)])
title('(c) Theta')
```

```
subplot(224), plot(t, X(:,3)*180/pi,'-r')
xlabel('time (s)')
ylabel('Angle (deg)')
legend(['phi, init=',num2str(phiinit)])
title('(d) Phi')


%       all plots won't all fit in one figure window, unfortunately
figure('Name','Angular displacement history');
subplot(321), plot(t, X(:,2)*180/pi,'.g')
xlabel('time (s)')
ylabel('Angular rates (deg/s)')
legend(['thetadot, init=',num2str(thetadotinit)])
title('(a) Thetadot')

subplot(322), plot(t,X(:,4)*180/pi,'-r')
xlabel('time (s)')
ylabel('Angular rates (deg/s)')
legend(['phidot, init=',num2str(phidotinit)])
title('(b) Phidot')

subplot(223), plot(X(:,1)*180/pi, X(:,2)*180/pi)
xlabel('Theta (degrees)')
ylabel('Thetadot (deg/s)')
title('(c) Phase plane plot of Theta vs Thetadot')

subplot(224), plot(X(:,3)*180/pi, X(:,4)*180/pi)
xlabel('Phi (degrees)')
ylabel('Phidot (deg/s)')
title('(d) Phase plane plot of Phi vs Phidot')
```

---

```
%     Integrating the Beletsky and Levin massless tether differential
equations
%     This process assumes tether is fully deployed upwards from
asteroid surface

%     Filename:  attach2.m
%
function Xdot=attach2(t,X)
%
%X is [theta, thetadot,phi,phidot, r, rdot]

global  omegasuninit theta omega omegainit mspace maxlength muast r T ;

F=helio(t,X);           %ugly, but you can't integrate these time
dependent equations otherwise
%Fhist=[Fhist;t F'];

Xdot(1)=X(2);
Xdot(2)=-2*(X(2)+1)*(X(6)/X(5) - X(4)*tan(X(3)))-3*sin(X(1))*cos(X(1))-
F(2)/(X(5)*cos(X(3)));
Xdot(3)=X(4);
```

```
Xdot(4)=-2*(X(6)/X(5))*X(4)-
sin(X(3))*cos(X(3))*((X(2)+1)^2+3*(cos(X(1)))^2)-F(3)/(X(5));
if X(5)< maxlength;      %r, such that it can grow to "maxlength"
      Xdot(5)=X(6);
else
      Xdot(5)=0;
end
Xdot(6)=omega*(X(4)^2+(X(2)+1)^2*(cos(X(3)))^2+3*(cos(X(3)))^2*(cos(X(1)
))^2-1)-T/mspace -F(1);
```

## C.3 Crawler retrieval.

The equations for a crawler mass are a slightly modified version of the Glickman and Rybak equations. Heliocentric contributions are neglected. The files used in the sample retrieval integration are

| | |
|---|---|
| crawl1.m | Main program and plotting subroutines |
| crawl2.m | The ode45 integration routine |

---

```
%     Filename:   crawl1.m
%     Subject:    Crawler EOM per Glickman and Rybak
%     Files called: crawl2.m
%
clear all;
%     Constants
global omega k EHA z;
omega=4.36e-4;                              %2 hr--8.73e-4, 1 day = 7.27e-
5

%     Tether characteristics
mt=5;                                       %SAIC tether mass 5 kg
A=pi*.003^2/4;                              %tether cross-section area
(3mm tether)
L=500;                          %Deployed tether length (fixed), meters
mcrawl=300; mspace=700;         %mass: crawler payload, spacecraft (kg)
rho=mt/(A*L);                   %SAIC: 500 m, tether mass density
k1=rho*A*(L^3)/mcrawl;          %integration constant (unadulterated
version)
k2=3*mspace*L^2/mcrawl;         %moment of inertia and grav. gradient for
spacecraft
k=k1+k2;                        %adulterated constant for the integration
routine


% For a test case of Glickman and Rybak, use L=100000,
mt=400,mp=500,mspace=70000,EHAdeg=0.9

%     Initial parameters
EHAdeg=5;                       %degrees of constant hangoff angle
EHA=EHAdeg*pi/180;              %Convert degrees EHA to radians
```

```
y0=0.1; y0dot=0;              %Initial crawler position,velocity
t0=0; tf=1800;

[t,y]=ode45('crawl2',t0,tf,y0);


%     Extract ydot for plots
zsize=size(z);
      time=z(:,1);
      why =z(:,2);
      whydot=z(:,3);
timesplit=round(zsize(1)/4);  %initial impulse makes graphing difficult,
so break it apart

%     Estimate acceleration
why2dot=[time(1) whydot(1)];
for i=1:round(timesplit/3);
      temp=[time(i+1) (whydot(i+1)-whydot(i))/(time(i+1)-time(i));];
      why2dot=[why2dot;temp];
end

%     Estimate jerk
jerk=[time(1) why2dot(1)];
for i=1:round(timesplit/3);
      temp=[time(i+1) (why2dot(i+1)-why2dot(i))/(time(i+1)-time(i));];
      jerk=[jerk;temp];
end


figure('name','Crawler position characteristics')
%     Figure 1: Crawler position vs time
subplot(221),plot(t,y,'g')
legend(['EHA = ',num2str(EHAdeg),' deg'])
xlabel('time (sec)')
ylabel('Position (m)')
title('Crawler position on tether')

%     Figure 2: Retrieval rate vs time
subplot(222), plot(t,y,':r')
xlabel('time (sec)')
ylabel('deployment rate (m/s)')
title('Deployment rate as a function of time')

figure('name','Velocity and acceleration of the crawler')
%     Figure : Initial impulsive motion
subplot(221), plot(time(1:timesplit),whydot(1:timesplit),'g')
xlabel('time (s)')
ylabel('crawler velocity (m/s)')
title('Initial motion of the crawler')

%     Figure : Post impulse motion
subplot(222),
plot(time(3*timesplit:zsize(1)),whydot(3*timesplit:zsize(1)),'g')
xlabel('time (s)')
ylabel('crawler velocity (m/s)')
title('Subsequent motion of the crawler')

%     Figure : Initial impulsive motion
subplot(223), plot(why2dot(:,1),why2dot(:,2),'g')
```

```
xlabel('time (s)')
ylabel('crawler acceleration (m/s2)')
title('Initial acceleration of the crawler')

%     Figure : Impulse
subplot(224), plot(jerk(:,1),jerk(:,2),'r')
xlabel('time (s)')
ylabel('crawler "jerk" (m/s3)')
title('"Jerk" of the crawler')
```

## C.4 Miscellaneous.

These following files are listed here

| | |
|---|---|
| Fhistory.m | Plot option for heliocentric forces in orbiting frame |
| helio.m | Heliocentric "perturbing" forces |
| cross.m | Cross product (e.g. cross(*vector1*,*vector2*)) |

---

```
%      Filename:  Fhistory.m
%      Plots the heliocentric correction in local reference frame coords
%

global omegasuninit theta omega omegainit ma mspace muast r T Fhist;

period=2*pi/omega;

figure('Name','Inertial acceleration correction');
subplot(221), plot(Fhist(:,1)/period,Fhist(:,3))
xlabel('time (fraction of orbital period)')
ylabel('acceleration (m/s2)')
title('(a) In-plane acceleration due to sun (m/s2)')
%legend(['x (m), speed=',num2str(speed),' m/s '],['y (m),
theta=',num2str(ejectiontheta),' degrees'], ['total length (m)'])

subplot(222), plot(Fhist(:,1)/period,Fhist(:,4))
xlabel('time (fraction of orbital period)')
ylabel('acceleration (m/s2)')
title('(b) Out-of-plane acceleration due to sun')

subplot(223), plot(Fhist(:,1)/period,Fhist(:,2))
xlabel('time (fraction of orbital period)')
ylabel('acceleration (m/s2)')
title('(c) Radial acceleration due to sun')

subplot(224), plot(Fhist(:,2),Fhist(:,3))
xlabel('In-plane acceleration (m/s2)')
ylabel('Out-of-plane acceleration (m/s2)')
title('(d) Angular accelerations due to sun')
```

---

```
%Does the grunt work to feed deploy2.m

function [F]=helio(t,X)
%
%X is [theta, thetadot,phi,phidot, r, rdot]
%x1=X(1); x2=X(2); x3=X(3);x4=X(4);x5=X(5); x6=X(6);

global  omegasuninit theta omega omegainit ma mspace muast r T F ;

omegasun=1.990971e-7; R=1.4959965e11; musun=1.3271544e20;
OMsun=[0 0 omegasun];OM=[0 0 omega];

%3-1-3 rotation angles PSI, TH, PHI
PSI=omegasun.*t+omegasuninit; TH=0*pi/180; PHI=omega.*t+omegainit
      RPSI=[cos(PSI) sin(PSI) 0;-sin(PSI) cos(PSI) 0; 0 0 1];
      RTH =[1 0 0; 0 cos(TH) sin(TH); 0 -sin(TH) cos(TH)];
      RPHI=[cos(PHI) sin(PHI) 0;-sin(PHI) cos(PHI) 0; 0 0 1];
C=RPHI*RTH*RPSI;

Ras=R*[cos(PSI); sin(PSI); 0];  Ras2dot=-omegasun^2.*Ras;
rma=r*[cos(X(3))*cos(PHI); cos(X(3))*sin(PHI); sin(X(3))];
      magrma=(rma(1)^2 + rma(2)^2 + rma(3)^2)^.5;
Rms=C*Ras+rma;
      magRms=(Rms(1)^2 + Rms(2)^2 + Rms(3)^2)^.5;

Finert=musun.*Rms/magRms^3-C*Ras2dot+muast.*rma/magrma^3-
2*cross(C*OMsun',cross(OM,rma))-cross(C*OMsun',cross(C*OMsun',rma));
F=   [cos(X(5))*cos(X(3)) sin(X(5))*sin(X(3)) sin(X(3)); -sin(X(5))
cos(X(5)) 0; -cos(X(5))*sin(X(3)) -sin(X(5))*sin(X(3))
cos(X(3))]*Finert;

%     Tension in a tether can be related by
u=X(4)^2+(X(2)+1)^2*(cos(X(3)))^2+3*(cos(X(3)))^2*(cos(X(1)))^2-1;
T=mspace*omega^2*X(5)*u;
```

---

```
function xprod=cross(A,B);
%
%     This returns a 3x1 cross product to the user.
%
xp1=A(2)*B(3)-A(3)*B(2);
xp2=-A(3)*B(1)+A(1)*B(3);
xp3=A(1)*B(2)-A(2)*B(1);
xprod=[xp1; xp2; xp3];
end
```

# Bibliography


1. Alvarez, Luis W. "Extraterrestrial Cause for the Cretaceous-Tertiary Extinction." *Science*, 208:1095-1108 (1980)

2. Anselmo, Joseph C. "NRO Orbiting Spacecraft Studies Tether Survivability." *Aviation Week and Space Technology*, Vol 145, No. 1:24 (July 1, 1996)

3. Arnett, Bill. "Asteroids." Internet article. July 1996 (URL: http://bozo.lpl.arizona.edu/nineplanets/asteroids.html)

4. Arnold, David A. "The Behavior of Long Tethers in Space." *Advances in the Astronautical Sciences, Volume 62*, P. Bainum, editor, 35-50. San Diego: Univelt Inc, 1986

5. Bate, Roger R. and others. *Fundamentals of Astrodynamics*. New York: Dover Publications, Inc., 1971

6. Beletsky, Vladimir V. And Evgenii M. Levin. "Dynamics of Space Tether Systems" *Advances in the Astronautical Sciences, Volume 83*. San Diego: Univelt Inc, 1993

7. Berkowitz, Bruce D. "More Moon Probe for Your Money." *Technology Review*, Vol 98, No 3:25-31, April 1995

8. Canavan, Gregory H. and others. "Near-Earth Object Interception Workshop." In *Hazards Due to Comets and Asteroids*, Tom Gehrels, editor, 93-126. Tucson: University of Arizona Press, 1994

9. Chapman, Clark R. and others. "Physical Properties of Near-Earth Asteroids: Implications for the Hazard Issue." In *Hazards Due to Comets and Asteroids*, Tom Gehrels, editor, 537-549, Tucson: University of Arizona Press, 1994

10. Cheng, Andrew F. and others. "Missions to Near-Earth Objects." In *Hazards Due to Comets and Asteroids*, Tom Gehrels, editor, 651-670. Tucson: University of Arizona Press, 1994

11. Chobotov, Vladimir A. *Spacecraft Attitude Dynamics and Control*. Malabar: Krieger Publishing Co., 1991

12. European Space Agency. "Rosetta/CNSR A Comet-Nucleus Sample-Return Mission." *Mission and System Definition Document.* Noordwijk: ESA Publications Division, 1991

13. Gehrels, T. ed. *Hazards Due to Comets and Asteroids.* Tucson:University of Arizona Press, 1994.

14. Glickman, Ronald E. and Samuel C. Rybak. "Gravity Gradient Enhancement During Tethered Payload Retrieval." *Advances in the Astronautical Sciences, Volume 62,* P. Bainum, editor, 317-337. San Diego: Univelt Inc, 1986

15. Goldman, Stuart J. "Clementine Maps the Moon." *Sky and Telescope*, Vol 88, No 2:21-24, August 1994

16. Haughton, James and others. "System Level Mechanical Testing of the Clementine Spacecraft." *18th Space Simulation Conference: Space Mission Success Through Testing*, Baltimore, MD 31 October - 3 November 1994 (NASA CP 3280)

17. Hyman, Nelson L. and Jeong H. Kim. "Thermal Design Verification of the Clementine Spacecraft: Quick, Cheap, and Useful." *18th Space Simulation Conference: Space Mission Success Through Testing*, Baltimore, MD 31 October - 3 November 1994 (NASA CP 3280)

18. Lang, D.D. and R. R. Nolting. "Operations with Tethered Space Vehicles." *Gemini Summary Conference*, Houston, TX, February 1-2, 1967 ( NASA SP-138, pp. 55-66)

19. Larson, Wiley J. and James R. Wertz. ed. *Space Mission Analysis and Design, Second Edition.* Torrance: Microcosm, Inc. 1992.

20. Likins, Peter W. *Elements of Engineering Mechanics.* New York: McGraw-Hill Book Company, 1973.

21. Martin Marietta Corporation. "Study of Sample Drilling Techniques for Mars Sample Return Missions" Denver: Martin Marietta Corp, 1979 (NASA CR 160723)

22. Minor Planet Center. "Unusual Minor Planets." Internet article, November 1996. (URL:http//cfa-www.harvard.edu/~graff/lists/Unusual.html)

23. Morrison, David, editor. *The Spaceguard Survey: Report of the NASA International Near-Earth Object Interception Workshop*, Washington D.C.: NASA, 1992

24. National Aeronautics and Space Administration. *Tethers in Space Handbook, Second Edition.* Washington D.C.: NASA, 1989

25. National Aeronautics and Space Administration. "NSSDC Master Catalog Display: NEAR." Internet article, July 1995 (URL: http://nssdc.gsfc.nasa.gov/planetary/near.html)

26. Penzo, Paul A. "A Survey of Tether Applications to Planetary Exploration." Pasadena: Jet Propulsion Lab, 1986

27. Pisacane, Vincent L. and Robert C. Moore, Editors. *Fundamentals of Space Systems.* New York: Oxford University Press, 1994.

28. Rabinowitz, David L. and others. "The Population of Earth-Crossing Asteroids." In *Hazards Due to Comets and Asteroids*, Tom Gehrels, editor, 285-312. Tucson: University of Arizona Press, 1994

29. Rahe, J. and others. "Properties of Cometary Nuclei." In *Hazards Due to Comets and Asteroids*, Tom Gehrels, editor, 597-634. Tucson: University of Arizona Press, 1994

30. Redd, Frank. "Tether Platform Applications" Internet article, August 1996 (URL: http//www.engineering.usu.edu/Dep...papers/carroll/carroll)

31. Science Applications International Corporation. "Asteroid Prospector Sample Return Study." Schaumburg: SAIC, October 20, 1995

32. Schilling, K. and others. "Autonomous On-Comet Operations Aspects of the Rosetta Mission." *Control Engineering Practice*, Vol. 2, No. 3:499-507, March 1994

33. Shoemaker, Eugene M. and others. "Asteroid and Comet Flux in the Neighborhood of Earth." *Global Catastrophes in Earth History*, V. L. Sharpton and P.D. Ward, editors, 155-170. Boulder: Geological Society of America, 1990. (Geological Society of America Special Paper 247.)

34. Shoemaker, Eugene M. *Near-Earth Asteroid Returned Sample (NEARS) Final Technical Report.* Lowell Observatory, 1994 (NASA CR 197297)

35. Stuhlinger, E. and others. "Comet Nucleus Sample Return Missions .With Electrically Propelled Spacecraft." *Journal of the British Interplanetary Society*, Vol. 39, No. 6:273-281, June 1986.

36. Sutton, George P. *Rocket Propulsion Elements, An Introduction to the Engineering of Rockets, Sixth Edition.* New York: John Wiley and Sons. 1986

37. Swet, C.J. and J.M. Whisnant. *Deployment of a Tethered Orbiting Interferometer.* Johns Hopkins University Technical Memorandum TG 1080. Silver Springs: Applied Physics Laboratory, August 1969. (AD 707327)

38. Personal communications with Mr Alan Willoughby of the ANALEX Corporation, March 1995 - February 1996

# Vita

Captain John W. Wong [redacted]. He graduated from Hueneme High School, Port Hueneme, California in June 1980 and subsequently enlisted in the United States Air Force in a cryptographic specialty field. AIC Wong applied to the United States Air Force Academy and was inducted into the Class of 1985 in June 1981. Cadet Wong graduated from the USAF Academy in May 1985 with dual degrees in General Chemistry and Engineering Physics, and entered the fledgling Space Operations career field.

His first assignment as a commissioned officer was at Sunnyvale AFS, in Sunnyvale, California, where he managed the development of satellite operations training for the Air Force Satellite Control Network. During this assignment, he also held the position of Operations Director in the Resource Scheduling and Planning Branch of the AFSCN, and later returned to a training directorate to develop the training for MILSTAR ground equipment maintainers.

In September 1992, Captain Wong became a Missile Warning Crew Commander at Clear AS, Alaska, and provided both space surveillance and missile warning functions to NORAD. Capt Wong transferred from Clear AS to Wright-Patterson AFB in May 1994 to work on a M.S. degree in Space Operations at the Air Force Institute of Technology. He finished the degree post-AFIT at his follow-on assignment to the Office of Aerospace Studies, Kirtland AFB, New Mexico, in June 1997.

Captain Wong was married to Jennifer Ingalls from [redacted] and has one daughter, Janelle, [redacted]

[redacted]

Current assignment: OAS/DRA
3550 Aberdeen Dr SE
Kirtland AFB, NM 87117
(505) 846-8243 (DSN 246)

| REPORT DOCUMENTATION PAGE | Form Approved OMB No. 0704-0188 |
|---|---|



| 1. AGENCY USE ONLY *(Leave blank)* | 2. REPORT DATE | 3. REPORT TYPE AND DATES COVERED |
|---|---|---|
| | June 1997 | Masters Thesis |

**4. TITLE AND SUBTITLE**
Analysis of Tethers in Sampling Near Earth Objects

**5. FUNDING NUMBERS**

**6. AUTHOR(S)**
John W. Wong, Capt, USAF

**7. PERFORMING ORGANIZATION NAME(S) AND ADDRESS(ES)**
Air Force Institute of Technology, WPAFB OH 45433-6583

**8. PERFORMING ORGANIZATION REPORT NUMBER**
AFIT/GSO/ENY/97J-1

**9. SPONSORING/MONITORING AGENCY NAME(S) AND ADDRESS(ES)**
Mr John J. Nieberding
Space Directorate Office
NASA Lewis Research Center/ Bldg 3-6
21000 Brookpark Road
Cleveland, OH 44135

**10. SPONSORING/MONITORING AGENCY REPORT NUMBER**

**11. SUPPLEMENTARY NOTES**

**12a. DISTRIBUTION AVAILABILITY STATEMENT**
Approved for public release; distribution unlimited

**12b. DISTRIBUTION CODE**
A

**13. ABSTRACT** *(Maximum 200 words)*

This study investigated the feasibility of a SAIC proposal to sample Near Earth Objects (NEOs) from an orbiting spacecraft using a tethered landing device. The parameters for suitable targets were derived from an analysis of a proposed point design as applied to current knowledge of NEOs. Tether strength and lifetime for the point design were also assessed. First order modeling of tether dynamics showed that deployment and attachment to a NEO are feasible. The dynamics of retrieving a sample via a crawler unit which crawls up the tether requires further exploration.

**14. SUBJECT TERMS**
Tethers, Near Earth Objects, Asteroids, Spacecraft, Sample Collection, Space

**15. NUMBER OF PAGES**
134

**16. PRICE CODE**

| 17. SECURITY CLASSIFICATION OF REPORT | 18. SECURITY CLASSIFICATION OF THIS PAGE | 19. SECURITY CLASSIFICATION OF ABSTRACT | 20. LIMITATION OF ABSTRACT |
|---|---|---|---|
| Unclassified | Unclassified | Unclassified | UL |

Standard Form 298 (Rev. 2-89) (EG)
Prescribed by ANSI Std. 239.18
Designed using Perform Pro, WHS/DIOR, Oct 94